UNIVERSITY OF KWAZULU-NATAL

Double Spatial Media Based Modulation

Ronald Tafireyi Tsvaki

2019

Double Spatial Media Based Modulation

Ronald Tafireyi Tsvaki

211558511

Submitted in fulfillment of the academic requirements of
Master of Science in Engineering

Discipline of Electrical, Electronic and Computer Engineering
School of Engineering, College of Agriculture, Engineering and Science
University of KwaZulu-Natal, Durban, South Africa

Supervisor: Dr. Narushan Pillay
Co-Supervisor: Prof. HongJun Xu

December 2019

Preface

The research contained in this dissertation was completed by the candidate while based in the School of Engineering, Discipline of Electrical, Electronic and Computer Engineering, in the College of Agriculture, Engineering and Science, University of Kwazulu-Natal, Howard College, South Africa.

The contents of this work have not been submitted in any form to another university and, except where the work of others is acknowledged in the text, the results reported are due to investigations carried out by the candidate.

As the candidate's supervisor, I agree to the submission of this dissertation.

Signed:

Dr Narushan Pillay

Date:

Declaration 1

Plagiarism

I, Ronald Tafireyi Tsvaki, declare that:

i. the research reported in this dissertation, except where otherwise indicated, is my original research;

ii. this dissertation has not been submitted for any degree or examination at any other university;

iii. this dissertation does not contain other person's data, pictures, graphs or other information unless specifically acknowledged as being sourced from other persons;

iv. this dissertation does not contain other person's writing unless specifically acknowledged as being sourced from other researchers. Where other written sources have been quoted, then

   a. their words have been re-written but the general information attributed to them has been referenced,

   b. where their exact words have been used, then their writing has been placed in italics and inside quotation marks, and referenced;

v. this dissertation does not contain texts, graphics or tables copied from the internet, unless specifically acknowledged, and the source being detailed in the dissertation and in the reference section.

Signed:

Ronald T. Tsvaki

Date:

Declaration 2

Publications

DETAILS OF CONTRIBUTION TO PUBLICATIONS that form part and/or include research presented in this dissertation (include publications in preparation, submitted, *in press* and published and give details of the contributions of each author to the experimental work and writing of each publication).

Publication 1:

R. Tsvaki, N. Pillay, H. Xu,"Double Spatial Media-based Modulation with RF Mirrors" *International Journal of Communication Systems (IJCS)* [under review].

Signed:

Ronald T. Tsvaki

Date:

Dedication

This thesis is dedicated to my beloved late mother, Ms Jesmine T. Kutsawa.

Acknowledgements

I would like to express my deepest appreciation supervisor, Dr Narushan Pillay, for his continued support and guidance during the course of this research. I sincerely appreciate the diligent advice that has helped to advance my academic writing skills and I a grateful to have had the opportunity to work under his vigilante care.

My gratitude also goes to Professor Hongjun Xu, who played a significant role in helping me to improve my research. I also wish to express my gratitude to all my colleagues with whom I have had the pleasure to work with during research.

A special and heartfelt thanks goes to my family, who thorough-out the journey have continued to encourage and support me in all ways during good times and bad times.

Lastly, I would like to thank God his blessing, and allowing me to advance to this stage in my academic career. I would like to thank him for granting me the strength in diligence and perseverance to complete this research and all other blessings.

Abstract

Multiple-input multiple-out (MIMO) systems have become an increasingly popular technology in wireless communications due to their high data rates and increased reliability. However, several drawbacks degrade the performance of MIMO systems. Inter-channel interference, inter-antenna synchronization, low energy efficiency, and relatively high-complexity receive algorithms are several of the challenges that MIMO systems face. As such, spatial modulation (SM) was introduced as a scheme that is capable of exploiting the advantages of MIMO systems, while simultaneously mitigating its drawbacks. SM provided an excellent method of exploiting spatial diversity, which eventually replaced MIMO systems. However, as the use of SM became more prominent, its drawbacks became more apparent. The spectral efficiency of SM is limited by the logarithmic relationship between spectral efficiency and the number of transmit antennas.

Several SM-based transmission schemes, such as quadrature spatial modulation and double spatial modulation (DSM), were introduced with the prospect of improving the spectral efficiency of SM. These schemes have a single radio frequency (RF) chain; therefore, relatively low-complexity receive algorithms are employed. Conventional transmission techniques are referred to as source-based modulation (SBM).

Media-based modulation (MBM) is a new attractive transmission scheme that has been recently receiving increased research attention. MBM employs the use of RF mirrors to vastly improve the error performance and/or spectral efficiency of modulation schemes. It has been demonstrated that MBM, coupled with SBM techniques, vastly improves the error performance and can potentially increase the spectral efficiency of these systems.

In this dissertation, DSM is extended to employ MBM, such as to improve error performance. The proposed transmission scheme is called double spatial media-based modulation (DSMBM). The theoretical average bit error probability (ABEP) of DSMBM over an independent and identically distributed Rayleigh frequency-flat fading channel in the presence of additive white

Gaussian noise is formulated. The theoretical ABEP of DSMBM is validated by Monte Carlo simulations, where the error performance matches the theoretical ABEP at high signal-to-noise ratios (SNRs).

Lastly, coded channels are investigated. Typically soft-output detection coupled with soft-input channel decoding yields a significant SNR gain. Motivated by this, this dissertation further proposes a soft-output maximum-likelihood detector for the DSM and DSMBM schemes.

Contents

List of Figures

List of Tables

List of Acronyms

ABEP	Average Bit Error Probability
AMPS	Advanced Mobile Phone System
APM	Amplitude/Phase Modulation
AWGN	Additive White Gaussian Noise
BER	Bit Error Rate
CSI	Channel State Information
DSMBM	Double Spatial Media-Based Modulation
DSM	Double Spatial Modulation
FEC	Forward Error Correction
G	Generation
GSM	Generalised Spatial Modulation
HDMLD	Hard Decision Maximum-likelihood Detection/Detector
IM	Index Modulation
IAS	Inter-Antenna Synchronization
ICI	Inter-Channel Interference
IEEE	Institute of Electrical and Electronic Engineers
i.i.d.	Independent and Identically Distributed
IoT	Internet of Things
LLR	Log-Likelihood Ratio
LTE	Long Term Evolution
MAP	Mirror Activation Pattern

MBM	Media-Based Modulation
MBM-TU	Media-Based Modulation Transmit Unit
MGF	Moment Generating Function
MIMO	Multiple-Input Multiple-Output
ML	Maximum-Likelihood
PDF	Probability Density Function
PEP	Pairwise Error Probability
PSK	Phase Shift Keying
QAM	Quadrature Amplitude Modulation
QSMBM	Quadrature Spatial Media-Based Modulation
QSM	Quadrature Spatial Modulation
RF	Radio Frequency
RV	Random Variable
SBM	Source-Based Modulation
SER	Symbol Error Rate
SIMO	Single-Input Multiple-Output
SIMO-MBM	Single-Input Multiple-Output Media-Based Modulation
SM	Spatial Modulation
SNR	Signal-to-Noise Ratio
SOMLD	Soft-output Maximum-likelihood Detection/Detector
USTLD	Uncoded Space-Time Labeling Diversity
WCS	Wireless Communication System
Wi-Fi	Wireless-Fidelity
WiMAX	Worldwide Interoperability for Microwave Access
WLAN	Wireless Local Area Network

Chapter 1

Introduction

1.1 Introduction

In the recent half-century, wireless communication systems (WCS) have experienced an immense advancement in the communication industry [1]. The introduction of the first standardized mobile phone was in 1982, and since then, wireless mobile communications have undergone considerable growth, which has advanced from the first generation (1G) to the fifth-generation (5G) [2]. The mobile wireless generation (G) generally refers to a change in the nature of WCS in terms of compatible transmission technology, frequency, speed, technology, and data capacity [2,3]. WCS aims to provide high quality and reliable communication, and each new generation of wireless communications is based upon the research and development of the previous generation [4, 5].

The first WCS was called the Advanced Mobile Phone System (AMPS). This system was later referred to as the 1G network [3]. AMPS was a form of analogue communication that only provided voice call services. Analogue networks were not robust systems, and these networks only offered limited security over voice calls. AMPS was later replaced by the second generation (2G) mobile systems, which were introduced in 1991. The evolution from 1G to 2G was mainly influenced by the shift from analogue to digital communications. Digital communications were well received since the shift from analogue to digital represented higher data capacity, reduced cost, improved speed, system flexibility, and power efficiency of digital hardware [3, 4]. The main aim of this generation was to provide secure and reliable communication channels. The two leading technologies that supported this network were code-division multiple access and global system for mobile communication [1]. While 2G networks initially provided voice services, these systems gradually evolved to support data services such as short messaging, internal roaming and conference calls.

The third-generation (3G) of WCS technology was commercially introduced in 2001. The main aim of 3G was to facilitate greater voice and data capacity, which would support a broad range of applications at a lower cost. As a result, web browsing, emails, multimedia services, and other smartphone technology were brought about by 3G networks. The 3G systems mainly utilized a technology called universal mobile telecommunications systems as a core network architecture [4]. This technology employed aspects of 2G systems and combined them with new technology and protocols that delivered significant data rates. These 3G networks continued to advance to the 3.5G, 3.75G, and eventually brought about a further shift to the fourth generation (4G) [3]. The 4G standard was made possible due to the significant advancements in technology that limited the previous generations. Demanding high data rate applications such as high-definition mobile streaming, enterprise software applications, Internet of Things (IoT) and cloud computing were made possible by 4G [6]. The key technologies utilized in 4G systems are multiple-input multiple-output (MIMO) and orthogonal frequency division multiplexing. The standards at which these technologies operate are IEEE 802.11n, also known as wireless fidelity (Wi-Fi), IEEE 802.11n, also known as worldwide interoperability for microwave access (WiMAX), and Long Term Evolution (LTE) [7, 8]. Fifth-generation (5G) WCS have recently been deployed; however, they are not yet commercially available worldwide. Technology such as Millimeter Wave Mobile Communications is employed in 5G. This technology has introduced relatively new communication systems such as Massive MIMO, millimeter-wave, small cells, and light-fidelity systems, which all show promising research prospects [9, 10].

The demand for wireless networks with increased data rates, improved error performance, and lower cost has been the main motivation for researchers to develop WCS that can support the advancing technological demands [2]. However, practical constraints, such as high power consumption, constringent hardware requirements, and high computational complexity, need to be mitigated to achieve robust wireless networks that deliver the required standard for emerging applications [1]. At a physical level, one of the main challenges facing WCS is the degradation/attenuation of signals transmitted in a channel with the presence of additive white Gaussian noise (AWGN) [11]. Noise arises from various natural phenomena, such as thermal noise, which is a product of passive components, including resistors and solid-state devices used in the construction of communication systems [12]. Another source of interference is black body noise, which arises from celestial sources such as solar radiation. These naturally-occurring noise components are typically modeled by random variables (RVs) that are assumed to follow

Gaussian distribution. The effect of thermal noise is assumed to be "white", which indicates that it is not frequency selective, and it is modeled at the receiver as a superimposed signal on the transmission [1, 12]. In communication systems, the effects of additive noise can be mitigated by increasing the signal transmit power in a channel. However, the power level in signal transmission is limited by the equipment and other practical constraints.

1.2 Multipath Propagation

Multipath propagation is the transmission of terrestrial radio waves through a wireless channel [1]. Due to effects such as ionospheric reflection and refraction, reflection from water bodies and terrestrial objects, a radio receiver in a wireless channel receives multiple different versions of the same signal, which vary in time due to different signal paths. This difference in arrival time is referred to as multipath [12]. Multipath propagation of radio waves through a wireless channel is a complicated phenomenon characterized by various effects, such as multipath-fading, path loss, absorption, reflection, diffraction, and shadowing. Mathematical descriptions of this phenomenon are either unknown or too complex for tractable communications systems analyses [12]. However, considerable efforts have been devoted to the statistical modeling and characterization of these different effects. Some models exist which represent amplitude distribution of fading coefficients, the most common of which are Rayleigh fading, Nakagami-q fading, and Rician fading. This dissertation focuses on the propagation environment and communication scenario for the Rayleigh fading model [1, 12].

1.2.1 Rayleigh Fading Model

Rayleigh fading is a statistical model of the effect of a propagation environment on radio signals in a wireless channel [1]. Fading is the deviation of the attenuation affecting a signal over a WCS, and fading accounts for effects such as reflection, refraction, and scattering which occur during radio wave transmission [1]. The Rayleigh fading model is most commonly applied in wireless channels that have no direct line-of-sight between the transmitter and receiver. The effect of fading introduces both amplitude distortion and phase delay to the transmitted symbol, allowing a complex fade coefficient to be modeled where both the real and imaginary components are modeled as independent and identically distributed (i.i.d.) Gaussian RVs [1, 11]. The fading coefficient is expressed as:

$$h = h^{\Re} + jh^{\Im} \tag{1.1}$$

where h is the fading coefficient, $h^{\Re}$ and $h^{\Im}$ are the real and imaginary components of the fading coefficient, respectively, which are Gaussian RVs with zero mean and variance of $\frac{1}{2}$. The Rayleigh fading coefficient can be represented in polar form as:

$$h = \alpha e^{j\phi}, \tag{1.2}$$

where $\alpha = \sqrt{|h^{\Re}|^2 + |h^{\Im}|^2}$ is the fading amplitude, and $\phi = arctan\left(\frac{h^{\Im}}{h^{\Re}}\right)$ is the fading phase angle. The probability density function (PDF) of the Rayleigh fading with a fading amplitude α is given by:

$$f(\alpha) = \frac{\alpha}{\sigma^2} \exp\left(\frac{-\alpha^2}{2\sigma^2}\right), \alpha \geq 0, \tag{1.3}$$

where σ^2 is the variance of α.

In this dissertation, in all fading scenarios, the statistical propagation environment that is assumed is the Rayleigh frequency-flat fading channel, unless otherwise stated.

1.3 Diversity

A popular technique used in wireless communications to improve error performance in the presence of fading is diversity [12]. Diversity refers to the reception of multiple copies of a signal through a channel so that independent copies of the signal experience different transmission paths in a wireless channel. Diversity is a technique that introduces redundancy in a wireless channel, ensuring that a transmitted signal does not experience a deep fade that affects all components of the signal in different paths simultaneously [1]. In turn, this decreases the probability that all transmitted signals via the multiple paths are subjected to substantial attenuation. The receiver combines several received signals via multiple paths and gives a more accurate estimation of the transmitted signal [12]. There are several traditional methods employed by WCS to achieve diversity, and these are grouped into several categories, which include time, antenna, frequency, field, polarization, angle, and multipath diversity [13–15].

1.4 SIMO

Single-input single-output (SIMO) systems are one of the earliest modulation techniques that were introduced in order to achieve diversity [1]. In SIMO systems, the receiver is supplied with multiple redundant copies of the same signal, which results in the system gaining receive diversity. Figure 1.1 illustrates the system model for SIMO system, where N_R represents the

number of receive antennas.

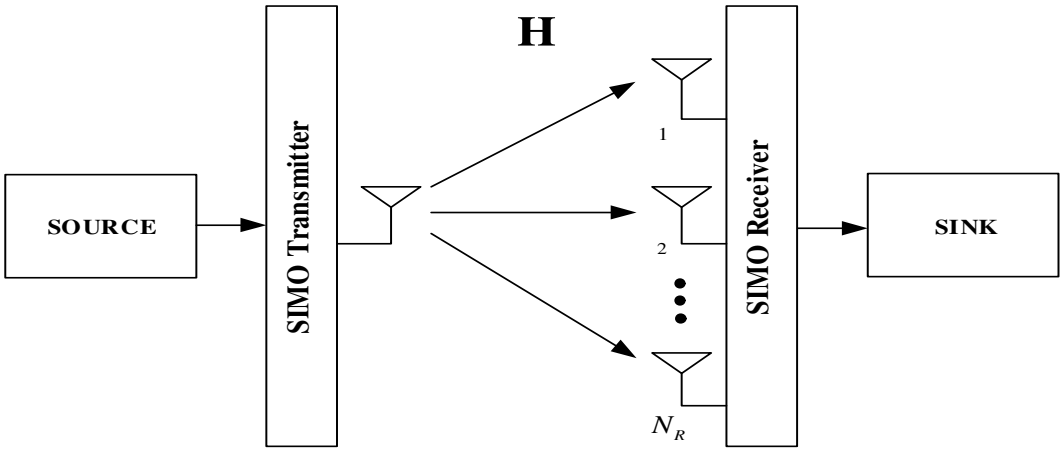

Figure 1.1: SIMO system model

At the receiver, all received signals are simultaneously processed to combine them with a suitable technique. The most common methods used to estimate the received signal are maximal ratio combining, selection combining and equal gain combining [1].

1.5 MIMO

As new wireless communication technologies emerge, there is still the desire for networks with significant improvements in data rates and error performance [2]. One conventional method of improving data rates is using transmission schemes that employ high modulation order amplitude and/or phase modulation (APM) constellation signals. However, the drawback is that such systems have poor reliability as the modulation order increases [1]. High order modulation schemes require high transmit power to yield a sufficiently good error performance; however, low order modulation schemes with low transmit power have better error performance as compared to high order schemes. As mentioned earlier, one method used to improve error performance is employing diversity to WCS [12, 16]. MIMO systems provide an efficient way to increase data rates and improve error performance by exploiting spatial diversity [17]. Spatial diversity in MIMO systems establishes multiple channels via the multiple antennas at both the transmitter and receiver [17, 18].

1.5.1 MIMO System Model

Figure 1.2 illustrates the system model for a MIMO system, where N_T and N_R, $N_T \leq N_R$, represents the number of transmit antennas and receive antennas, respectively.

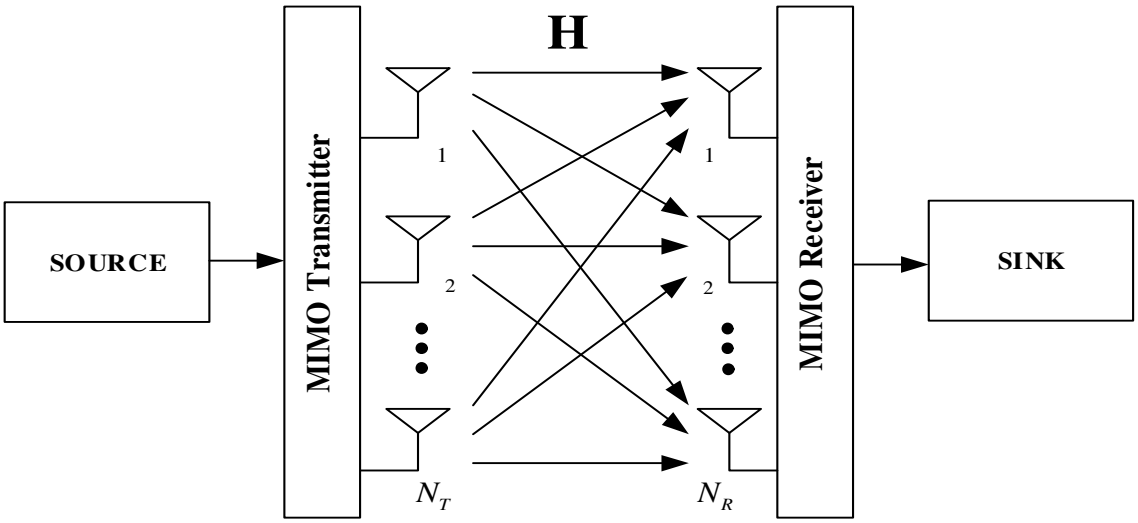

Figure 1.2: MIMO system model

In each transmission interval, the source provides an input bit stream of length m bits. The information bits are used to select APM signal constellation symbols which are transmitted via an $N_T \times 1$ transmit vector $\mathbf{x} = [x_1, \ldots, x_{N_T}]^T$, where $E\{|x_\ell|^2\} = 1,\ \ell \in [1 : N_T]$, over a Rayleigh frequency-flat fading channel $\mathbf{H}$ in the presence of AWGN. The fading channel gain matrix $\mathbf{H}$ is of dimension $N_R \times N_T$, and is given as [1]:

$$\mathbf{H} = \begin{bmatrix} h_{1,1} & \cdots & h_{1,N_T} \\ \vdots & \ddots & \vdots \\ h_{N_R,1} & \cdots & h_{N_R,N_T} \end{bmatrix}, \tag{1.4}$$

where each element in $\mathbf{H}$ is defined as $h_{k,\ell}$, which is a channel coefficient that corresponds to the k^{th} receive antenna and the ℓ^{th} transmit antenna, $k \in [1 : N_R],\ \ell \in [1 : N_T]$. AWGN is represented by an $N_R \times 1$ vector $\mathbf{n} = [n_1, \ldots, n_{N_R}]^T$. All elements of $\mathbf{H}$ and $\mathbf{n}$ are assumed to be i.i.d. entries with Gaussian distribution of zero mean and unit variance $\sim CN(0, 1)$. The received signal of MIMO is given as [1]:

$$\mathbf{y} = \sqrt{\rho}\mathbf{H}\mathbf{x} + \mathbf{n}, \tag{1.5}$$

where ρ is the average signal-noise ratio (SNR) at each receive antenna.

MIMO systems have been continuously receiving research attention due to the promising prospects of achieving high data rates and improved error performance, and as a result, these systems are now considered as one of the core techniques of improving wireless communication [19, 20]. To date, MIMO systems have become the essential element of wireless communication standards, including wireless local area network, Wi-Fi, WiMAX, and LTE [7].

Theoretically, the use of a large number of antennas allows for high antenna diversity gains for MIMO systems. However, physical devices in wireless networks such as mobile receivers have limited space available. Therefore, increasing the number of antennas in this constrained space leads to the distance between antennas decreasing. Decreasing the physical spacing between antennas of the MIMO systems induces spatial correlation, which degrades error performance and loss of diversity due to inter-channel interference (ICI) [1,17]. Despite the several benefits of MIMO, there are still limitations on a physical level, which include inter-antenna synchronization (IAS), highly complex receive algorithms, and low energy efficiency [12, 18].

1.6 Literature Survey

In this section, we present the summary of the literature that leads to the development of double spatial media-based modulation (DSMBM) transmitted over a Rayleigh frequency-flat fading channel. This summary is not necessarily presented in chronological order.

1.6.1 Index Modulation

Index modulation (IM) refers to a type of technique that employs alternative ways other than APM signal modulation to convey information through a wireless channel [21]. IM embeds information into indices of a distinct channel property, which alter the ON/OFF status of these indices. Some examples of channel properties are antennas, time-slots, and light-emitting diodes. Some advantages of IM are as follows [21, 22]:

1. In contrast to MIMO systems, which employ total transmission energy, IM can transfer saved transmission energy from inactive transmit components to the active components, therefore, improving the error performance.

2. IM provides an energy efficient method transmitting information via the activation and deactivation of components in a system.

3. A system that employs IM can increase spectral efficiency without increasing hardware complexity.

Based on its advantages, IM has become increasingly relevant as a candidate for next-generation wireless communications [21].

1.6.2 Spatial Modulation

Spatial Modulation (SM) is a relatively popular modulation scheme that was introduced by Mesleh *et al.* [23]. SM is an example of an IM modulation technique where information is conveyed through the selection of a transmit antenna index [21, 24]. The idea behind SM is to extend the conventional MIMO architecture to employ a third dimension, the spatial domain. SM operates by employing a single active transmit antenna index and subsequently transmitting an APM symbol via the active antenna in a transmission interval. SM provides an excellent method to exploit spatial multiplexing [22].

The use of spatial multiplexing in SM schemes provides a significant reduction in system complexity as compared to conventional MIMO systems. Since only a single transmit antenna is active with all other transmit antenna with zero power during transmission, SM schemes have the ability to mitigate ICI at the receiver, and IAS between the transmit antennas [22]. SM utilizes a single radio frequency (RF) chain, hence relatively low-complexity receive algorithms are employed in SM, improving energy efficiency. Apart from the reduced system complexity, SM also gives a high spectral efficiency transmission scheme, while the system maintains a relatively good error performance [23, 25]. Some advantages of SM are summarized as follows:

1. Only a single active transmit antenna is employed in a transmission interval; therefore, ICI and IAS are mitigated.

2. SM is an energy efficient scheme that only employs a single RF chain.

3. The error performance of SM is improved in contrast to conventional MIMO due to the use of the spatial domain.

4. SM systems have lower hardware costs and complexity.

Since the inception of SM, much research attention has been dedicated to SM due to its merits. However, SM still has several drawbacks that limit the full potential that this scheme can realize. The major drawbacks are summarized as follows:

1. SM has a logarithmic relationship between the spectral efficiency and the number of transmit antenna; therefore a high number of transmit antenna is required to achieve a substantial increase in spectral efficiency.

2. Binary data is used to encode the spatial domain; therefore, the number of transmit antenna has to be a numeral of 2^n, where $n \in \mathbb{N}$.

3. Due to the use of a single active transmit antenna at any transmission interval, SM is incapable of fully exploiting the transmit diversity potential of the MIMO configuration.

To address some of the challenges of SM, several significant SM-based schemes have been proposed in literature, and notable SM-based schemes have been presented in this dissertation.

1.6.3 Generalized Spatial Modulation

Generalized spatial modulation (GSM) is a scheme that was mainly introduced to enhance the spectral efficiency of SM [26, 27]. GSM improves the spectral efficiency of SM by increasing the number of active transmit antennas [27]. Multiple active transmit antenna indices are selected to transmit the same APM symbol in GSM, this differs from SM in that transmit antenna combinations are active during a transmission interval. The antenna spectral efficiency is calculated as base-two logarithm of the total number of transmit antenna combinations in GSM, which is an enhancement of conventional SM. In [28], the concept of GSM is presented in an alternative way of conventional GSM. GSM in [28] is extended to multiple-active transmit antenna, where different APM symbols are transmitted from the selected transmit antenna combinations to boost spectral efficiency further.

Although GSM improves the spectral efficiency of SM, there are still some limiting factors that degrade the performance of this system. The error performance of GSM is limited as compared to SM with the same number of antennas, and there is a higher cost in antenna design for GSM as IAS needs to be eliminated [26].

1.6.4 Quadrature Spatial Modulation

Quadrature spatial modulation (QSM) is a recently proposed IM transmission scheme which aims to improve the spectral efficiency of SM [29]. QSM employs additional information bits to select two active transmit antenna indices in a single transmission interval. The increase in the number of active transmit antenna indices directly increases the spectral efficiency of SM [29]. In QSM, the APM signal is decomposed into its constituent real and imaginary component before transmission via the two active transmit antenna indices. Since the real and imaginary components are orthogonal, QSM mitigates ICI [29].

The advantage of QSM is that the overall throughput of the SM system is enhanced by an additional base-two logarithm of the number of transmit antennas. QSM also inherits similar advantages of SM which include, the use of a single RF chain at the transmitter, and rela-

tively low-complexity receive algorithms. Investigations have demonstrated that QSM has an improved error performance as compared to conventional SM scheme; therefore, QSM provides a good potential replacement for the SM scheme [29].

1.6.5 Double Spatial Modulation

Double spatial modulation (DSM) is a recently proposed SM-based transmission scheme that effectively doubles the spectral efficiency of conventional SM [30]. DSM employs two independent SM transmission channels that are superimposed to transmit simultaneously during a transmission interval. The concept of DSM is inherited from the QSM, where the real and imaginary components of a signal are transmitted via two active transmit antenna indices. In contrast to QSM, DSM simultaneously transmits two AMP constellation symbols via two active transmit antenna indices [30].

The innovative idea that makes DSM possible is that constellation rotation is applied to one of the APM signal constellations, such that the receiver is able to distinguish all constellation points from APM signals of the independent SM channels. The rotation angle applied is optimized to a degree such that the bit error rate (BER) is minimized in the DSM channel [30, 31].

1.6.6 Media-Based Modulation

Media-based modulation (MBM) is a recently proposed concept in wireless communication that has been receiving much research attention. The innovative idea behind MBM is to vary the RF properties such as permittivity, permeability, and resistivity of the propagation environment around a transmit antenna [32]. One of the ways MBM achieves this effect is by placing a parasitic RF mirror near the transmit antenna [33]. Information bits are employed to adjust the ON/OFF status of the RF mirrors to create distinct channel fade realizations in a wireless channel. MBM offers a new dimension for the transmission of digital information by exploiting different fade realizations of wireless channels to create a modulation alphabet [21].

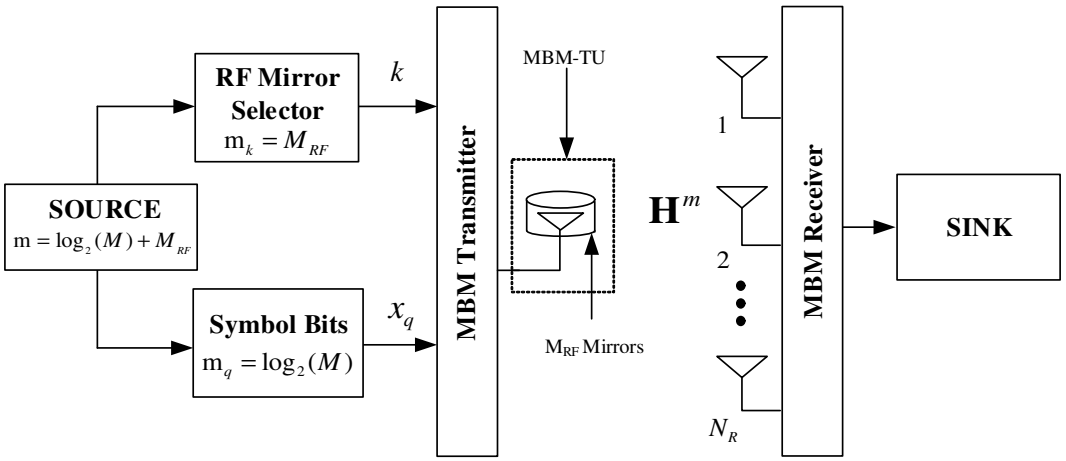

Figure 1.3: SIMO-MBM Transceiver with M_{RF} mirrors

Figure 1.3 illustrates a typical example of a single-input multiple-output (SIMO)-MBM system. The SIMO-MBM system has M_{RF} parasitic RF mirrors placed around the transmit antenna. The combination of a transmit antenna, and its corresponding RF mirror units are referred to as an "MBM transmit unit" (MBM-TU) [33]. An RF mirror can create two different channel fade realizations due to its ON/OFF status. Therefore, in an MBM-TU with M_{RF} RF mirrors, the total number of fade realizations is given by $N_m = 2^{M_{RF}}$ [33]. The RF mirror selector employs M_{RF} information bits to select an index k, $k \in [1 : N_m]$, which is employed by the MBM-TU to alter the field around the antenna according to the information bits. This property is the one that categorizes MBM as part of the IM family. The information bits conveyed to the MBM-TU via the index k activates a particular mirror pattern encoded by the binary data during each transmission interval, and the activated mirror pattern embeds an intentional fade realization into the channel. Each unique mirror pattern forms a channel fade constellation, and a collection of these channel fade constellation patterns is referred to as a mirror activation pattern (MAP) [32–34]. The input vector of $\log_2(M)$ bits, where M is the APM signal modulation order, are used to select an APM constellation symbol which is transmitted via the MBM-TU. The fading channel for SIMO-MBM is represented by the matrix $\mathbf{H}^m = [\mathbf{h}_1^m, \ldots, \mathbf{h}_{N_m}^m]$ of dimension $N_R \times N_m$ [33, 34]. The MBM receiver estimates the transmitted symbol, and the MAP index k used to convey information in each transmission interval [34].

This type of modulation is in contrast to the traditional wireless systems where the information is entirely embedded in the variations of the signal constellation and/or spatial domain. In this dissertation, we refer to traditional WCS with a single RF chain as source-based modulation (SBM) [32]. MBM offers several advantages over SBM which include:

1. MBM can increase the number of received constellation points without an increase in

energy. In SBM, spectral efficiency is improved by employing high modulation order APM signals, and this method results in an exponential increase in transmit power to meet a target error performance. In contrast to SBM, MBM can increase the spectral efficiency of the system without affecting the transmit power of the antennas. Obtaining a target error rate in MBM does not require high energy consumption, as in the case of SBM systems, this results in better energy efficiency for MBM systems.

2. The spectral efficiency of MBM increases linearly with an increase in the number of RF mirrors employed in an MBM-TU, given that the fade realizations generated are independent.

3. The spectral efficiency of MBM is significantly increased by SBM modulation schemes that employ MIMO architecture. SBM schemes such as SIMO, GSM, QSM, and SM can be effectively combined with MBM to produce systems with much-improved error performance and/or spectral efficiency. [33, 35, 36]. Space-time modulation schemes such as uncoded space-time labeling diversity (USTLD), and space-time block coded-SM can also be combined with MBM, and the result is a vast improvement in error performance as compared to the original scheme [37–39].

4. When comparing MBM and SBM systems operating at the same spectral efficiency, MBM provides a significantly better error performance compared to SBM systems. This is due to the Euclidean distance between MBM constellation points of the random fade realizations remaining constant with an increase in spectral efficiency, whereas, the Euclidean distance in SBM techniques decreases with an increase in spectral efficiency. The advantage of MBM further increases for high-order constellations and a large number of receive antennas.

5. MBM has inherent diversity that can easily mitigate slow fading. As the constellation points in MBM correspond to different channel realizations, deep fades do not have a persistent effect, which gives constellation diversity. As the constellation size increases, this feature essentially converts a static multipath fading channel into a non-fading AWGN channel with the effective signal energy equal to the received energy averaged over fading statistics.

6. In MBM it is possible to improve energy saving through selecting a subset of channel configurations which result in a better overall performance for a given energy and spectral efficiency.

7. There is no fundamental restriction on the size of the MBM-TU.

In contrast to its appealing advantages listed above, the major drawbacks of the MBM scheme are given as follows:

1. The arrangement of the constellation points is random, and the constellation points are used with equal probability, while in SBM, constellation points can be uniformly arranged. This may lead to degradation due to the random placement of constellation points and also points with equal probability.

2. MBM comes with challenging design and practical implementation difficulties. First, the design of MBM-TU that can support a high number of sufficiently different radiation patterns is not a straightforward task as the number of RF mirrors that can be effectively turned ON/OFF may be limited in practice.

3. One of the main drawbacks of the MBM is that obtaining the channel state information (CSI) is a challenging task. There is excessive channel sounding as the receiver has to be trained with pilot signals from all possible N_m channel states. In the case of fast fading environments, channel estimation at the receiver becomes an even more challenging task.

4. There is a possibility of correlation between the fade realizations, which degrades performance.

5. Similar to all IM-based schemes, the performance of MBM is not satisfactory with a small number of receive antennas.

As seen from the advantages and disadvantages summarized above, while MBM provides a new degree of freedom for data transmission, it presents a new technology that can pioneer the advancement of next-generation wireless networks, although it comes with challenging design issues and practical concerns [32, 34].

1.6.7 Channel Coding: Convolutional Codes

The main objective of wireless communication is to retrieve a transmitted signal in the presence of a fading channel and noise at the receiver. The received signal is processed, and the decoder estimates the most likely transmitted signal with minimum error probability. The decoder makes either a hard decision or a soft decision to estimate the transmitted signal.

In hard decision detection, a firm estimate is made at the receiver on the incoming signal, and the decision provides a single bit of information at the decoder. When a signal is received, it is compared to a certain threshold, and anything above that threshold is decoded as binary

"1" otherwise it is binary "0", a maximum-likelihood (ML) detector is an example of such a decoder. In the case of soft-detection, the decoder uses additional data encoded at the transmitter to provide a more accurate estimate of the transmitted signal. Soft-detectors not only determine whether the incoming signal is binary "1" or "0" based on a threshold, but they also provide a lower probability of error in the decision. In practice, these additional bits are exploited by the soft-decision decoder along with forward error coding (FEC) algorithms to provide a net coding gain [40].

In hard decision decoding, a received codeword is compared with all the possible codewords, and the codeword that gives the minimum Hamming distance is selected as the estimated codeword. In soft-decision decoding, the received codeword is compared to all possible codewords, and the codeword that gives the minimum Euclidean distance is selected as the decoded codeword. Thus the soft-decision decoding improves the decision process by supplying additional reliability information, which can be calculated as Euclidean distance or a log-likelihood ratio (LLR). Soft-decision decoders provide a higher net gain than hard-decision decoders when operating at the same rate. Soft decision detectors coupled with a soft input demodulator are examples of FEC systems that recover data more effectively [41–43]. Soft decision decoders use all of the information in the process of decision making, whereas the hard-decision decoders do not fully employ the information available at the receiver.

1.7 Research Motivation

As new generations of WCS emerge, there is an increasing demand for significant improvements in data rates and error performance. MIMO systems still hold promise to achieve such improvements and are considered as one of the core techniques in improving error performance and spectral efficiency [1]. MIMO systems have the ability to gain higher diversity gain through exploiting space diversity. However, MIMO systems face the challenge of spatial correlation, which degrades the performance of MIMO and loss of diversity due to ICI. Physical limitations, such as IAS, also degrade the performance of MIMO systems [17].

On this note, researchers developed a new innovative MIMO scheme called SM [23, 25]. SM is a scheme that extends conventional MIMO to the spatial dimension. The spatial domain employs additional data to select a single active transmit antenna index during a transmission interval. As a result, SM completely mitigates ICI and IAS. Furthermore, relatively low-complexity receive algorithms can be employed, and only a single RF chain is required [22]. As SM became

more prominent, its drawbacks became more apparent. The limitation of SM is that there is a logarithmic relationship between the number of transmit antenna and the spectral efficiency of the scheme. A vast number of transmit antennas are required to gain a substantial increase in spectral efficiency [23]. As a result, several SM-based schemes have been introduced in the literature, which enhance the spectral efficiency of SM.

QSM is a scheme that effectively increases the number of active transmit antenna indices employed in SM [29]. As a consequence, additional information bits are used to select two transmit antenna indices, therefore, increasing the spectral efficiency of SM. Significant improvement error performance is demonstrated when QSM is compared to SM. Since QSM decomposes an AMP symbol into its real and imaginary components, ICI is eliminated [29].

The general progression in the research of SM-based techniques yielded another type of scheme based on QSM called DSM [30]. DSM is proposed as a high rate data transmission scheme that aimed at increasing the spectral efficiency of QSM. DSM employs two independent SM channels that simultaneously transmits two AMP symbols on two active transmit antennas in a transmission interval. Although DSM does not enjoy the same ICI and IAS advantages as QSM, the error performance of DSM is better that QSM at the same spectral efficiency [30].

MBM with RF mirrors is a recently proposed wireless communication scheme that has attracted much research attention [32]. The investigations in [33] show that it is indeed possible and desirable to combine MBM with SBM schemes to achieve improved error performance and spectral efficiency. Modulation techniques such as SM, QSM, GSM, and space-time modulation techniques such as space-time block codes and USTLD have successfully combined with MBM to yield MBM-based schemes with superior data rates and error performance as compared to their natural SBM counterpart [33,35,38,39]. Evidence shows that MBM schemes coupled with MIMO techniques have much potential to be one of the leading technologies in next-generation wireless communications which can support demanding applications, such as IoT systems, enterprise software and cloud computing [10]. In light of this emerging technology, the motivation of this dissertation is to introduce a new MBM-based transmission scheme modeled after DSM. The motivation for this research stems from the fact that the SBM scheme DSM has a better error performance than QSM, and it has the potential to perform better than QSM at a higher spectral efficiency [30]. Therefore, the expectation is that the proposed scheme, DSMBM, has improved performance as compared to one of the benchmark schemes, quadrature spatial media-

based modulation (QSMBM) [35].

It is also desired that communication systems provide users with high data rates, in addition to ensuring reliability and power efficiency. In practice, the majority of wireless communications employ FEC to enhance information reliability in noisy channels. It has been demonstrated that soft-output detection coupled with soft-input channel decoding results in a significant net coding gain compared to the conventional hard-decision detection. Soft-output ML detectors (SOMLDs) for systems such as SM, QSM, and GSM have been presented in literature. Under coded conditions, significant improvement in error performance was demonstrated as compared to the hard-decision ML detectors (HDMLDs). Therefore, in this dissertation, the motivation is to further introduce SOMLD for DSM and DSMBM, which has not been presented in literature.

1.8 Research Objectives

Based on the motivation presented, the objectives of this dissertation are summarized as follows:

1. To improve the error performance of DSM, we propose an MBM scheme with RF mirrors based on DSM, hence the term DSMBM.
2. Formulation of the average bit error probability (ABEP) for DSMBM.
3. To achieve additional coding gain, we develop a SOMLD for DSM system.
4. To achieve additional coding gain, we develop a SOMLD for DSMBM system.

1.9 Overview of Dissertation Structure

In the previous sections of Chapter 1, we had a brief outlook on the evolution of WCS. Discussions are made on diversity, and we introduced MIMO systems and various other modulation techniques that improve wireless communication. MBM was discussed as a potential key modulation technique that can pioneer next-generation wireless technology. Our research motivation and objectives are stated in Section 1.6 and Section 1.7, respectively.

In Chapter 2, we present a detailed description of the SM scheme, which includes the SM system model, SM detection, and the performance analysis of SM. Monte Carlo simulation results are presented, which serve to validate the theoretical analysis of SM.

Chapter 3 is dedicated to the present QSM scheme. We discuss the system model, detection scheme, and performance analysis of QSM. Simulation results are presented to validate the theoretical analysis of QSM, and the error performance of QSM and SM systems are presented.

Chapter 4 discusses the base modulation scheme for this dissertation, DSM. We present the system model, detection scheme and performance analysis of DSM. The SOMLD for DSM is proposed. Simulation results are presented to validate the analytical performance and the proposed SOMLD.

Chapter 5 discusses MBM. The purpose of this chapter is to demonstrate how MBM improves SBM systems. We discuss the system model, detection scheme, and performance analysis for SIMO-MBM. Monte Carlo simulation results are presented, which serve to validate the theoretical analysis of SIMO-MBM.

In Chapter 6, we propose the MBM-based system DSMBM. We discuss the system model, detection scheme, and present the analytical performance of DSMBM. We further propose the SOMLD detector for DSMBM. Monte Carlo simulation results are presented to validate the theoretical analysis and the proposed SOMLD.

Finally, Chapter 7 concludes the achievements and key results presented in the dissertation and outlines possible future work.

1.10 Notation used in the Dissertation

Bold italics lower and upper case symbols denote column vectors and matrices, respectively, while regular letters represent scalar quantities. We use $(\cdot)^T$ for transpose, $|\cdot|$ for Euclidean norm, $\|\cdot\|_F$ for Frobenius norm, $(\cdot)!$ for factorial, and $E\{\cdot\}$ denotes the statistical expectation operator. $Q(\cdot)$ represents Gaussian Q-function, $\Gamma(\cdot)$ represents the gamma function, $\Re\{\cdot\}$ is the real part of a complex number, while $\Im\{\cdot\}$ is the imaginary part of a complex number. $\underset{w}{\text{argmin}}(\cdot)$ represents the minimum value of an argument with respect to w, and $(:)$ represents the binomial coefficient.

Chapter 2

Spatial Modulation

2.1 Introduction

In recent years of wireless communication development, MIMO systems have received increased research attention due to the potential that they possess to achieve networks with improved data rate and error performance [17]. MIMO systems transmit data in parallel streams, which are modulated by individual transmit antennas. During transmission, the data streams are received by multiple receive antennas, which are regarded as individual channels in the MIMO system [1]. These multiple channels give MIMO systems the ability to exploit spatial diversity at the transmitter and receiver [17]. Spatial diversity increases transmission range, data capacity, and improves the robustness of MIMO systems; as a result, MIMO systems have become increasingly beneficial to wireless communications [19, 22].

There are several challenges that MIMO systems need to overcome in order to maximize their potential. Due to the simultaneous transmission of data in MIMO systems, IAS is required between the transmit antennas, ICI at the receiver has to be mitigated; otherwise, there is loss of diversity, and MIMO systems employ relatively high-complexity receive algorithms [17, 18]. Several schemes have been investigated that mitigate the disadvantages of MIMO systems while exploiting its advantages [21]. The most popular scheme which offers an excellent method to exploit spatial multiplexing is SM, proposed by Mesleh *et al.* [23].

The innovative idea of SM is that it extends the conventional MIMO system to a third domain, the spatial dimension. The spatial domain employs additional information bits to select a single active transmit antenna index as a means to convey information. Note that the inactive transmit antennas have zero power during each transmission interval. As a result, SM mitigates

IAS at the transmitter, ICI at the receiver, and since a single RF chain is employed, relatively low-complexity receiver algorithms are utilized [25].

Based on its merits, SM provides a good candidate for the next generation of wireless communication. In this chapter, we present the system model, detection scheme, and the analytical error performance of SM. Monte Carlo simulations are presented, which serve to validate the analytical performance of SM.

2.2 System model for SM

Figure 2.1 illustrates an example of an SM system model with N_T and N_R representing the number of transmit antennas and receive antennas, respectively.

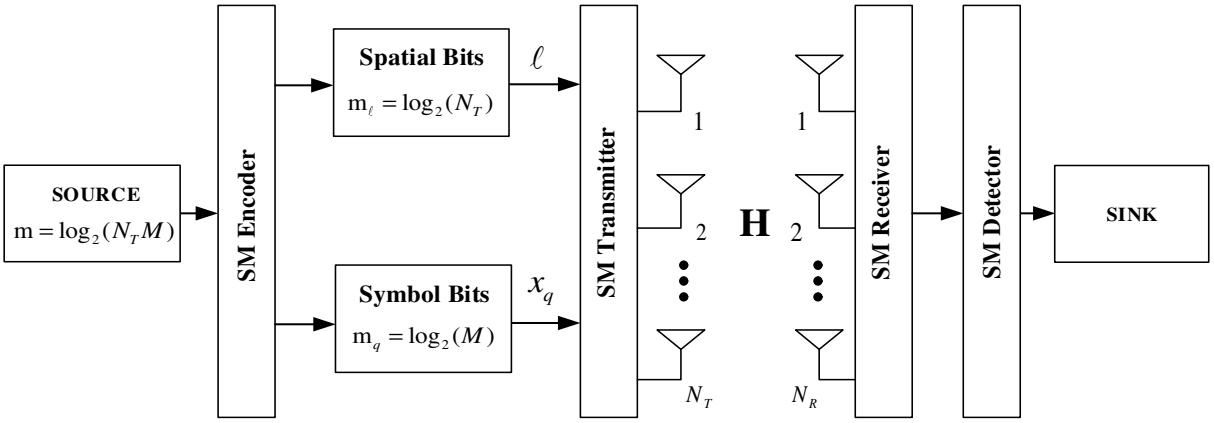

Figure 2.1: System Model for the SM scheme

In each transmission interval, the source provides an input bit vector of length $\mathrm{m} = \log_2(N_T M)$ bits, where M is the modulation order of the APM signal, into the SM encoder. The SM encoder divides the information into two parts. The first part is mapped such that $\mathrm{m}_\ell = \log_2 N_T$ bits are used to select a single transmit antenna index ℓ, $\ell \in [1 : N_T]$, while the second part is mapped such that $\mathrm{m}_q = \log_2 M$ bits are used to determine an APM constellation symbol x_q, $q \in [1 : M]$, to convey information. The APM symbols can either quadrature amplitude modulation (QAM) or phase-shift keying (PSK) modulated symbols. The spectral efficiency of SM is given as [25]:

$$\eta_{SM} = \log_2 M + \log_2 N_T \quad \text{b/s/Hz}. \tag{2.1}$$

The output of the SM transmitter is expressed as an $N_T \times 1$ transmission vector as:

$$\mathbf{x}_{q\ell} = \underset{\substack{\uparrow \\ 1^{st} \text{ position}}}{\begin{bmatrix} 0 \end}} \quad \underset{}{0} \quad \cdots \quad \underset{\substack{\downarrow \\ \ell^{th} \text{ position}}}{x_q} \quad \cdots \quad \underset{\substack{\uparrow \\ N_T^{th} \text{ position}}}{0 \end{bmatrix}^T}, \tag{2.2}$$

where $x_q,\ q \in [1 : M]$, represents the q^{th} symbol from the M-QAM/ M-PSK signal constellation with $E\{|x_q|^2\} = 1,$ and $\ell,\ \ell \in [1 : N_T]$, represents the active transmit antenna index.

In SM, only a single transmit antenna is active during a transmission interval; therefore, the transmission vector in (2.2) consists of $N_T - 1$ zero elements which corresponds to the inactive antennas, while the single non-zero element x_q at the ℓ^{th} position which correspond to the active transmit antenna index. Table 2.1 shows the Gray-coded constellation points used by 4-QAM. The example illustrated in Table 2.2 demonstrates the mapping procedure for a 4×4 Gray-coded 4-QAM SM transmission. In this example, we demonstrate the mapping procedure of SM with a spectral efficiency of 4 b/s/Hz, and we consider all possible constellation points.

Table 2.1: Gray-coded constellation for 4-QAM

Symbol Bits	M-**QAM Symbol**
[0 0]	$1 + i$
[0 1]	$-1 + i$
[1 0]	$-1 - i$
[1 1]	$1 - i$

Table 2.2: Illustration of the mapping procedure for SM

Index ℓ	**Source Bits** m	**Transmission Vector** $\mathbf{x}_{q\ell}$	**Index** ℓ	**Source Bits** m	**Transmission Vector** $\mathbf{x}_{q\ell}$
1	0 0 0 0	$\begin{bmatrix} 1+i & 0 & 0 & 0 \end{bmatrix}^T$	3	1 0 0 0	$\begin{bmatrix} 0 & 0 & 1+i & 0 \end{bmatrix}^T$
	0 0 0 1	$\begin{bmatrix} -1+i & 0 & 0 & 0 \end{bmatrix}^T$		1 0 0 1	$\begin{bmatrix} 0 & 0 & -1+i & 0 \end{bmatrix}^T$
	0 0 1 0	$\begin{bmatrix} -1-i & 0 & 0 & 0 \end{bmatrix}^T$		1 0 1 0	$\begin{bmatrix} 0 & 0 & -1-i & 0 \end{bmatrix}^T$
	0 0 1 1	$\begin{bmatrix} 1-i & 0 & 0 & 0 \end{bmatrix}^T$		1 0 1 1	$\begin{bmatrix} 0 & 0 & 1-i & 0 \end{bmatrix}^T$
2	0 1 0 0	$\begin{bmatrix} 0 & 1+i & 0 & 0 \end{bmatrix}^T$	4	1 1 0 0	$\begin{bmatrix} 0 & 0 & 0 & 1+i \end{bmatrix}^T$
	0 1 0 1	$\begin{bmatrix} 0 & -1+i & 0 & 0 \end{bmatrix}^T$		1 1 0 1	$\begin{bmatrix} 0 & 0 & 0 & -1+i \end{bmatrix}^T$
	0 1 1 0	$\begin{bmatrix} 0 & -1-i & 0 & 0 \end{bmatrix}^T$		1 1 1 0	$\begin{bmatrix} 0 & 0 & 0 & -1-i \end{bmatrix}^T$
	0 1 1 1	$\begin{bmatrix} 0 & 1-i & 0 & 0 \end{bmatrix}^T$		1 1 1 1	$\begin{bmatrix} 0 & 0 & 0 & 1-i \end{bmatrix}^T$

The source bits m, are mapped to the transmission vector $\mathbf{x}_{q\ell}$, which is transmitted over a Rayleigh frequency-flat fading channel $\mathbf{H}$ of dimension $N_R \times N_T$ in the presence of AWGN. AWGN is represented by vector $\mathbf{n}$ of dimension $N_R \times 1$. All elements of $\mathbf{H}$ and $\mathbf{n}$ are assumed to be i.i.d. entries with Gaussian distribution of zero mean and unit variance $\sim CN(0,1)$. The received signal is given by an $N_R \times 1$ vector $\boldsymbol{y}$ defined as [25]:

$$\boldsymbol{y} = \sqrt{\rho}\mathbf{H}\mathbf{x}_{q\ell} + \mathbf{n}\ , \tag{2.3}$$

where ρ is the average SNR at each receive antenna and the channel matrix $\mathbf{H}$ can be defined as:

$$\mathbf{H} = \begin{bmatrix} h_{1,1} & \cdots & h_{1,N_T} \\ \vdots & \ddots & \vdots \\ h_{N_R,1} & \cdots & h_{N_R,N_T} \end{bmatrix}, \tag{2.4}$$

where $h_{k,\ell}$ is the channel fading coefficient between the k^{th} receive antenna, $k \in [1 : N_R]$, and ℓ^{th} transmit antenna, $\ell \in [1 : N_T]$. Assuming the ℓ^{th} antenna is used in transmission, the received signal in (2.3) can be represented as:

$$\boldsymbol{y} = \sqrt{\rho}\mathbf{h}_\ell x_q + \mathbf{n}\ , \tag{2.5}$$

where $\mathbf{h}_\ell$ represents the ℓ^{th} column of the fading channel gain matrix $\mathbf{H}$.

2.3 SM Detection

In the detection of SM, we assume that perfect CSI is known at the SM receiver in all instances. The SM detector estimates the transmitted signal via an exhaustive ML search where all the possible antenna indices and signal constellation points are calculated. The detector selects the ML calculation with the minimum argument as the estimated received signal of the transmitted information. The ML detector for SM is given as [44]:

$$[\hat{\ell}, \hat{x}_q] = \underset{\substack{\ell \in [1:N_T] \\ q \in [1:M]}}{\operatorname{argmin}} \left(\|\boldsymbol{y} - \sqrt{\rho}\boldsymbol{h}_\ell x_q\|_F^2 \right). \tag{2.6}$$

If we let $\boldsymbol{g}_{q\ell} = \sqrt{\rho}\boldsymbol{h}_\ell \mathbf{x}_{q\ell}$, and expand the Frobenius norm in (2.6), then the ML detector can be simplified to yield:

$$[\hat{\ell}, \hat{x}_q] = \underset{\substack{\ell \in [1:N_T] \\ q \in [1:M]}}{\operatorname{argmin}} \left\{ \|\boldsymbol{g}_{q\ell}\|_F^2 - 2\Re\{\boldsymbol{y}^H \boldsymbol{g}_{q\ell}\} \right\}. \tag{2.7}$$

Note, the expression in (2.7) is the optimal ML detector for the SM scheme.

2.4 Performance Analysis of SM

In this section, the analytical lower bound performance analysis approach is used to calculate the ABEP for SM. Naidoo *et al.* in [25] proposed that the symbol error probability and antenna error probability for SM can be evaluated independently. Therefore, the lower bound analytical performance evaluates an ABEP that is given as a combination of the symbol error probability and antenna error probability [23, 25]:

$$P_e \geq P_a + P_b - P_a P_b \,, \tag{2.8}$$

where P_e is the ABEP, P_a is the bit error probability of the antenna index considering that the symbol is perfectly detected, while P_b is the bit error probability of the estimated symbol considering that the antenna index is perfectly detected [25, 44].

2.4.1 Performance Analysis for Symbol Estimation

The bit error probability for the transmit symbol is evaluated from the symbol error rate (SER) [25]. The SER for M-QAM over i.i.d. Rayleigh frequency-flat fading channel is given as [23, 25]:

$$\text{SER} = \frac{a}{c}\left[\frac{1}{2}\left(\frac{2}{b\rho+2}\right)^{N_R} - \frac{a}{2}\left(\frac{1}{b\rho+1}\right)^{N_R} + (1-a)\sum_{i=1}^{c-1}\left(\frac{\beta_i}{b\rho+\beta_i}\right)^{N_R} + \sum_{i=c}^{2c-1}\left(\frac{\beta_i}{b\rho+\beta_i}\right)^{N_R}\right], \tag{2.9}$$

where $a = 1 - \frac{1}{\sqrt{M}}$, $b = \frac{3}{M-1}$, $\beta_i = 2\sin^2\theta_i$, $\theta_i = \frac{i\pi}{4c}$, and c is the number of iterations of convergence, $c = 10$. The BER at high SNR can be approximated from the SER as:

$$P_b \cong \frac{\text{SER}}{n}, \tag{2.10}$$

where $n = \log_2 M$.

2.4.2 Analytical BER of Transmit Antenna Index Estimation

The bit error probability of the transmit antenna is computed in a similar manner presented in [25]. Given that the transmit symbol is decoded perfectly, the average BER of the transmit antenna is calculated using the union bounded approach and is given as [25]:

$$P_a \leq \sum_{q=1}^{M}\sum_{\ell=1}^{N_T}\sum_{\hat{\ell}=1}^{N_T}\frac{N(\ell,\hat{\ell})P(\mathbf{x}_{q\ell}\rightarrow\mathbf{x}_{q\hat{\ell}})}{MN_T}\,, \tag{2.11}$$

where $P(\mathbf{x}_{q\ell}\rightarrow\mathbf{x}_{q\hat{\ell}})$ is the pairwise error probability (PEP) of selecting $\mathbf{x}_{q\hat{\ell}}$ given that $\mathbf{x}_{q\ell}$ was transmitted, and $N(\ell,\hat{\ell})$ is the number of bit errors between the transmit antenna index ℓ and the estimated transmit antenna index $\hat{\ell}$. The conditional PEP of the channel is given as [25]:

$$P(\mathbf{x}_{q\ell}\rightarrow\mathbf{x}_{q\hat{\ell}}|\mathbf{H}) = P(\|\boldsymbol{y}-\sqrt{\rho}\mathbf{h}_{\hat{\ell}}x_q\|_F < \|\boldsymbol{y}-\sqrt{\rho}\mathbf{h}_{\ell}x_q\|_F) = Q(\sqrt{k}), \tag{2.12}$$

where k is a central chi-squared RV with $2N_R$ degrees of freedom and is defined as:

$$k = \frac{\rho}{2}\|(\mathbf{h}_{\ell}x_q - \mathbf{h}_{\hat{\ell}}x_q)\|_F^2 = \sum_{n=1}^{2N_R}\alpha_n^2, \tag{2.13}$$

where $\alpha_n \sim N(0,\sigma_\alpha^2)$ and the variance $\sigma_\alpha^2 = \frac{\rho}{2}|x_q|^2$. The PDF of k is defined as [25]:

$$p_k(\upsilon) = \frac{\upsilon^{N_R-1}e^{\frac{-\upsilon}{2\sigma_\alpha^2}}}{\left(2\sigma_\alpha^2\right)^{N_R}\Gamma\left(N_R\right)} \quad,\ \upsilon \geq 0. \tag{2.14}$$

Since the distribution of k is known, the PEP in (2.11) is calculated as [25]:

$$P(\mathbf{x}_{q\ell} \to \mathbf{x}_{q\hat{\ell}}) = \int_{\upsilon=0}^{\infty} Q(\sqrt{\upsilon}) p_k(\upsilon) \mathrm{d}\upsilon. \tag{2.15}$$

The closed-form representation for (2.15) is given as [25]:

$$P(\boldsymbol{x}_{q\ell} \to \boldsymbol{x}_{q\hat{\ell}}) = \mu_\alpha^{N_R} \sum_{k=0}^{N_R-1} \binom{N_R - 1 + k}{k} [1 - \mu_\alpha]^k, \tag{2.16}$$

where $\mu_\alpha = \frac{1}{2}\left(1 - \sqrt{\frac{\sigma_\alpha^2}{\sigma_\alpha^2+1}}\right)$.

2.5 Numerical Analysis of the Analytical and Simulated BER Performance of SM

In this section, the ABEP for SM formulated using the analytical lower bound approach is presented. Monte Carlo simulation results are executed in a Matlab environment, and are presented to validate the analytical result in Section 2.4. All Monte Carlo simulations are performed over i.i.d. Rayleigh frequency-flat fading channels in the presence of AWGN, and Gray-coded M-QAM signal constellations are employed. It is assumed that complete CSI is known at the receiver in all instances.

Monte Carlo simulations for SM with spectral efficiencies of η_{SM} = 4, 5, 6, 7 and 8 b/s/Hz are presented in graphs of average BER versus SNR. The notation used to denote an $N_T \times N_R$ SM system with an APM modulation order of M is (N_T, N_R, M, η_{SM}).

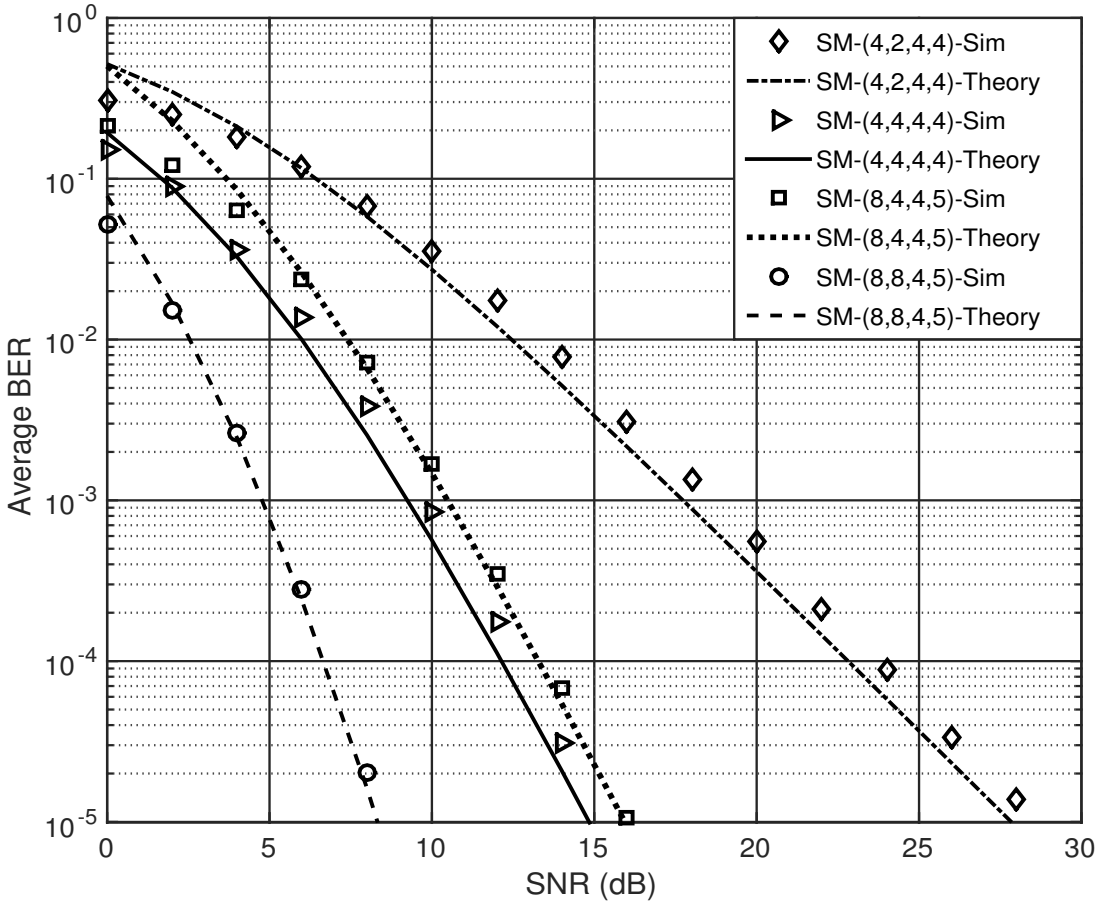

Figure 2.2: Theoretical and simulated BER performance of SM for $\eta_{SM} = 4$, 5 b/s/Hz.

In Figure 2.2, the analytical and Monte Carlo simulation results for $4 \times 2,\ 4 \times 4,\ 8 \times 4,$ and 8×8 SM systems with spectral efficiencies of $\eta_{SM} = 4$ and 5 b/s/Hz are presented. The Monte Carlo BER performance is relatively tight and matches the analytical BER performance, therefore, verifying the theoretical performance of SM. An investigation of the results shows that the BER performance of SM improves with an increase in the number of receive antennas for systems with the same spectral efficiency. At a BER of 10^{-5}, 4×4 4-QAM SM has an SNR gain of 12.5 dB over 4×2 4-QAM SM, and at a BER of 10^{-5}, 8×8 4-QAM SM has an SNR gain of 7.4 dB over 8×4 4-QAM SM.

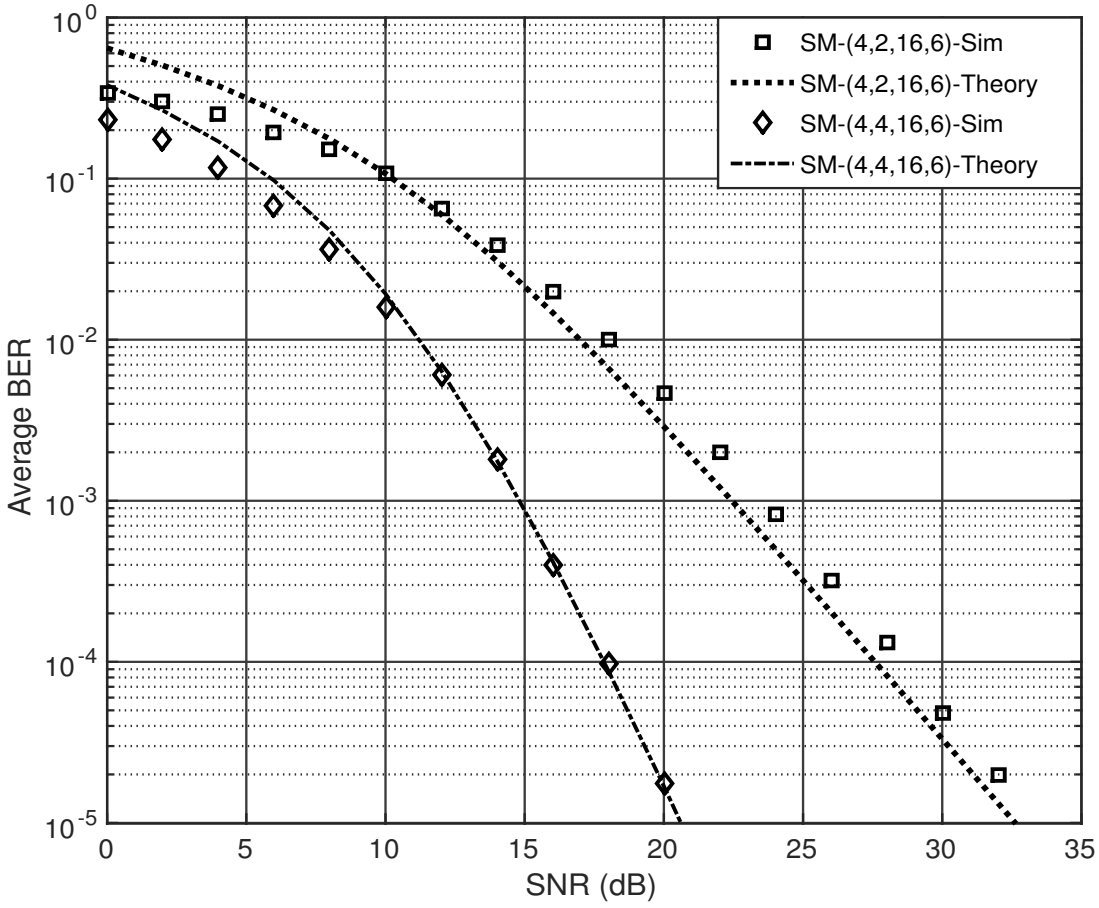

Figure 2.3: Theoretical and simulated BER performance of SM for $\eta_{SM} = 6$ b/s/Hz.

In Figure 2.3, the analytical and Monte Carlo simulation results for 4×2 and 4×4 SM systems with spectral efficiency of $\eta_{SM} = 6$ b/s/Hz are presented. An investigation of the results shows that the BER performance of SM improves with an increase in the number of receive antennas for systems with the same spectral efficiency. At a BER of 10^{-5}, 4×4 16-QAM SM has an SNR gain of 12.8 dB over 4×2 16-QAM SM. The Monte Carlo simulation results validate the analytical performance of SM as it is demonstrated that the analytical results are closely matched by the simulation result.

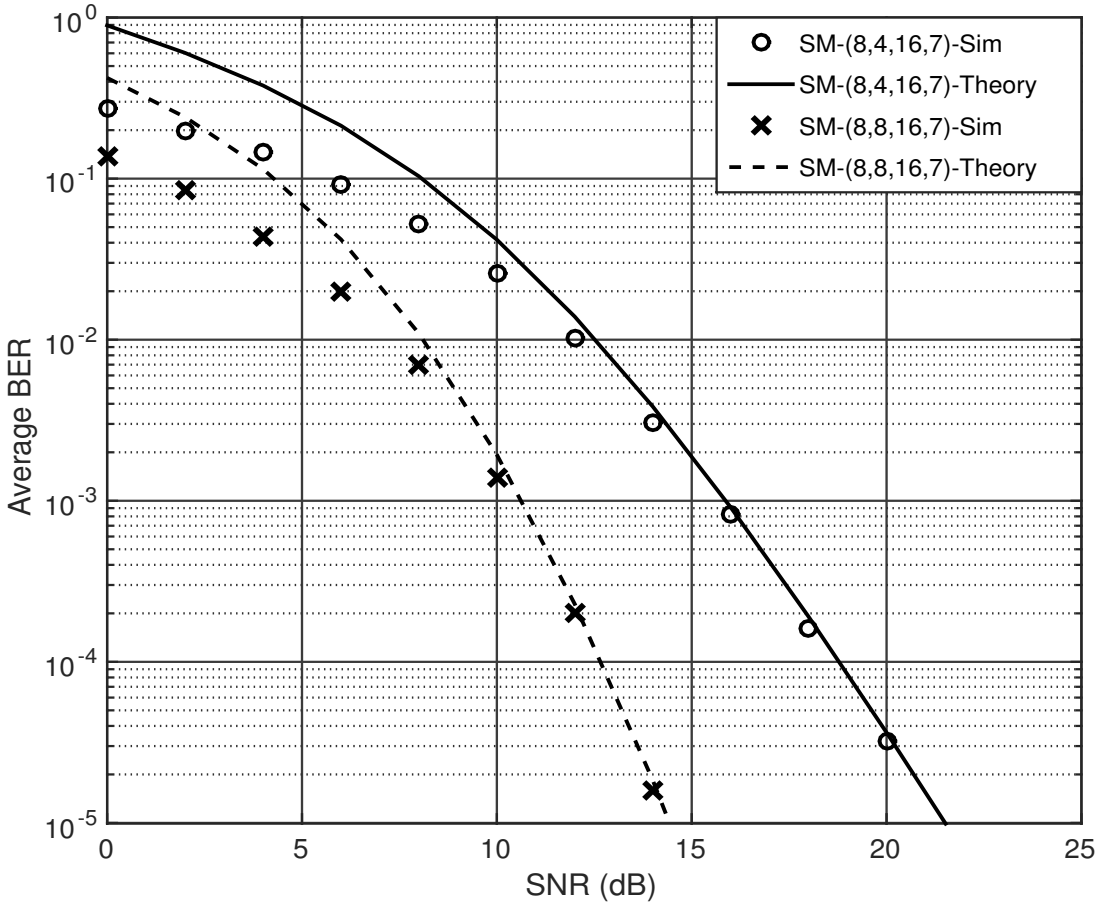

Figure 2.4: Theoretical and simulated BER performance of SM for $\eta_{SM} = 7$ b/s/Hz.

In Figure 2.4, the analytical and Monte Carlo simulation results for 8×4 and 8×8 SM systems with spectral efficiency of $\eta_{SM} = 7$ b/s/Hz are presented. Analysis of the BER performance of SM shows that an increase in the number of receive antennas improves the error performance. At a BER of 10^{-5}, 8×8 16-QAM SM has an SNR gain of 7.1 dB over 8×4 16-QAM SM. The Monte Carlo simulations are consistent with the analytical error performance showing a relatively tight match, validating the theoretical performance of SM.

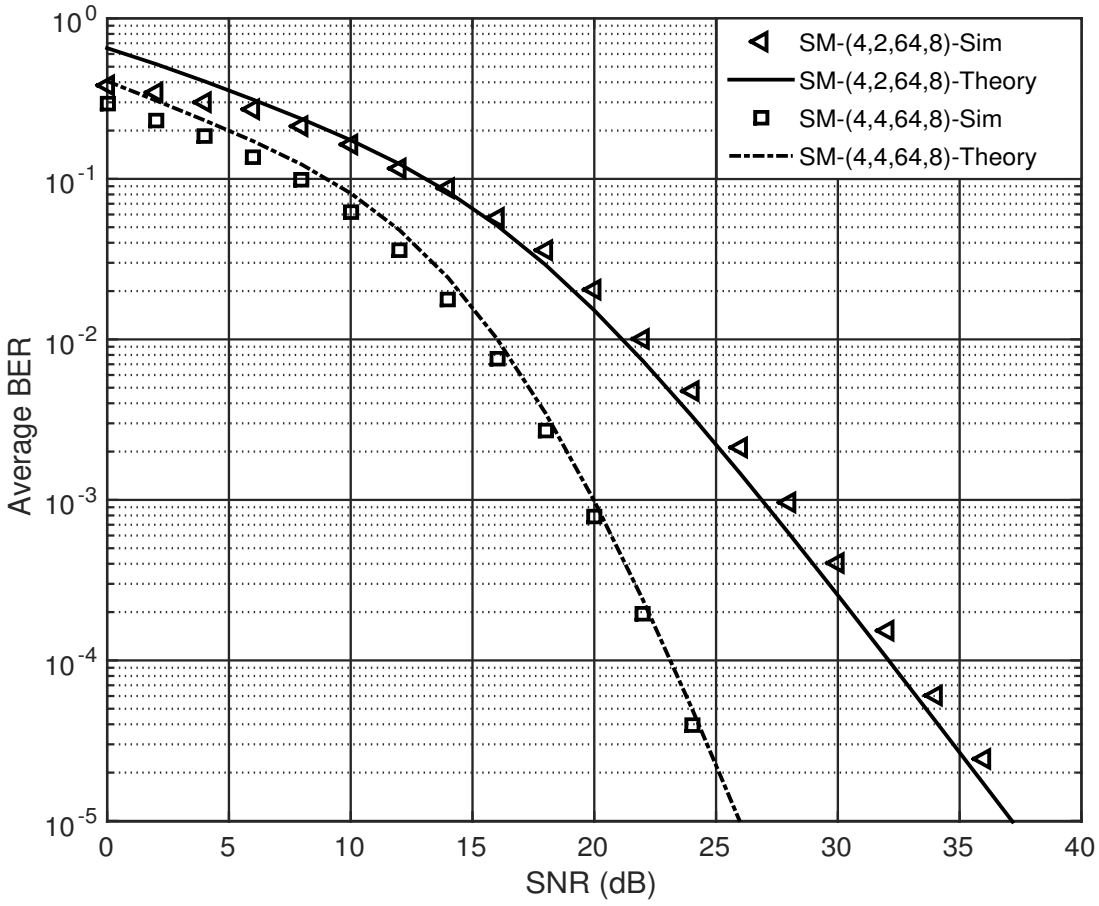

Figure 2.5: Theoretical and simulated BER performance of SM for $\eta_{SM} = 8$ b/s/Hz.

In Figure 2.5, the analytical and Monte Carlo simulation results for 4×2 and 4×4 SM systems with spectral efficiency of $\eta_{SM} = 8$ b/s/Hz are presented. At a BER of 10^{-5}, 4×4 64-QAM SM has an SNR gain of 12.1 dB over 4×2 64-QAM SM. The simulation results validate the theoretical analysis as the performance of the SM closely matches the theoretical result.

2.6 Summary

The performance analysis for SM employing the lower bound approach to calculate the average BER performance over i.i.d. Rayleigh frequency-flat fading channels was presented. Monte Carlo simulations were presented, and the analytical results were relatively tight with the simulated BER, therefore validating the theoretical performance of SM.

Chapter 3

Quadrature Spatial Modulation

3.1 Introduction

MIMO systems have shown much promise with regards to the potential of achieving networks with increased data rates, and improved error performance [1]. However, MIMO systems face challenges on a physical level, such as the need for IAS at the transmit antenna array and reduction of ICI at the receive antennas [17,18]. SM proposed by Mesleh *et al.* [23,25] has emerged in the last few decades as a technique that extends the conventional MIMO to the spatial dimension. SM utilizes both the signal constellation in the form of an APM symbol and the spatial dimension in which an index is used to select a single active transmit antenna as a means to convey information.

SM provides an innovative method of exploiting spatial diversity while mitigating the adverse effects of MIMO, such as ICI and IAS. However, SM does not have the benefit of transmit diversity since only a single transmit antenna is active during a transmission interval, and SM cannot substantially increase data rate due to the logarithmic relationship between the number of transmit antennas and the spectral efficiency [25]. This drawback on spectral efficiency has motivated researchers to introduce an SM-based scheme that enhances the spectral efficiency of conventional SM called QSM [29].

QSM employs an additional active transmit antenna index to SM to enhance the spectral efficiency of the system. The APM symbol in QSM is decomposed into its constituent real and imaginary components, which are subsequently transmitted via the two active transmit antenna indices in the spatial domain. QSM effectively increases the number of active transmit antenna during a transmission interval, therefore, directly increasing the spectral efficiency of the SM-

based technique. Since the real and imaginary components are transmitted via orthogonal sine and cosine carriers, respectively, QSM remains ICI free [29].

QSM has a single RF chain that allows the scheme to have a relatively low-complexity receive algorithm. Significant improvement in terms of BER is demonstrated by QSM when compared to SM of the same spectral efficiency [29]. In this chapter, we present the system model, detection scheme, and the analytical error performance of QSM. Monte Carlo simulation results are presented, which serve to validate the analytical performance of QSM, and the BER performance of SM and QSM are presented.

3.2 System model for QSM

Figure 3.1 illustrates an example of a QSM system model with N_T and N_R representing the number of transmit antennas and receive antennas, respectively.

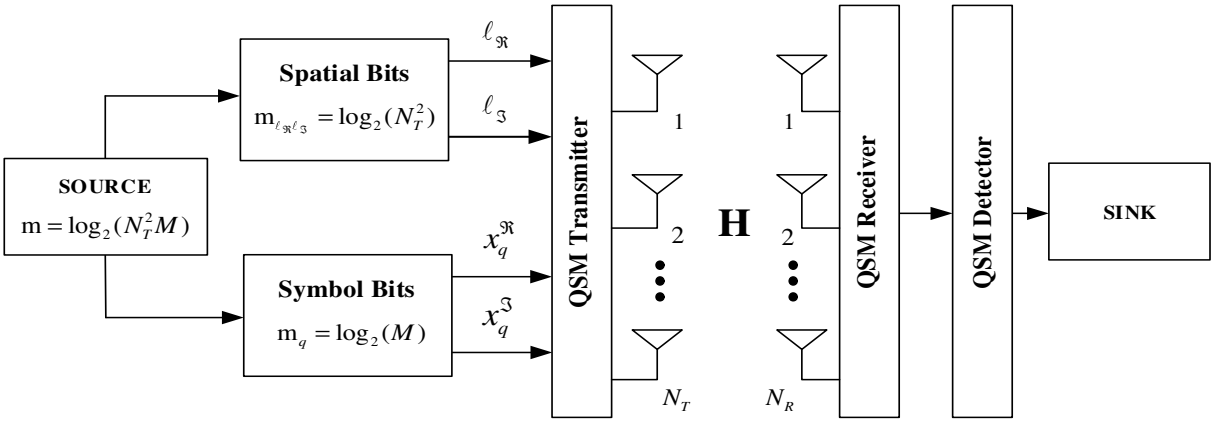

Figure 3.1: System model for the QSM scheme

In each transmission interval, the source provides an input vector of length $\mathrm{m} = \log_2(N_T^2 M)$ bits, where M is the modulation order of the APM signal. The source bits are divided into two parts. The first $\mathrm{m}_{\ell_\Re \ell_\Im} = \log_2(N_T^2)$ bits are mapped to select two transmit antenna indices $\ell_\Re$ and $\ell_\Im$, $\ell_\Re, \ell_\Im \in [1 : N_T]$, while the remaining $\mathrm{m}_q = \log_2(M)$ bits are used to determine an M-QAM symbol $x_q = x_q^\Re + i x_q^\Im$, $q \in [1 : M]$. The M-QAM symbol is split into its constituent real and imaginary parts, and these are transmitted via transmit antennas with index $\ell_\Re$ and $\ell_\Im$ in each transmission interval, respectively. The spectral efficiency of QSM is given as [29]:

$$\eta_{QSM} = \log_2 M + 2\log_2 N_T \quad \text{b/s/Hz.} \tag{3.1}$$

The output of the QSM transmitter is an $N_T \times 1$ vector given as:

$$\mathbf{x}_{q\ell_{\Re}\ell_{\Im}} = \begin{matrix} & & \ell_{\Re}^{th} \text{ position} & \ell_{\Im}^{th} \text{ position} & \\ & & \downarrow & \downarrow & \\ \big[\, 0 & \cdots & x_q^{\Re} & ix_q^{\Im} & \cdots \; 0 \,\big]^T, \\ & \uparrow & & & \uparrow \\ & 1^{st} \text{ position} & & & N_T^{th} \text{ position} \end{matrix} \tag{3.2}$$

where $x_q^{\Re}$ and $x_q^{\Im}$ represent the real and imaginary parts of the q^{th} symbol from an M-QAM signal constellation with $E\{|x_q^{\Re}|^2\} = E\{|x_q^{\Im}|^2\} = 1$, and $\ell_{\Re}$ and $\ell_{\Im}$ represent the real and imaginary transmit antenna indices, respectively.

Note in QSM; it is possible to have the real and imaginary transmit antenna indices $\ell_{\Re}$ and $\ell_{\Im}$ mapped to the same transmit antenna index. In that case, QSM is modeled after SM where the modulated symbol is given by $x_q = x_q^{\Re} + ix_q^{\Im}$ with $E\{|x_q|^2\} = 1$, and we denote the index when $\ell_{\Re} = \ell_{\Im}$ as ℓ, $\ell \in [1 : N_T]$. The example illustrated in Table 3.1 demonstrates the mapping procedure of 4×4 Gray-coded 4-QAM QSM with a spectral efficiency of 6 b/s/Hz, only a few random data streams are considered.

Table 3.1: Illustration of the mapping procedure for QSM

Source Bits	**Transmit Antenna Pairs**		**Symbols Bits**	**Transmit Vector**
$\mathrm{m} = \log_2(N_T^2 M)$	$\ell_{\Re}$	$\ell_{\Im}$	$\mathrm{m}_q = \log_2(M)$	$\mathbf{x}_{q\ell_{\Re}\ell_{\Im}}$
[0 0 1 0 0 0]	[0 0] = 1	[1 0] = 3	[0 0] = $1+i$	[1 0 $+i$ 0]^T
[0 1 1 1 0 1]	[0 1] = 2	[1 1] = 4	[0 1] = $-1+i$	[0 -1 0 $+i$]^T
[1 0 1 0 1 1]	[1 0] = 3	[1 0] = 3	[1 1] = $1-i$	[0 0 $1-i$ 0]^T
[1 1 0 0 1 0]	[1 1] = 4	[0 0] = 1	[1 0] = $-1-i$	[$-i$ 0 0 -1]^T
[0 1 0 1 0 0]	[0 1] = 2	[0 1] = 2	[0 0] = $1+i$	[0 $1+i$ 0 0]^T
[1 1 1 0 1 0]	[1 1] = 4	[1 0] = 3	[1 0] = $-1-i$	[0 0 $-i$ -1]^T
[0 0 1 1 1 1]	[0 0] = 1	[1 1] = 4	[1 1] = $1-i$	[1 0 0 $-i$]^T
[1 0 0 0 0 1]	[1 0] = 3	[0 0] = 1	[0 1] = $-1+i$	[$+i$ 0 -1 0]^T

The source bits m are mapped to the transmission vector $\mathbf{x}_{q\ell_{\Re}\ell_{\Im}}$ and are transmitted over a Rayleigh frequency-flat fading channel $\mathbf{H}$ of dimension $N_R \times N_T$ in the presence of AWGN. AWGN is represented by vector $\mathbf{n}$ of dimension $N_R \times 1$. All elements of $\mathbf{H}$ and $\mathbf{n}$ are assumed

to be i.i.d. entries with Gaussian distribution of zero mean and unit variance $\sim CN(0,1)$. The received signal is given by an $N_R \times 1$ vector $\boldsymbol{y}$ given as [29]:

$$\boldsymbol{y} = \sqrt{\rho}\mathbf{H}\mathbf{x}_{q\ell_{\Re}\ell_{\Im}} + \mathbf{n}, \tag{3.3}$$

where ρ is the average SNR at each receive antenna. The fading channel gain matrix $\mathbf{H}$ is defined as:

$$\mathbf{H} = \begin{bmatrix} h_{1,1} & \cdots & h_{1,N_T} \\ \vdots & \ddots & \vdots \\ h_{N_R,1} & \cdots & h_{N_R,N_T} \end{bmatrix}, \tag{3.4}$$

where $h_{k,\ell}$ is the channel fading coefficient between the k^{th} receive antenna, $k \in [1 : N_R]$, and ℓ^{th} transmit antenna, $\ell \in [1 : N_T]$. Assuming that the $\ell_{\Re}^{th}$ and $\ell_{\Im}^{th}$ antennas are used in the transmission of the real and imaginary parts of the symbol, respectively, the received signal in (3.3) can be further expressed as [29]:

$$\boldsymbol{y} = \sqrt{\rho}\big(\mathbf{h}_{\ell_{\Re}} x_q^{\Re} + j\mathbf{h}_{\ell_{\Im}} x_q^{\Im}\big) + \mathbf{n}, \tag{3.5}$$

where $\mathbf{h}_{\ell_{\Re}}$ and $\mathbf{h}_{\ell_{\Im}}$ represent the $\ell_{\Re}^{th}$ and $\ell_{\Im}^{th}$ column of the fading channel gain matrix $\mathbf{H}$.

3.3 QSM Detection

In the detection of QSM, we assume that perfect CSI is known at the receiver in all instances. The QSM detector estimates the transmitted signal via an exhaustive ML search where all possible antennas and signal constellation points are calculated. The detector selects the ML calculation with the minimum argument as the estimated received signal of the transmitted information [23, 25]. The ML detector for QSM is given as:

$$\big[\,\hat{\ell}_{\Re},\ \hat{\ell}_{\Im},\ \hat{x}_{\hat{q}}^{\Re},\ \hat{x}_{\hat{q}}^{\Im}\big] = \underset{\hat{\ell}_{\Re},\ \hat{\ell}_{\Im},\ \hat{x}_{\hat{q}}^{\Re},\ \hat{x}_{\hat{q}}^{\Im}}{\operatorname{argmin}} \|\boldsymbol{y} - \sqrt{\rho}\big(\mathbf{h}_{\ell_{\Re}} x_q^{\Re} + i\mathbf{h}_{\ell_{\Im}} x_q^{\Im}\big)\|_F^2. \tag{3.6}$$

If we let $\boldsymbol{g} = \sqrt{\rho}\big(\mathbf{h}_{j_{\Re}} x_q^{\Re} + i\mathbf{h}_{j_{\Im}} x_q^{\Im}\big)$, then expanding the Frobenius norm simplifies (3.6) to yield:

$$\big[\hat{\ell}_{\Re},\ \hat{\ell}_{\Im},\ \hat{x}_{\hat{q}}^{\Re},\ \hat{x}_{\hat{q}}^{\Im}\big] = \underset{\hat{\ell}_{\Re},\ \hat{\ell}_{\Im},\ \hat{x}_{\hat{q}}^{\Re},\ \hat{x}_{\hat{q}}^{\Im}}{\operatorname{argmin}} \left\{ \|\boldsymbol{g}\|_F^2 - 2\Re\{\boldsymbol{y}^H\boldsymbol{g}\} \right\}. \tag{3.7}$$

Note, the expression in (3.7) is the optimal ML detector for the QSM scheme.

3.4 Performance Analysis of QSM

In this section, the analytical error performance of QSM is formulated employing an asymptotic tight union bound approach shown in [29, 45]. For the initial stage of the derivation, we assume that $N_R = 1$ for simplicity, a generalized expression for an arbitrary number of receivers is presented at the end of the section. Considering the received signal in (3.5) and if we let $\hat{\boldsymbol{g}} = \sqrt{\rho}\big(\hat{\mathbf{h}}_{\ell_\Re}\hat{x}_q^\Re + i\hat{\mathbf{h}}_{\ell_\Im}\hat{x}_q^\Im\big)$, then the PEP of QSM is given as [29]:

$$P\big(\boldsymbol{g} \to \hat{\boldsymbol{g}}|\mathbf{H}\big) = P(d_{\boldsymbol{g}} \to d_{\hat{\boldsymbol{g}}}|\mathbf{H}) = Q\big(\sqrt{\zeta}\big), \tag{3.8}$$

where $d_{\boldsymbol{g}} = \|\boldsymbol{g}\|_F^2 - 2\Re\{\boldsymbol{y}^H\boldsymbol{g}\}$ and ζ is an exponential RV given by [29]:

$$\zeta = \frac{\rho}{2}\|\boldsymbol{g} - \hat{\boldsymbol{g}}\|_F^2. \tag{3.9}$$

If we let:

$$A = \big[\ \Re\big(\mathbf{h}_{\ell_\Re}\hat{x}_\Re\big) - \Im\big(\mathbf{h}_{\ell_\Im}\hat{x}_\Im\big) - \Re\big(\hat{\mathbf{h}}_{\ell_\Re}\hat{x}_\Re\big) + \Im\big(\hat{\mathbf{h}}_{\ell_\Im}\hat{x}_\Im\big)\ \big]$$

$$B = \big[\ \Im\big(\mathbf{h}_{\ell_\Re}\hat{x}_\Re\big) + \Re\big(\mathbf{h}_{\ell_\Im}\hat{x}_\Im\big) - \Im\big(\hat{\mathbf{h}}_{\ell_\Re}\hat{x}_\Re\big) - \Re\big(\hat{\mathbf{h}}_{\ell_\Im}\hat{x}_\Im\big)\ \big]$$

Then the equation in (3.9) can be written as:

$$\zeta = \frac{\rho}{2}|A + iB|^2. \tag{3.10}$$

Note that, ζ is an exponential RV with the following mean:

$$\overline{\zeta} = \begin{cases} \frac{\rho}{2}\big(|x_q^\Re|^2 + |x_q^{\hat{\Re}}|^2 + |x_q^\Im|^2 + |x_q^{\hat{\Im}}|^2\big), & \text{if } \mathbf{h}_{\ell_\Re} \neq \mathbf{h}_{\hat{\ell}_\Re}, \mathbf{h}_{\ell_\Im} \neq \mathbf{h}_{\hat{\ell}_\Im} \\ \frac{\rho}{2}\big(|x_q^\Re - x_q^{\hat{\Re}}|^2 + |x_q^\Im|^2 + |x_q^{\hat{\Im}}|^2\big), & \text{if } \mathbf{h}_{\ell_\Re} = \mathbf{h}_{\hat{\ell}_\Re}, \mathbf{h}_{\ell_\Im} \neq \mathbf{h}_{\hat{\ell}_\Im} \\ \frac{\rho}{2}\big(|x_q^\Re - x_q^{\hat{\Re}}|^2 + |x_q^\Im - x_q^{\hat{\Im}}|^2\big), & \text{if } \mathbf{h}_{\ell_\Re} = \mathbf{h}_{\hat{\ell}_\Re}, \mathbf{h}_{\ell_\Im} = \mathbf{h}_{\hat{\ell}_\Im} \\ \frac{\rho}{2}\big(|x_q^\Re|^2 + |x_q^{\hat{\Re}}|^2 + |x_q^\Im - x_q^{\hat{\Im}}|^2\big), & \text{if } \mathbf{h}_{\ell_\Re} \neq \mathbf{h}_{\hat{\ell}_\Re}, \mathbf{h}_{\ell_\Im} = \mathbf{h}_{\hat{\ell}_\Im}. \end{cases} \tag{3.11}$$

Hence, assuming a single receive antenna is employed, the average PEP can be written as [29]:

$$\overline{P}_e(\boldsymbol{g}_\delta \to \hat{\boldsymbol{g}}_{\hat{\delta}}) = \frac{1}{2}\left(1 - \sqrt{\frac{\overline{\zeta}/2}{1 + \overline{\zeta}/2}}\right). \tag{3.12}$$

The ABEP of QSM is evaluated using the following asymptotically tight union bound:

$$P_b \leq \frac{1}{2^{\eta_{QSM}}} \sum_{\delta}^{2^{\eta_{QSM}}} \sum_{\hat{\delta}}^{2^{\eta_{QSM}}} \frac{1}{\eta_{QSM}} \overline{P}_e(\boldsymbol{g} \to \hat{\boldsymbol{g}}) N(\delta, \hat{\delta}), \tag{3.13}$$

where $N(\delta, \hat{\delta})$ is the number of bit errors associated with the corresponding PEP event. If the receiver has N_R receive antennas, the instantaneous PEP is given by [29]:

$$P_e(\boldsymbol{g}_\delta \to \hat{\boldsymbol{g}}_{\hat{\delta}}) = Q\left(1 - \sqrt{\sum_{k=1}^{N_R}}\right), \tag{3.14}$$

and the average PEP can be written as [12, 29]:

$$\overline{P}_e(\boldsymbol{g}_\delta \to \hat{\boldsymbol{g}}_{\hat{\delta}}) = \mu^{N_R} \sum_{k=0}^{N_R-1} \binom{N_R - 1 + k}{k} [1-\mu]^k, \tag{3.15}$$

where $\mu = \frac{1}{2}\left(1 - \sqrt{\frac{\overline{\zeta}/2}{\overline{\zeta}/2+1}}\right)$. Taking the Taylor series of (3.15) and ignoring high-order terms yields the following asymptotic average PEP for QSM [29]:

$$P_b = \overline{P}_e(\boldsymbol{g}_\delta \to \hat{\boldsymbol{g}}_{\hat{\delta}}) = \frac{2^{N_R-1}\Gamma(N_R + 0.5)}{\sqrt{\pi(N_R)!}} \left(\frac{1}{\overline{\zeta}}\right)^{N_R}. \tag{3.16}$$

3.5 Numerical Analysis of the Analytical and Simulated BER Performance of QSM

In this section, the ABEP for QSM formulated using the analytical union bound approach is presented. Monte Carlo simulation results are executed in a Matlab environment and are presented to validate the analytical result in Section 3.4. All Monte Carlo simulations are performed over i.i.d. Rayleigh frequency-flat fading channels in the presence of AWGN and Gray-coded M-QAM signal constellations are employed. It is assumed that complete CSI is known at the receiver in all instances.

Monte Carlo simulations for QSM with spectral efficiencies of $\eta_{QSM} = 4$, 6, 8, and 10 b/s/Hz are presented in graphs of BER versus SNR. The notation used to denote an $N_T \times N_R$ QSM configuration with an APM modulation order of M is $(N_T, N_R, M, \eta_{QSM})$.

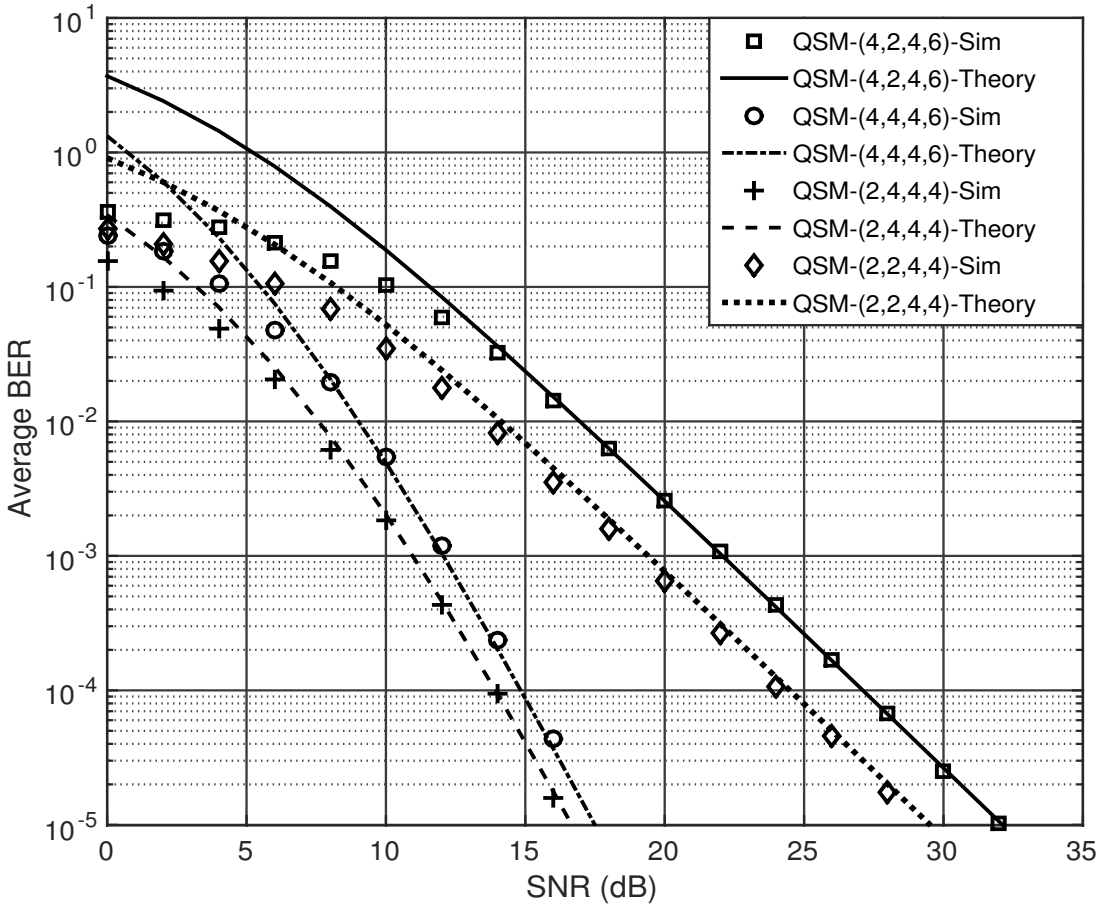

Figure 3.2: Theoretical and simulated BER performance of QSM for $\eta_{QSM} = 4$, 6 b/s/Hz.

In Figure 3.2, the analytical and Monte Carlo simulation results for 2×2, 2×4, 4×2, and 4×4 QSM systems with spectral efficiencies of $\eta_{QSM} = 4$ and 6 b/s/Hz are presented. The analysis of the results shows that the Monte Carlo BER error performance is consistent with the analytical performance at high SNR values, which validates the theoretical analysis of QSM. An investigation of the results shows that the BER performance of QSM improves with an increase in the number of receive antennas for systems with the same spectral efficiency. At a BER of 10^{-5}, 4×4 4-QAM QSM has an SNR gain of 14.7 dB over 4×2 4-QAM QSM, and at a BER of 10^{-5}, 2×4 4-QAM QSM has an SNR gain of 12.9 dB over 2×2 4-QAM QSM.

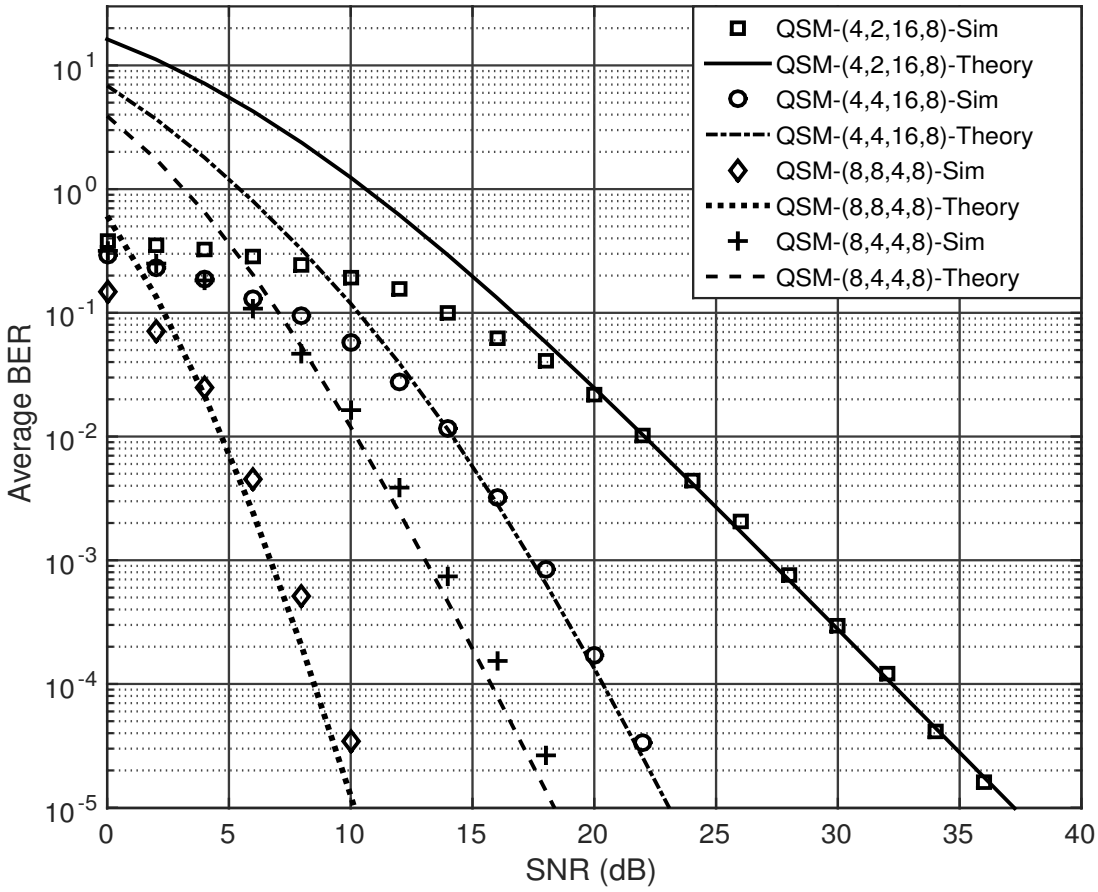

Figure 3.3: Theoretical and simulated BER performance of QSM for $\eta_{QSM} = 8$ b/s/Hz.

In Figure 3.3, the analytical and Monte Carlo simulation results for 4×2, 4×4, 8×4, and 8×8 QSM systems with spectral efficiency of $\eta_{QSM} = 8$ b/s/Hz are presented. The Monte Carlo simulation results validate the analytical performance of QSM as the error performance of the Monte Carlo simulation closely matches the analytical performance at high SNR regions. At a BER of 10^{-5}, 4×4 16-QAM QSM has an SNR gain of 13.6 dB over 4×2 16-QAM QSM, and at a BER of 10^{-5}, 8×8 4-QAM QSM has an SNR gain of 8.1 dB over 8×4 4-QAM QSM.

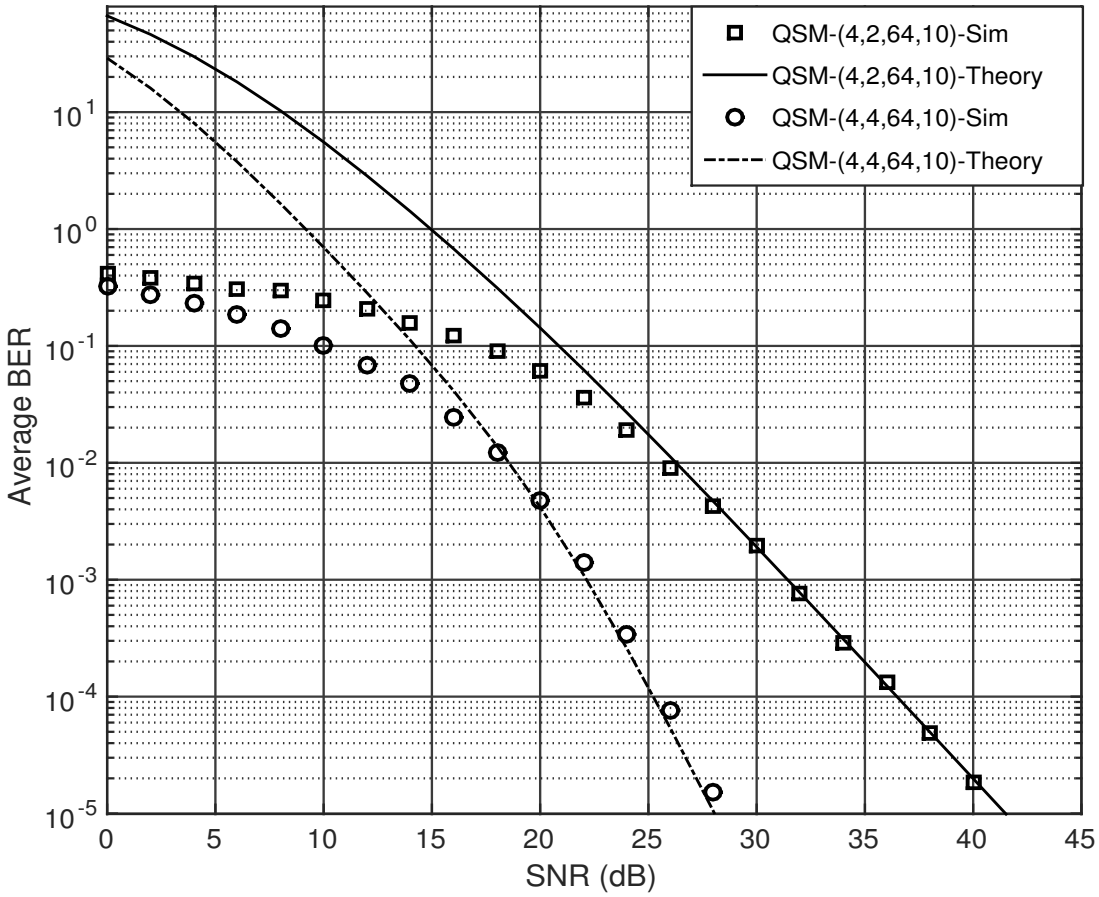

Figure 3.4: Theoretical and simulated BER performance of QSM for $\eta_{QSM} = 10$ b/s/Hz.

In Figure 3.4, the analytical and Monte Carlo simulation results for 4×2, and 4×4 QSM systems with spectral efficiency of $\eta_{QSM} = 10$ b/s/Hz are presented. The Monte Carlo simulation results show consistency with the analytical error performance at high SNR regions. This is the expected result since the upper bound approach is used to determine the analytical performance. At a BER of 10^{-5}, 4×4 64-QAM QSM has an SNR gain of 12.8 dB over 4×2 64-QAM QSM.

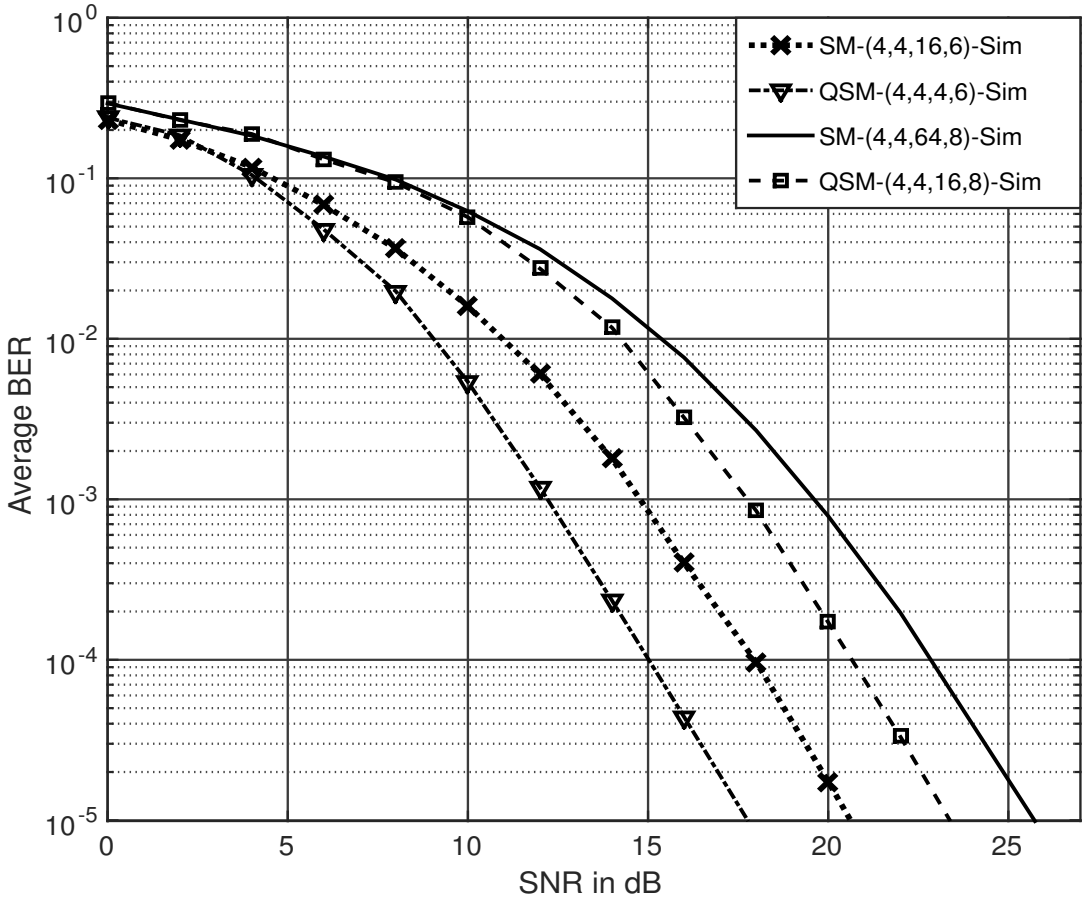

Figure 3.5: BER performance of SM and QSM for $\eta_{QSM}, \eta_{SM} = 6, 8$ b/s/Hz.

In Figure 3.5, simulations of the BER performance of SM and QSM systems with spectral efficiencies of 6 and 8 b/s/Hz are presented. All simulations have a 4×4 configuration and identical spectral efficiencies for the purpose of making fair comparisons. At a BER of 10^{-5}, 4-QAM QSM with $\eta_{QSM} = 6$ b/s/Hz has an SNR gain of 2.9 dB over 16-QAM SM with $\eta_{SM} = 6$ b/s/Hz. At a BER of 10^{-5}, 16-QAM QSM with $\eta_{QSM} = 8$ b/s/Hz has an SNR gain of 2.3 dB over 64-QAM SM with $\eta_{SM} = 8$ b/s/Hz. Low order modulation schemes require low transmit power to achieve better error performance as compared to high order schemes, therefore for the same spectral efficiency, QSM has a better error performance than SM.

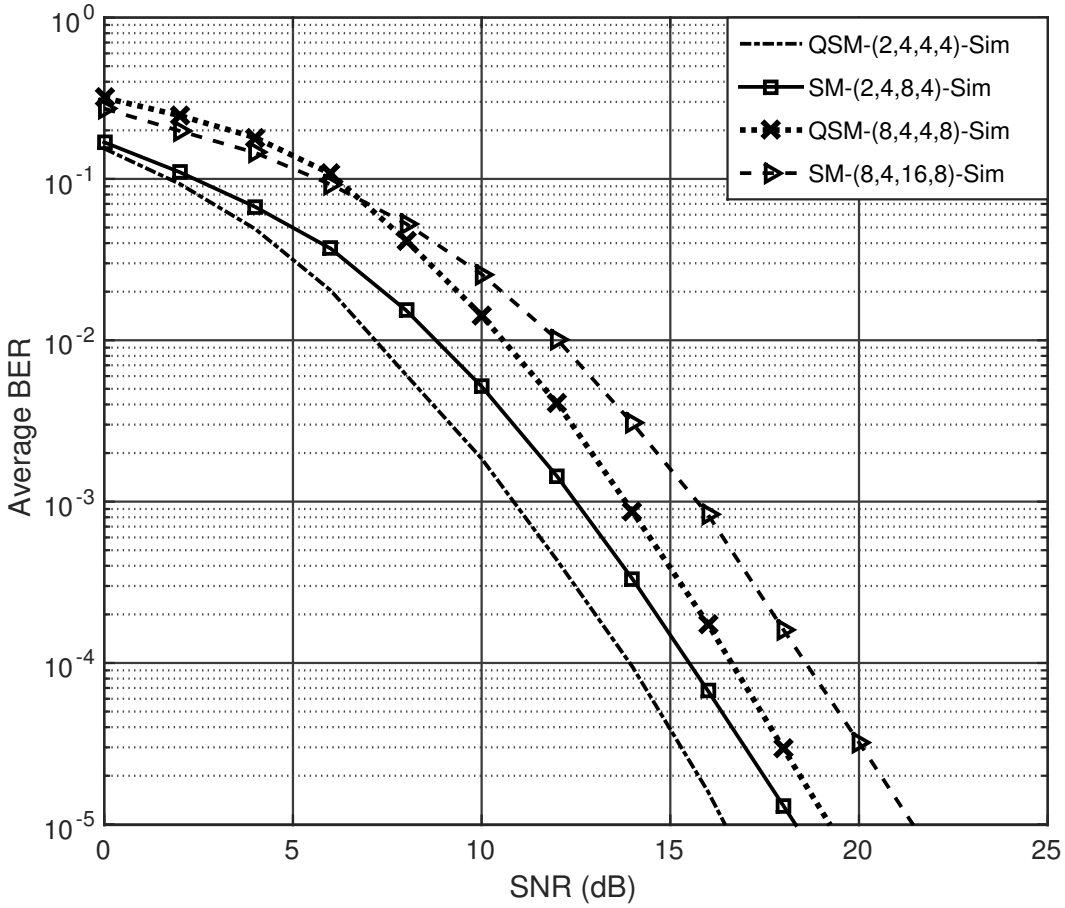

Figure 3.6: BER performance of SM and QSM for $\eta_{QSM}, \eta_{SM} = 4, 8$ b/s/Hz.

In Figure 3.6, simulations of the BER performance of SM and QSM systems with spectral efficiencies of 4 and 8 b/s/Hz are presented. Systems with 2×4 and 8×4 configurations are presented. At a BER of 10^{-5}, 2×4 4-QAM QSM has an SNR gain of 1.9 dB over 2×4 8-QAM SM. At a BER of 10^{-5}, 8×4 4-QAM QSM has an SNR gain of 2.2 dB over 8×4 16-QAM SM. Low order modulation schemes require low transmit power to achieve the same error performance as high order modulation schemes with the same spectral efficiency. Therefore , QSM has a better error performance than SM.

3.6 Summary

The performance analysis for QSM employing the asymptotic union bound approach to calculate the average BER performance over i.i.d. Rayleigh frequency-flat fading channel was formulated. The analytical results were consistent with the Monte Carlo simulations at high SNR regions, therefore validating the theoretical performance of QSM. The BER performance of SM and QSM is presented, and it is demonstrated that QSM has a better error performance than SM for systems with identical spectral efficiency.

Chapter 4

Double Spatial Modulation

4.1 Introduction

IM techniques have recently received much research attention as possible candidates for the next-generation of wireless communication [21,46]. IM improves the spectral efficiency of MIMO systems by conveying extra information via the spatial domain. SM is a promising IM-based scheme that presents an energy efficient implementation of MIMO systems [23, 44]. SM is a scheme that completely mitigates ICI and IAS which degrade the performance of MIMO systems, and relatively low-complexity receive algorithms are utilized in SM, this is due to the use of a single RF chain in the system. [17, 24, 25].

QSM is one recently proposed SM based scheme, which provides significant improvement in spectral efficiency as compared to the traditional SM [25,45]. QSM employs two active transmit antenna indices during a single transmission interval. The increase in the number the active transmit antennas directly increases the spectral efficiency of QSM. Since QSM employs orthogonal sine and cosine carriers, ICI is mitigated. QSM employs a single RF chain at the receiver, therefore relatively low-complexity receive algorithms are required [29].

Due to the increase in demand for improved data rates, DSM is a recently proposed SM-based modulation scheme that aims to double the spectral efficiency of traditional SM [30]. DSM simultaneously employs two independent SM transmission channels that are superimposed to simultaneously transmit two APM constellation symbols in a single transmission interval [30]. The innovative idea in DSM is that constellation rotation is applied to one of the APM signal constellations such that the receiver is capable of distinguishing all signal constellation points of the two independent SM channels. The rotation angle applied is optimized to a degree such

that the BER is minimized between the SM channels and/or the minimum Euclidean distance is maximised between the signal constellation sets [30, 31].

In practice, the majority of wireless communications employ FEC to enhance data reliability in noisy channels [40]. It has been demonstrated that soft-output detection coupled with soft-input channel decoding results in a significant net coding gain [41, 42]. SOMLDs for systems such as SM, QSM, and GSM have been proposed, and under coded conditions, significant improvement in error performance is demonstrated [43, 47, 48]. In this chapter, we present the system model, detection scheme, and analytical error performance of DSM. Furthermore, this chapter proposes an SOMLD for DSM, and simulation results are presented to validate the analytical performance and the SOMLD.

4.2 System Model for DSM

Figure 4.1 illustrates the system model for DSM, where N_T and N_R represent the number of transmit antennas and receive antennas, respectively.

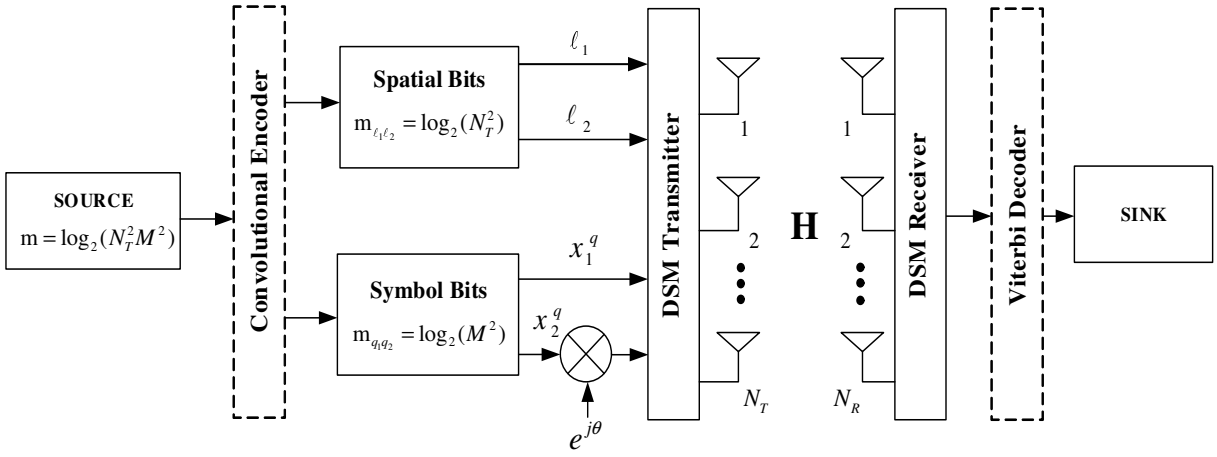

Figure 4.1: System Model for the DSM scheme

In each transmission interval, the source provides an input vector of length $\mathrm{m} = \log_2(N_T^2 M^2)$, where M is the APM signal modulation order, into the DSM encoder. Note, we refer the dashed convolutional encoder in Figure 4.1 as the DSM primary bit splitter for uncoded cases. The DSM encoder divides the source bits into four partitions. The first and second partitions are mapped such that $\mathrm{m}_{\ell_1\ell_2} = \log_2 N_T^2$ bits are used to select two transmit antenna indices ℓ_1 and ℓ_2, $\ell_1, \ell_2 \in [1 : N_T]$, respectively, while the third and fourth partitions are mapped such that $\mathrm{m}_{q_1 q_2} = \log_2(M^2)$ bits are used to select two symbols x_1^q and x_2^q, $q \in [1 : M]$ which are drawn from a Gray-coded M-QAM or M-PSK signal constellation set. The first data symbol

x_1^q is transmitted via the active transmit antenna with index ℓ_1 whereas the second data symbol x_2^q is rotated through an optimized angle θ before transmission via the second active transmit antenna with index ℓ_2. The spectral efficiency of DSM is given as [30]:

$$\eta_{DSM} = 2\log_2 M + 2\log_2 N_T \ \text{ b/s/Hz.} \tag{4.1}$$

Note that in DSM, it is possible to have the active transmit antenna indices $\ell_1 = \ell_2$; in this case, we denote the active transmit antenna index as ℓ, $\ell \in [1 : N_T]$, and the transmitted symbol is a summation of the symbols x_1^q and the rotated $x_2^q e^{j\theta}$. Due to this property, the DSM signal constellation for the independent SM channels must have one of two properties that permit the optimal performance of the scheme at the detector, and these are listed as:

1. To improve the performance of the ML detector, the minimum Euclidean distance between the two signal constellation must be maximized [31].

2. The signal constellation points for the symbols must be unique such that they can be distinguished at the receiver [30].

In Figure 4.2, the BER performance for 4×4 DSM systems with BPSK, 4-QAM, and 8-QAM constellations versus rotation angle is presented. A heuristic approach is used to determine the optimum rotation angle for the constellations that give the best ML detector performance. At an SNR of 16 dB, the optimal rotation for BPSK ranges from 60° to 120°. At an SNR of 16 dB, the optimum rotation angle range for 4-QAM rests in two regions, from 40° to 55° and from 125° to 140°. At an SNR of 20 dB, the optimum rotation angle range for 8-QAM rests in two regions, from 55° to 65° and from 115° to 125°. In this dissertation, we set the optimum rotation angle θ, for BPSK, 4-QAM and 8 QAM as 90°, 45° and 60°, respectively [30].

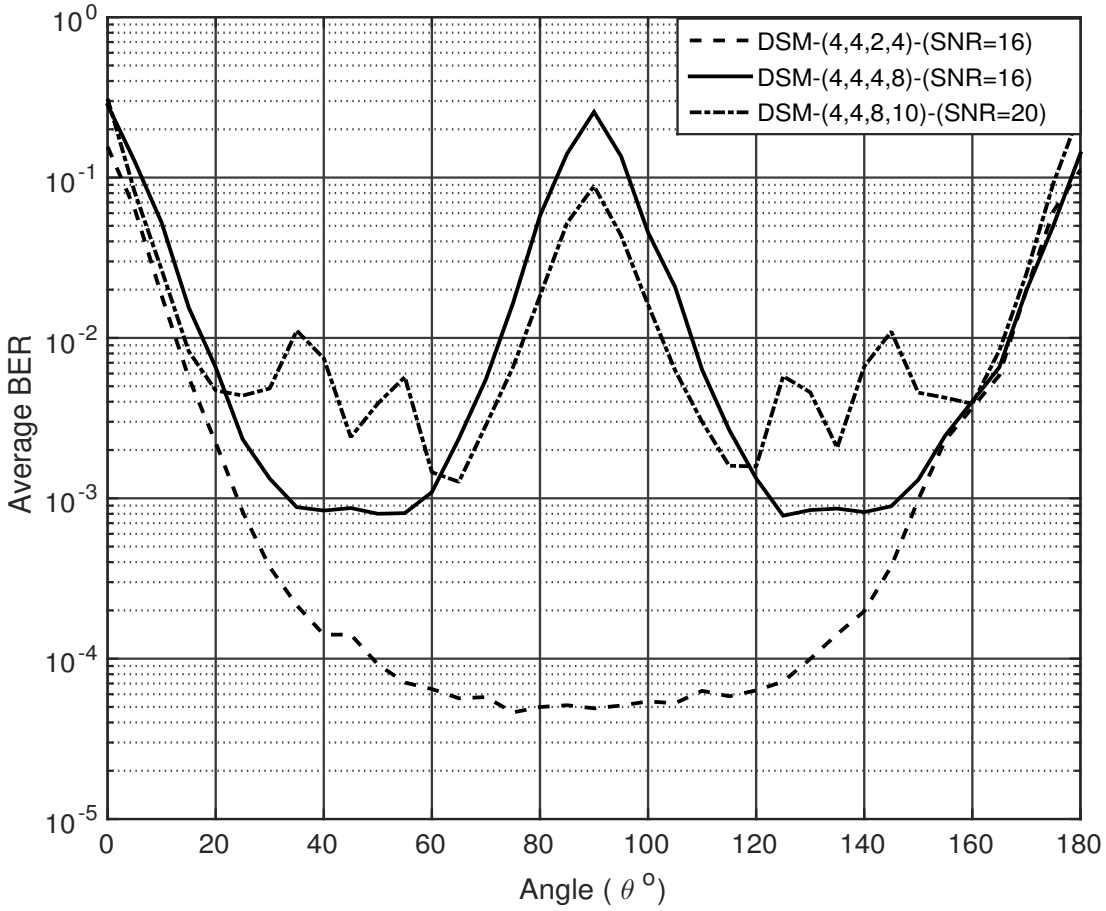

Figure 4.2: BER versus rotation angle in degrees for BPSK, 4-QAM and 8-QAM.

The output of the DSM mapper is expressed as an $N_T \times 1$ transmission vector given as:

$$\mathbf{x} = \underset{\substack{\uparrow \\ 1^{st} \text{ position}}}{\big[\, 0 \;\; \cdots} \quad \underset{\substack{\ell_1^{th} \text{ position} \\ \downarrow}}{x_q^1} \quad \underset{\substack{\ell_2^{th} \text{ position} \\ \downarrow}}{x_q^2 e^{j\theta}} \quad \underset{\substack{\uparrow \\ N_T^{th} \text{ position}}}{\cdots \;\; 0 \,\big]^T}, \tag{4.2}$$

where x_1^q and $x_2^q e^{j\theta}$, $q \in [1 : M]$, represent the transmit symbols drawn from M-QAM or M-PSK signal constellation sets with $E\{|x_1^q|^2\} = E\{|x_2^q e^{j\theta}|^2\} = 1$, and ℓ_1 and ℓ_2, $\ell_1, \ell_2 \in [1 : N_T]$ represent the active transmit antenna indices for x_1^q and $x_2^q e^{j\theta}$, respectively, and θ represents the optimum rotation angle. Note that in (4.3), as previously stated, it is possible to have the active transmit antenna indices $\ell_1 = \ell_2$, therefore we represent the two indices as a single active transmit antenna index ℓ, $\ell \in [1 : N_T]$, and the signal transmitted on index ℓ is a summation of symbols x_1^q and $x_2^q e^{j\theta}$, respectively.

The example illustrated in Table 4.1 demonstrates the mapping procedure for a 4×4 Gray-coded 4-QAM DSM. In this example, we demonstrate the mapping procedure of a DSM system with spectral efficiency of 8 b/s/Hz; only two random data streams are considered.

Table 4.1: Illustration of the mapping procedure for DSM

Source Bits	**Mapping Partition**				**Transmit Vector**
$\mathrm{m} = \log_2(N_T^2 M^2)$	1	2	3	4	$\mathbf{x}$
0 1 1 1 0 1 1 0 $\theta = 45°$ $N_T = 4$ $M = 4$	$\log_2 N_T = 2$ 0 1 $\ell_1 = 2$ $\mathbf{h}_{\ell_1}$	$\log_2 N_T = 2$ 1 1 $\ell_2 = 4$ $\mathbf{h}_{\ell_2}$	$\log_2 M = 2$ 0 1 x_1^q $-1 - j$	$\log_2 M = 2$ 1 0 $x_2^q e^{j\theta}$ $(1 + j)\ e^{j\theta}$	$\begin{bmatrix} 0 \\ x_1^q \\ 0 \\ x_2^q e^{j\theta} \end{bmatrix}$
1 0 1 0 0 0 1 1 $\theta = 45°$ $N_T = 4$ $M = 4$	$\log_2 N_T = 2$ 1 0 $\ell = 3$ $\mathbf{h}_{\ell}$	$\log_2 N_T = 2$ 1 0 $\ell = 3$ $\mathbf{h}_{\ell}$	$\log_2 M = 2$ 0 0 x_1^q $-1 + j$	$\log_2 M = 2$ 1 1 $x_2^q\ e^{j\theta}$ $(1 - j)\ e^{j\theta}$	$\begin{bmatrix} 0 \\ 0 \\ x_1^q + x_2^q e^{j\theta} \\ 0 \end{bmatrix}$

The source bits m are mapped to the transmission vector $\mathbf{x}$, which is transmitted over a Rayleigh frequency-flat fading channel $\mathbf{H}$ of dimension $N_R \times N_T$ in the presence of AWGN. AWGN is represented by vector $\mathbf{n}$ of dimension $N_R \times 1$. All elements of $\mathbf{H}$ and $\mathbf{n}$ are assumed to be i.i.d. entries with Gaussian distribution of zero mean and unit variance given by $\sim CN(0, 1)$. The received signal is given by an $N_R \times 1$ vector $\boldsymbol{y}$, is defined as [30]:

$$\boldsymbol{y} = \sqrt{\rho/2}\mathbf{H}\mathbf{x} + \mathbf{n}\ , \tag{4.3}$$

where $\rho/2$ is the average SNR at each receive antenna and the channel matrix $\mathbf{H}$ can be defined as:

$$\mathbf{H} = \begin{bmatrix} h_{1,1} & \cdots & h_{1,N_T} \\ \vdots & \ddots & \vdots \\ h_{N_R,1} & \cdots & h_{N_R,N_T} \end{bmatrix}, \tag{4.4}$$

where $h_{k,\ell}$ is the channel fading coefficient between the k^{th} receive antenna, $k \in [1 : N_R]$, and ℓ^{th} transmit antenna, $\ell \in [1 : N_T]$. Assuming the ℓ_1^{th} and ℓ_2^{th} antennas are used in the transmission of x_1^q and $x_2^q e^{j\theta}$, respectively, the received signal in (4.4) can be represented as:

$$\boldsymbol{y} = \sqrt{\rho/2}\ \left(\mathbf{h}_{\ell_1} x_1^q + \mathbf{h}_{\ell_2} x_2^q e^{\theta}\right) + \mathbf{n}, \tag{4.5}$$

where $\mathbf{h}_{\ell_1}$ and $\mathbf{h}_{\ell_2}$ denote the ℓ_1^{th} and ℓ_2^{th} columns of the channel gain matrix $\mathbf{H}$, respectively.

4.3 DSM Detection

In the detection of DSM, we assume that perfect CSI is known at the receiver in all instances. The DSM detector estimates the transmitted signal via an exhaustive ML search were all possible antenna indices ℓ_1 and ℓ_2 and the M-QAM/M-PSK constellation symbols x_1^q and $x_2^q e^{j\theta}$ are calculated. The detector selects the ML calculation with the minimum argument as the estimated received signal of the transmitted information. The ML detector is given as [30]:

$$\big[\hat{x}_1^{\hat{q}},\ \hat{x}_2^{\hat{q}},\ \hat{\ell}_1,\ \hat{\ell}_2\big] = \underset{\hat{x}_1^{\hat{q}},\ \hat{x}_2^{\hat{q}},\ \hat{\ell}_1,\ \hat{\ell}_2}{\operatorname{argmin}} \|\boldsymbol{y} - \sqrt{\rho/2}\big(\mathbf{h}_{\ell_1} x_1^q + \mathbf{h}_{\ell_2} x_2^q e^{j\theta}\big)\|_F^2. \tag{4.6}$$

If we let:

$$\boldsymbol{g} = \sqrt{\rho/2}\big(\mathbf{h}_{\ell_1} x_1^q + \mathbf{h}_{\ell_2} x_2^q e^{j\theta}\big), \tag{4.7}$$

then, expanding the Frobenius norm simplifies (4.7) to yield:

$$\big[\hat{x}_1^{\hat{q}},\ \hat{x}_2^{\hat{q}},\ \hat{\ell}_1,\ \hat{\ell}_2\big] = \underset{\hat{x}_1^{\hat{q}},\ \hat{x}_2^{\hat{q}},\ \hat{\ell}_1,\ \hat{\ell}_2}{\operatorname{argmin}} \left\{ \|\boldsymbol{g}\|_F^2 - 2\Re\{\boldsymbol{y}^H \boldsymbol{g}\} \right\}. \tag{4.8}$$

Note, the expression in (4.8) is the optimal ML detector for the DSM scheme.

4.4 Performance Analysis of DSM

In this section, we derive the theoretical ABEP of DSM in i.i.d. Rayleigh frequency-flat fading channels. The union bound method is employed to formulate the theoretical ABEP for DSM, and it is defined as [30]:

$$\text{ABEP} \leq \frac{1}{M^2 N_T^2} \sum_{\mathbf{x}} \sum_{\hat{\mathbf{x}}} \frac{N(\mathbf{x}, \hat{\mathbf{x}}) P(\mathbf{x} \to \hat{\mathbf{x}})}{\eta_{DSM}}, \tag{4.9}$$

where $\mathbf{x}$ is the codeword given in (4.2), $P(\mathbf{x} \to \hat{\mathbf{x}})$ is the PEP that the transmitted codeword $\mathbf{x}$ is detected as $\hat{\mathbf{x}}$ at the receiver and $N(\mathbf{x}, \hat{\mathbf{x}})$ is the number of bit errors associated with the corresponding PEP event $P(\mathbf{x} \to \hat{\mathbf{x}})$. The conditional PEP is given as:

$$P(\mathbf{x} \to \hat{\mathbf{x}} | \mathbf{H}) = P(\|\boldsymbol{y} - \hat{\mathbf{x}}\|_F^2 < \|\boldsymbol{y} - \mathbf{x}\|_F^2). \tag{4.10}$$

The conditional PEP in (4.17) may be simplified using the method shown by Xu *et al.* [49] which gives:

$$P(\mathbf{x} \to \hat{\mathbf{x}}|\mathbf{H}) = Q(\sqrt{k}), \tag{4.11}$$

where k is a central chi-squared RV with $2N_R$ degrees of freedom and is defined as:

$$k = \frac{\rho}{8}\|\mathbf{H}\|_F^2 \cdot \|\mathbf{x} - \hat{\mathbf{x}}\|_F^2 = \sum_{n=1}^{2N_R} \alpha^2, \tag{4.12}$$

where $\alpha \sim N(0, \sigma_\alpha^2)$ and the variance $\sigma_\alpha^2 = \frac{\rho}{8} \cdot \|\mathbf{x} - \hat{\mathbf{x}}\|_F^2$. The PDF of k is defined as:

$$f_k(\upsilon) = \frac{\upsilon^{N_R-1} e^{\frac{-\upsilon}{2\sigma_\alpha^2}}}{\left(2\sigma_\alpha^2\right)^{N_R}\left(N_R-1\right)!} \quad , \ \upsilon \geq 0. \tag{4.13}$$

Averaging the conditional PEP over the i.i.d. RVs we arrive at:

$$P\big(\mathbf{x} \to \hat{\mathbf{x}}\big) = \int_0^\infty P\big(\mathbf{x} \to \hat{\mathbf{x}}|\mathbf{H}\big) \cdot f_k\big(\upsilon\big)\partial\upsilon. \tag{4.14}$$

Employing the trapezoidal rule approximation of the Q-function which is given as:

$$Q(\phi) \approx \frac{1}{2c}\left[\frac{1}{2}\exp\left(\frac{-\phi^2}{2}\right) + \sum_{k=1}^{c-1}\exp\left(\frac{-\phi^2}{2\sin^2\left(\frac{k\pi}{2c}\right)}\right)\right], \tag{4.15}$$

where c is the number of iterations of convergence, $c = 10$. Using the moment generating function (MGF), we arrive at the unconditional PEP given as [49]:

$$P\big(\mathbf{x} \to \hat{\mathbf{x}}\big) = \frac{1}{2c}\left[\frac{1}{2}M\left(\frac{1}{2}\right) + \sum_{k=1}^{c-1} M\left(\frac{1}{2\sin^2\left(\frac{k\pi}{2c}\right)}\right)\right], \tag{4.16}$$

where the MGF $M(\cdot)$ is defined as:

$$M(s) = \int_0^\infty e^{s\upsilon}\frac{\upsilon^{N_R-1}e^{\frac{-\upsilon}{2\sigma_\alpha^2}}}{\left(2\sigma_\alpha^2\right)^{N_R}\left(N_R-1\right)!}\partial\upsilon = \left(\frac{1}{1+2\sigma_\alpha^2 s}\right)^{N_R}. \tag{4.17}$$

4.5 DSM Soft-Output Detector

The system model in Figure 4.1 is extended to include channel coding and decoding, and we refer to the dashed line blocks in Figure 4.1 for the coded model understudy in this section. For the proposed soft-output detector, we assume the following [42]:

1. Data symbols and antenna indices are uncorrelated.

2. Data symbols are independent and generated with equal probability.

3. Antenna bits are independent and generated with equal probability.

4. Full CSI is available at the receiver.

4.5.1 SOMLD for DSM

The SOMLD for DSM is formulated as an LLR based on the ML detector in (4.9) [43]. An LLR expression is a formula that is used to calculate the value of each significant bit that makes up the binary data of an index. The SOMLD for DSM is formed from the combination of the LLR expressions for the first antenna index ℓ_a, the second antenna index ℓ_b, first symbol x_a, and the second symbol x_b. The LLR expression for the first antenna index ℓ_a is formulated as:

$$LLR(\ell_a) = \log \frac{P\big(\ell_a = 1|\mathbf{y}\big)}{P\big(\ell_a = 0|\mathbf{y}\big)}. \tag{4.18}$$

The LLR expression in (4.18) can be written as:

$$LLR(\ell_a) = \log \frac{\sum\limits_{\substack{\hat{\ell}_a \in \boldsymbol{\ell}_a^1 \\ \hat{\ell}_b \in \mathbf{L}_b}} \sum\limits_{\substack{\hat{x}_a^q \in \boldsymbol{\Omega}_a \\ \hat{x}_b^q \in \boldsymbol{\Omega}_b}} P\big(\mathbf{y}|\ell_a = \hat{\ell}_a, \ell_b = \hat{\ell}_b, x_a^q = \hat{x}_a^q, x_b^q = \hat{x}_b^q\big) P\big(\ell_a = \hat{\ell}_a\big)}{\sum\limits_{\substack{\hat{\ell}_a \in \boldsymbol{\ell}_a^0 \\ \hat{\ell}_b \in \mathbf{L}_b}} \sum\limits_{\substack{\hat{x}_a^q \in \boldsymbol{\Omega}_a \\ \hat{x}_b^q \in \boldsymbol{\Omega}_b}} P\big(\mathbf{y}|\ell_a = \hat{\ell}_a, \ell_b = \hat{\ell}_b, x_a^q = \hat{x}_a^q, x_b^q = \hat{x}_b^q\big) P\big(\ell_a = \hat{\ell}_a\big)}, \tag{4.19}$$

where $\boldsymbol{\ell}_a^1$ and $\boldsymbol{\ell}_a^0$ are vectors which contain the indices of the first antenna $\hat{\ell}_a$ with binary '1' and '0' that corresponds to a particular significant bit of the binary data of the index in question, respectively. $\mathbf{L}_b$ is a set of all possible indices $\hat{\ell}_b$ for the second antenna index. $\boldsymbol{\Omega}_a$ and $\boldsymbol{\Omega}_b$ represent a set of all possible symbols for $\hat{x}_a$ and $\hat{x}_b$, respectively. Applying Bayes' theorem to the demodulator output in (4.19), the LLR for the first antenna ℓ_a is calculated as:

$$LLR(\ell_a) = \log \frac{\sum\limits_{\hat{\ell}_a \in \boldsymbol{\ell}_a^1} \sum\limits_{\ell_b \in \mathbf{L}_b} \sum\limits_{\hat{x}_a^q \in \boldsymbol{\Omega}_a} \sum\limits_{\hat{x}_b^q \in \boldsymbol{\Omega}_b} \exp(A)}{\sum\limits_{\hat{\ell}_a \in \boldsymbol{\ell}_a^0} \sum\limits_{\ell_b \in \mathbf{L}_b} \sum\limits_{\hat{x}_a^q \in \boldsymbol{\Omega}_a} \sum\limits_{\hat{x}_b^q \in \boldsymbol{\Omega}_b} \exp(B)}, \tag{4.20}$$

where $A = B = \frac{-\|\mathbf{y} - \sqrt{\frac{P}{2}}\left(\mathbf{h}_{\hat{\ell}_a}\hat{x}_a^q + \mathbf{h}_{\hat{\ell}_b}\hat{x}_b^q e^{j\theta}\right)\|_F^2}{2\sigma^2}$ and σ^2 is the variance of the AWGN channel in (4.5). Based on the procedure shown in (4.18) and (4.19), the LLR expression for the second antenna

index ℓ_b is given as:

$$LLR(\ell_b) = \log \frac{\sum_{\hat{\ell}_b \in \boldsymbol{\ell}_b^1} \sum_{\hat{\ell}_a \in \mathbf{L}_a} \sum_{\hat{x}_a^q \in \boldsymbol{\Omega}_a} \sum_{\hat{x}_b^q \in \boldsymbol{\Omega}_b} \exp(A)}{\sum_{\hat{\ell}_b \in \boldsymbol{\ell}_b^0} \sum_{\hat{\ell}_a \in \mathbf{L}_a} \sum_{\hat{x}_a^q \in \boldsymbol{\Omega}_a} \sum_{\hat{x}_b^q \in \boldsymbol{\Omega}_b} \exp(B)}, \tag{4.21}$$

where $\boldsymbol{\ell}_b^1$ and $\boldsymbol{\ell}_b^0$ are vectors which contain the indices of the second antenna index $\hat{\ell}_b$ with binary '1' and '0' that corresponds to a particular significant bit of the binary data of the index in question, respectively, $\mathbf{L}_a$ is a set of all possible antenna indices $\hat{\ell}_a$ for the first antenna index. The LLR expression for the first symbol x_a^q is calculated using the same procedure shown in (4.18) and (4.19) and is given as:

$$LLR(x_a^q) = \log \frac{\sum_{\hat{x}_a^q \in \boldsymbol{\Omega}_a^1} \sum_{\hat{x}_b^q \in \boldsymbol{\Omega}_b} \sum_{\hat{\ell}_a \in \mathbf{L}_a} \sum_{\hat{\ell}_b \in \mathbf{L}_b} \exp(A)}{\sum_{\hat{x}_a^q \in \boldsymbol{\Omega}_a^0} \sum_{\hat{x}_b^q \in \boldsymbol{\Omega}_b} \sum_{\hat{\ell}_a \in \mathbf{L}_a} \sum_{\hat{\ell}_b \in \mathbf{L}_b} \exp(B)}, \tag{4.22}$$

where $\boldsymbol{\Omega}_1^a$ and $\boldsymbol{\Omega}_0^a$ are vectors which contain the indices of the first symbol $\hat{x}_a^q$ with binary '1' and '0' that corresponds to a particular significant bit of the binary data of symbol in question, respectively. $\boldsymbol{\Omega}_b$ is a set representing all possible $\hat{x}_b^q$ symbols. $\mathbf{L}_a$ and $\mathbf{L}_b$ are a set of all possible antenna indices $\hat{\ell}_a$ and $\hat{\ell}_b$ for the first and second antenna indices, respectively. Lastly, the LLR expression for the second symbol x_b^q is calculated using the procedure shown in (4.18) and (4.19) and is given as:

$$LLR(x_b^q) = \log \frac{\sum_{\hat{x}_b^q \in \boldsymbol{\Omega}_b^1} \sum_{x_b^q \in \boldsymbol{\Omega}_a} \sum_{\hat{\ell}_a \in \mathbf{L}_a} \sum_{\hat{\ell}_b \in \mathbf{L}_b} \exp(A)}{\sum_{\hat{x}_b^q \in \boldsymbol{\Omega}_b^0} \sum_{x_b^q \in \boldsymbol{\Omega}_a} \sum_{\hat{\ell}_a \in \mathbf{L}_a} \sum_{\hat{\ell}_b \in \mathbf{L}_b} \exp(B)}, \tag{4.23}$$

where $\boldsymbol{\Omega}_b^1$ and $\boldsymbol{\Omega}_b^0$ are vectors which contain the indices of the second symbol index $\hat{x}_b^q$ with binary '1' and '0' that corresponds to a particular significant bit of the binary data of the symbol in question, respectively, and $\boldsymbol{\Omega}_a$ is a set representing all possible $\hat{x}_a$ symbols.

4.6 Numerical Analysis of the Analytical and Simulated BER Performance of DSM

In this section, the ABEP for DSM formulated using the union bound approach is presented. Monte Carlo simulation results executed in a Matlab environment and are presented to validate the analytical result in Section 4.5. All Monte Carlo simulations are performed over i.i.d.

Rayleigh frequency-flat fading channels in the presence of AWGN, and Gray-coded M-QAM or M-PSK signal constellations are employed. It is assumed that complete CSI is known at the receiver in all instances.

In Section 4.2, uncoded data is transmitted, and Gray-coded M-ary constellation sets are employed. Monte Carlo simulations are presented for spectral efficiencies of 6, 8, and 10 b/s/Hz, and results are presented in terms of average BER versus SNR. The notation used to denote $N_R \times N_T$ DSM configuration is $(N_T, N_R, M, \eta_{DSM})$.

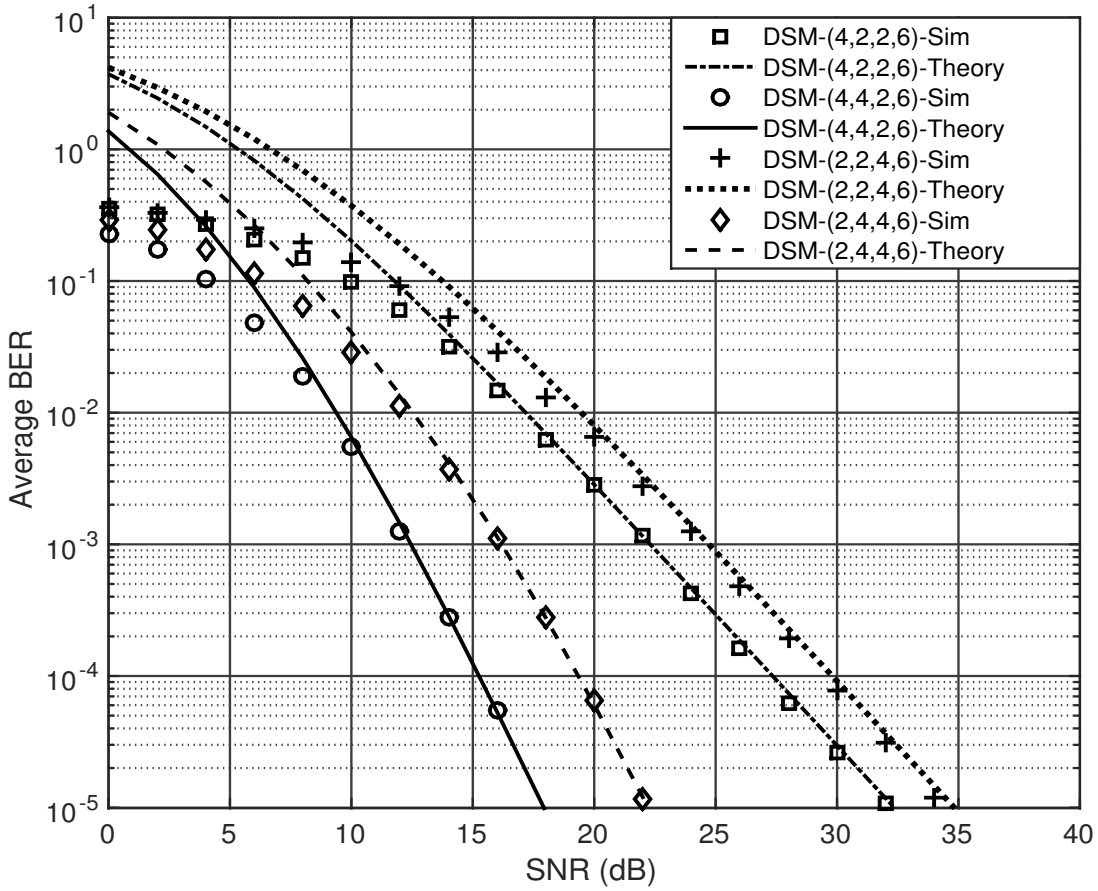

Figure 4.3: Theoretical and simulated BER performance of DSM for $\eta_{DSM} = 6$ b/s/Hz.

In Figure 4.3, the analytical and Monte Carlo simulation results for 2×2, 2×4, 4×2, and 4×4 DSM systems with spectral efficiency of $\eta_{DSM} = 6$ b/s/Hz are presented. The analysis of the results shows that the Monte Carlo error performance is consistent with the analytical error performance at high SNR values. This is the expected results since the theoretical analysis employs an upper bound approach, a match in high SNR regions validates the theoretical analysis of DSM. An investigation of the results shows that the BER performance of QSM improves with an increase in the number of receive antennas for systems with the same spectral efficiency. At a BER of 10^{-5}, 4×4 4-QAM DSM has an SNR gain of 14.1 dB over 4×2 4-QAM DSM, and

at a BER of 10^{-5}, 2×4 BPSK has an SNR gain of 12.2 dB over 2×2 BPSK for DSM.

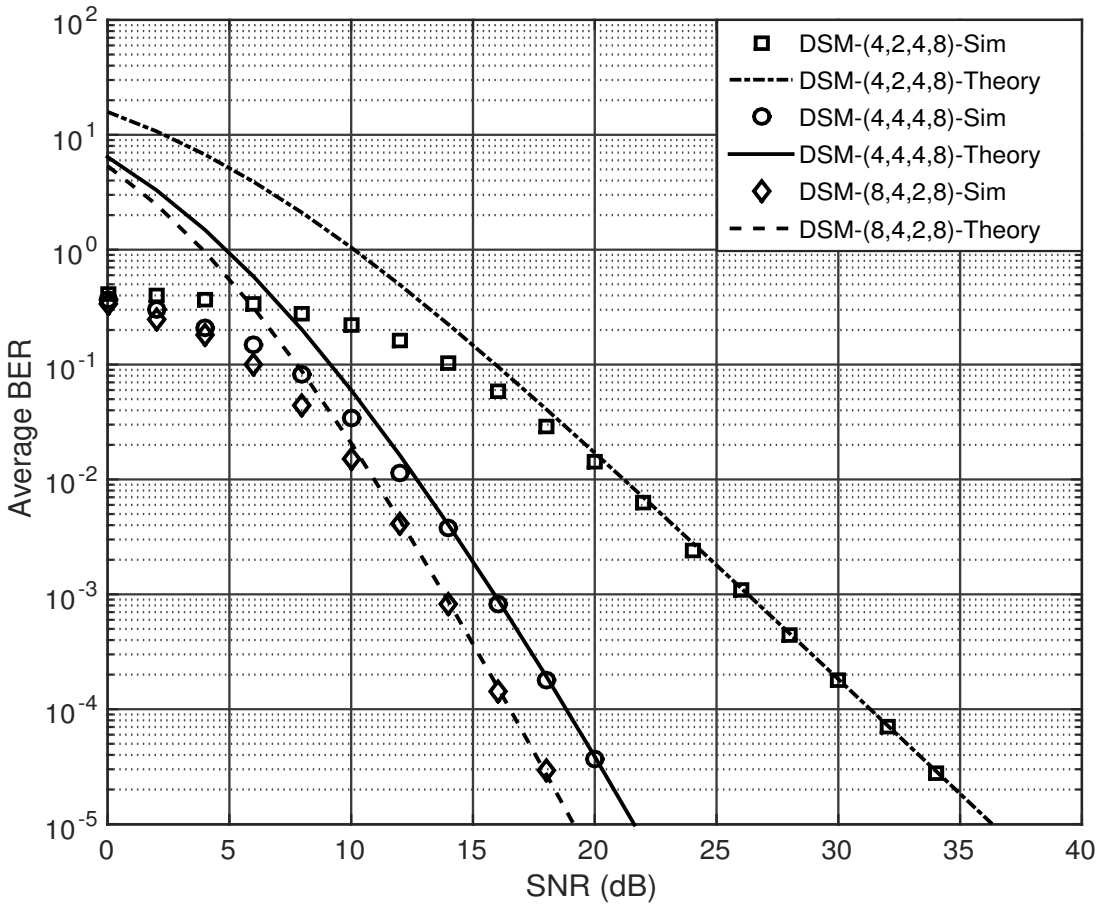

Figure 4.4: Theoretical and simulated BER performance of DSM for $\eta_{DSM} = 8$ b/s/Hz.

In Figure 4.4, the analytical and Monte Carlo simulation results for 4×2, 4×4, and 8×4 DSM systems with spectral efficiency of $\eta_{DSM} = 8$ b/s/Hz are presented. The Monte Carlo simulation results validate the analytical performance of DSM as the simulation closely matches the analytical performance at high SNR. At a BER of 10^{-5}, 4×4 4-QAM QSM has an SNR gain of 14.3 dB over 4×2 4-QAM for DSM.

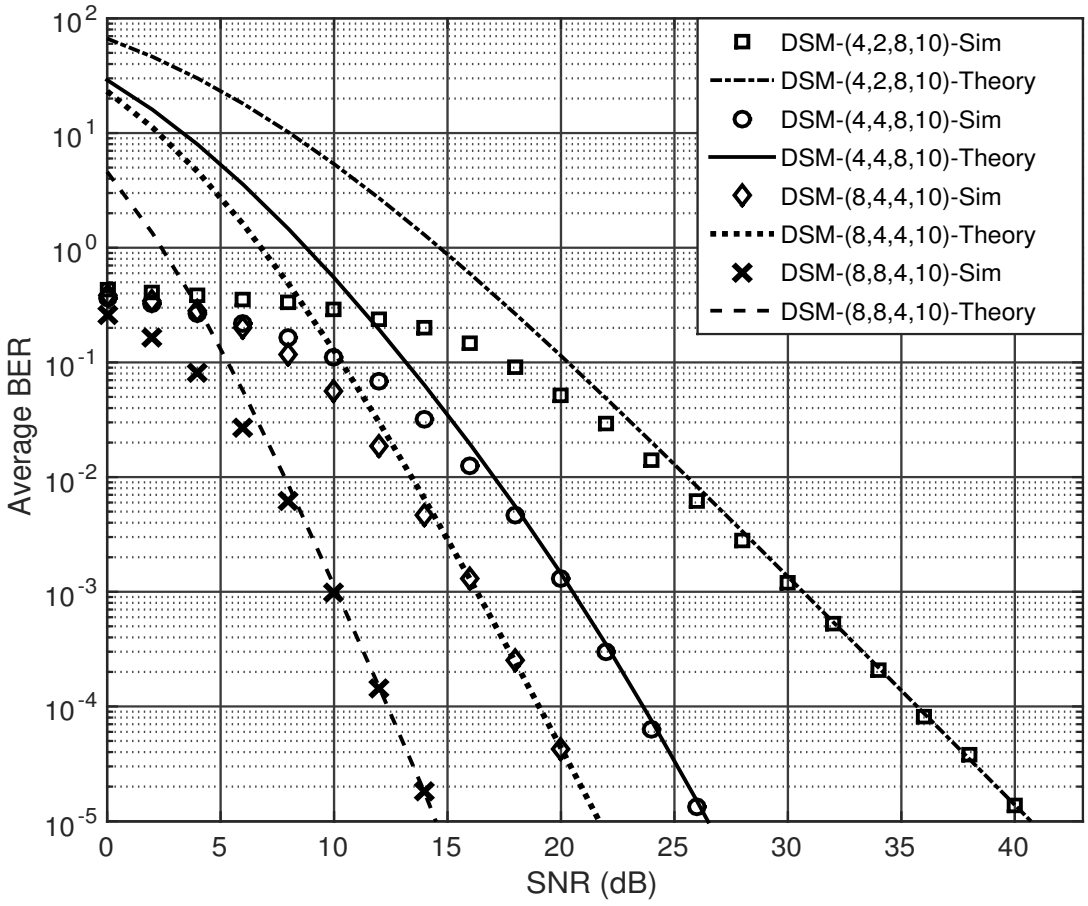

Figure 4.5: Theoretical and simulated BER performance of DSM for $\eta_{DSM} = 10$ b/s/Hz.

In Figure 4.5, the analytical and Monte Carlo simulation results for 4×2, 4×4, 8×4, and 8×8 DSM systems with spectral efficiency of $\eta_{DSM} = 10$ b/s/Hz are presented. The Monte Carlo simulation results validate the analytical performance of DSM as the simulation closely matches the analytical performance at high SNR regions. An investigation on the BER shows that DSM error performance improves with an increase in the number of receive antennas for systems with the same spectral efficiency. At a BER of 10^{-5}, 4×4 8-QAM DSM has an SNR gain of 14.3 dB over 4×2 8-QAM DSM, and at a BER of 10^{-5}, 8×8 4-QAM has an SNR gain of 7.5 dB over 8×4 4-QAM for DSM.

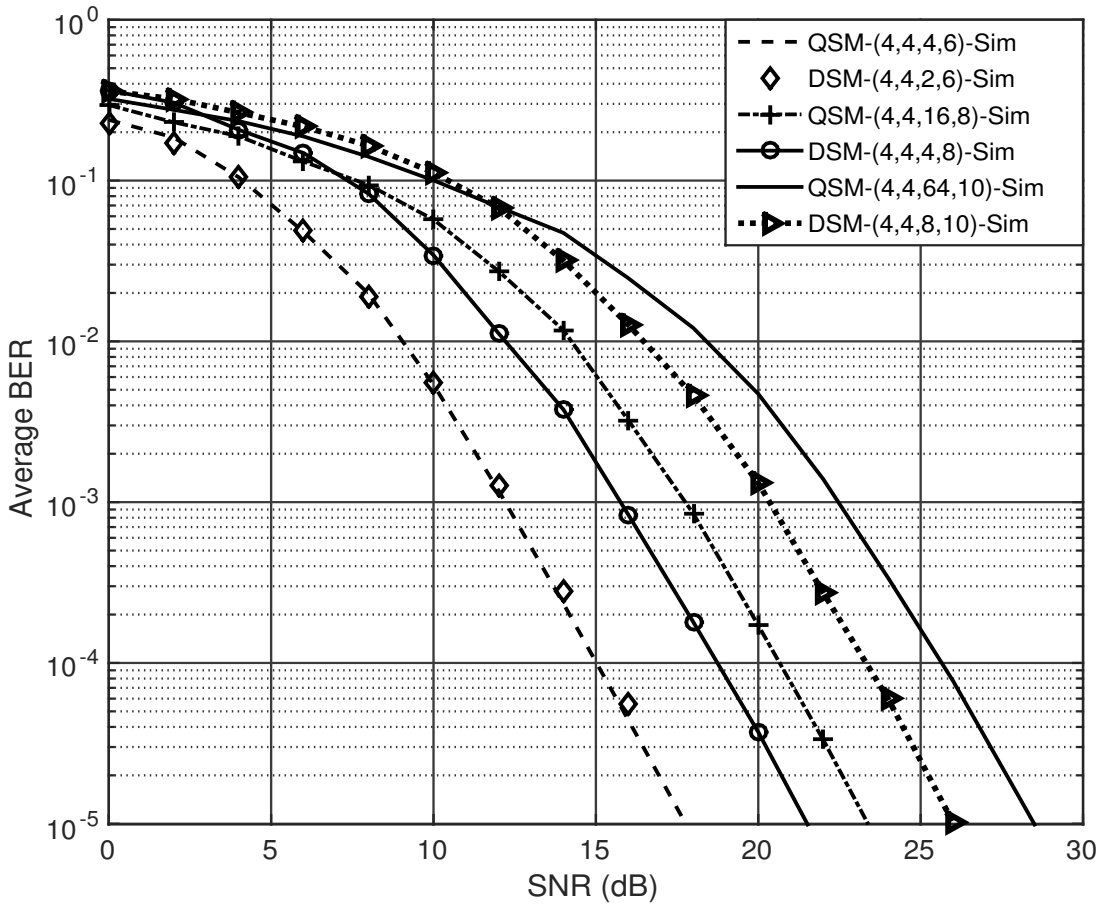

Figure 4.6: BER performance of QSM and DSM for η_{QSM}, η_{DSM} = 6, 8, 10 b/s/Hz.

In Figure 4.6, the BER performance of 4×4 QSM and DSM systems are compared for spectral efficiencies of $\eta_{QSM} = \eta_{DSM} = 6$, 8, and 10 b/s/Hz. Note that, the error performance of QSM and DSM with spectral efficiency of $\eta_{QSM} = \eta_{DSM} = 6$ b/s/Hz is closely matched at all SNR points. If we consider the optimum rotation angle for BPSK given, at $\theta = 90°$, the second transmission symbol is fundamentally equal to $(\pm j)$, and the first transmission symbol $x_1^q = (\pm 1)$. The summation of these two symbols essentially gives a 4-QAM constellation symbol as $(\pm 1 \pm j)$; therefore, the error performance of DSMBM and QSMBM is identical [30]. As the modulation order of the two systems is increased, DSM demonstrates an improved error performance as compared to QSM. At a BER of 10^{-5}, 4-QAM DSM with η_{DSM}=8 b/s/Hz has an SNR gain of 2.9 dB over 16-QAM QSM with η_{QSM}=8 b/s/Hz. At a BER of 10^{-5}, 8-QAM DSM with η_{DSM}=10 b/s/Hz has an SNR gain of 2.3 dB over 64-QAM QSM with η_{QSM}=10 b/s/Hz.

4.6.1 BER performance of DSM SOMLD

In Section 4.4, the setting for all coded cases, a $\frac{1}{2}$-rate convolutional encoder was employed to encode the information bits under the constraint length of 9 with code generator matrices

$g_1 = (561)_{octal}$; $g_2(753)_{octal}$ [41, 42, 50]. At the detector, the proposed SOMLD is employed, and the output is fed into a soft-input Viterbi channel decoder in order to estimate the transmitted information [40].

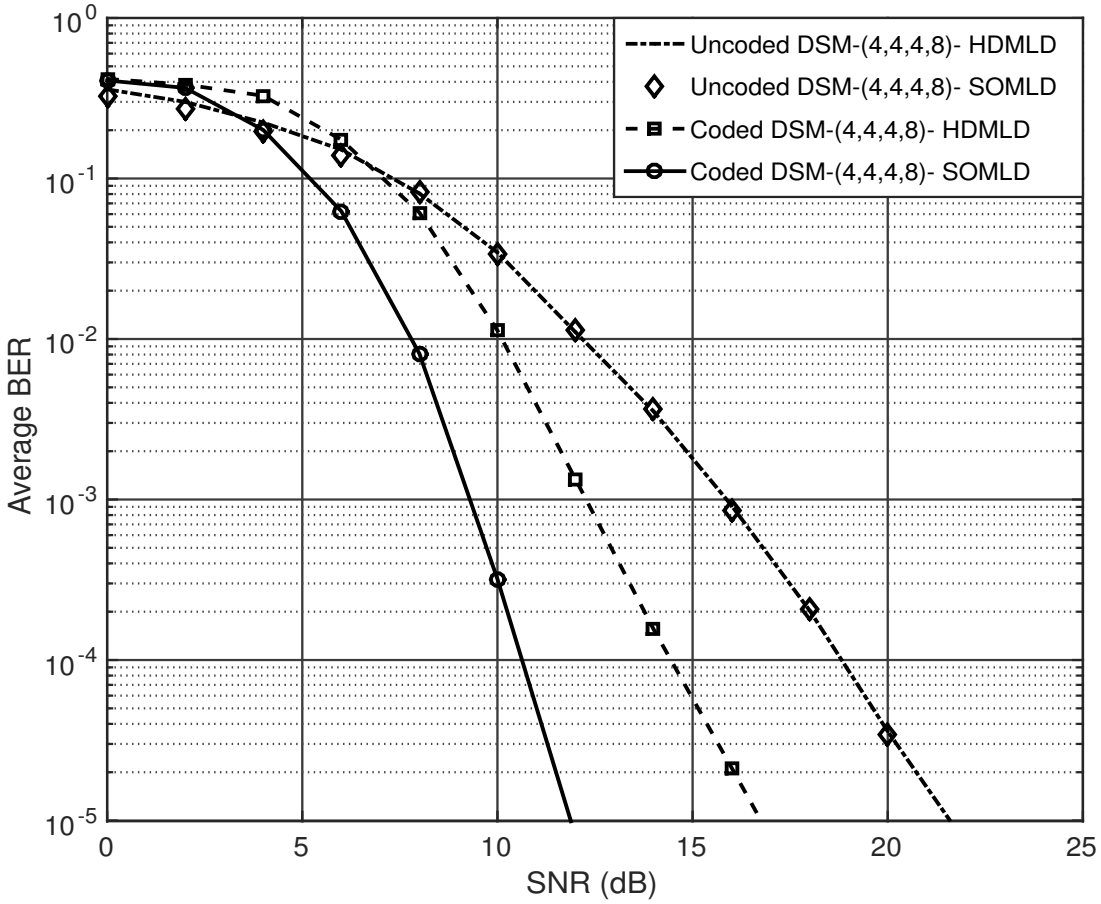

Figure 4.7: BER performance of DSM for the SOMLD and HDMLD with $\eta_{DSM} = 8$ b/s/Hz.

Figure 4.7 shows the simulation results for uncoded channels for the proposed SOMLD and the HDMLD for DSM at spectral efficiency of η_{DSM}= 8 b/s/Hz. The optimal detector given in (4.9) is regarded as the HDMLD for DSM. The uncoded cases show that the HDMLD matches the SOMLD error performance. This is the expected result since SOMLDs only has an effect in coded channels with a soft input decoder at the receiver can give coding gain [50]. For coded channels, the proposed SOMLD for DSM demonstrates coding gain over the uncoded SOMLD. At a BER of 10^{-5}, coded SOMLD outperforms uncoded SOMLD with an SNR gain of 9.6 dB, while coded HDMLD has an SNR gain of 4.8 dB as compared to uncoded HDMLD.

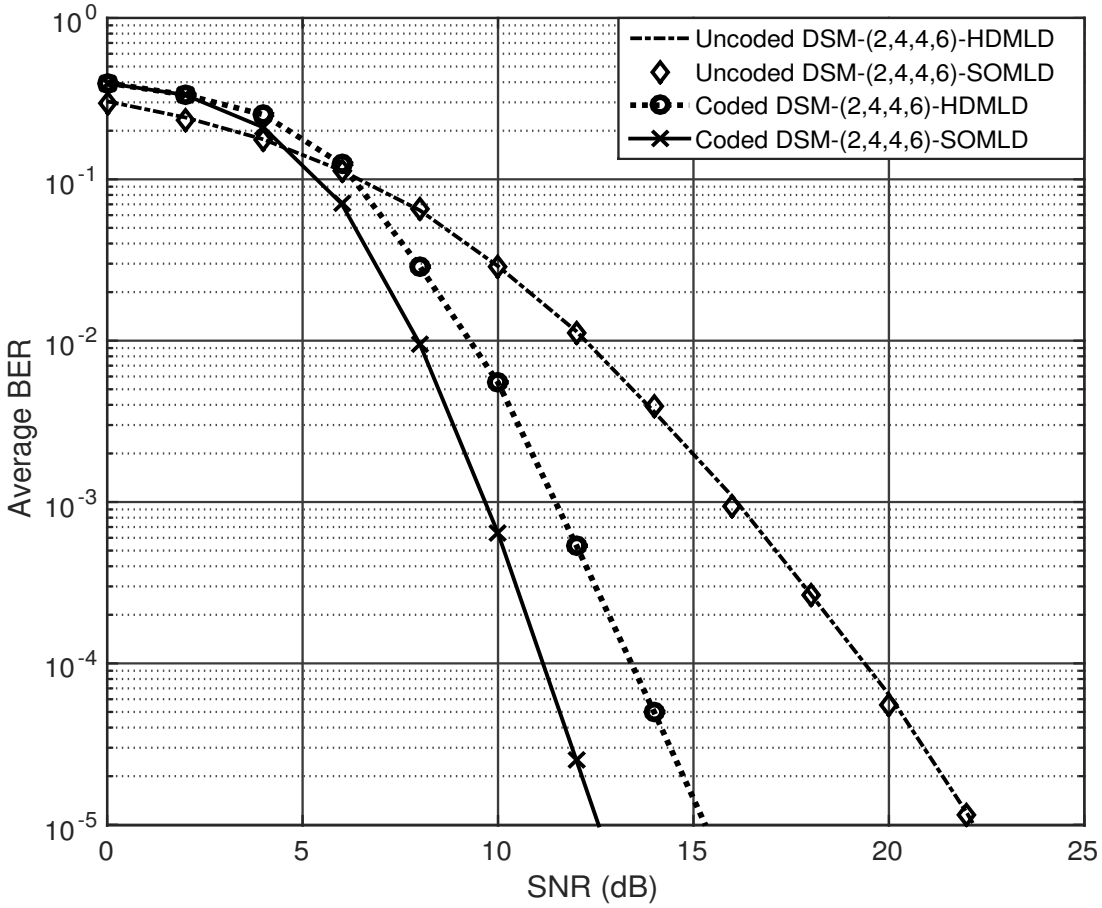

Figure 4.8: BER performance of DSM for the SOMLD and HDMLD with $\eta_{DSM} = 6$ b/s/Hz.

Figure 4.8 shows the simulation results for uncoded channels for the proposed SOMLD and the HDMLD for DSM at spectral efficiency of $\eta_{DSM} = 6$ b/s/Hz. For uncoded cases, the SOMLD error performance is consistent with the uncoded HDMLD error performance, therefore validating the detector. For coded channels, the proposed SOMLD for DSM demonstrates coding gain over the uncoded SOMLD. At a BER of 10^{-5}, coded SOMLD outperforms uncoded SOMLD with an SNR gain of 9.5 dB, while coded HDMLD has an SNR gain of 6.7 dB as compared to uncoded HDMLD.

4.7 Summary

The performance analysis for DSM employing the asymptotic union bound approach to calculate the average BER performance over i.i.d. Rayleigh frequency-flat fading channel was formulated. The analytical results were consistent with the Monte Carlo simulations at high SNR regions, therefore validating the theoretical performance of DSM. The BER performance of DSM and QSM are presented and demonstrated that DSM has a better error performance than QSM

for systems with identical spectral efficiency given that the APM modulation order for DSM is higher than two. The proposed SOMLD is validated by the results shown from the simulation of uncoded HDMLD and SOMLD systems. In coded channels, both the HDMLD and SOMLD demonstrated significant SNR gains.

Chapter 5

Media Based Modulation

5.1 Introduction

The next-generation wireless communications require substantial improvements in data rates and error performance in order to support the proliferating media applications such as IoT, cloud computing, and enterprise software applications [6, 7]. MIMO systems still hold promise to achieve these improvements and are considered one of the core techniques for improving data rates and error performance [17, 19]. However, drawbacks such as ICI, IAS, and relatively high-complexity receive algorithms have limited the potential of MIMO and has motivated researchers to investigate other modulation schemes.

MBM with RF mirrors is a recently proposed wireless communication technique, which has attracted much research attention [32–34]. The innovative idea of MBM involves embedding information into a channel state by varying RF properties, such as permittivity, permeability, and resistivity around a transmit antenna [33]. One of the methods employed to vary the channel state is to place RF mirrors around a transmit antenna, then switch the RF mirrors ON/OFF. Each individual state of these RF mirrors is referred to as a MAP, and each MAP creates a rich scattering environment at the transmit antenna, which results in independent end-to-end channel realizations at the receiver. Several advantages of MBM can be summarized as follows [32–34]:

1. A single transmit antenna can achieve multiple fade paths.

2. Spectral efficiency can be improved by increasing the number of receive constellation points without an increase in transmit power.

3. MAPs give MBM inherent diversity due to an increased constellation size, since there

are good and bad channel realizations; constellation diversity effectively converts a static multi-path fading channel into an AWGN channel with effective signal energy equal to the average received energy.

4. The increase in constellation diversity does not require the system to sacrifice data rate.

5. There is no fundamental restriction on the size of the RF mirror transmit unit.

6. It is possible to save energy through the selection of a subset of channel configurations from the MAP constellations resulting in overall improved performance.

Several schemes, such as SM, GSM, and QSM, have been extended to include MBM, and significant improvements in spectral efficiency and error performance was demonstrated [33, 35, 36]. Evidently, the application of MBM to traditional SBM techniques improves error performance and/or spectral efficiency. The purpose of this chapter is to present the MBM concept by demonstrating its application to SIMO systems [33]. SIMO systems, coupled with MBM, are referred to as SIMO-MBM. In this chapter, we present the system model, detection scheme, and analytical error performance of SIMO-MBM. Monte Carlo simulations are presented, which serve to validate the analytical performance of SIMO-MBM.

5.2 System model for SIMO-MBM

Figure 5.1 illustrates the system model of SIMO-MBM with a single MBM-TU containing M_{RF} mirrors and N_R receive antennas.

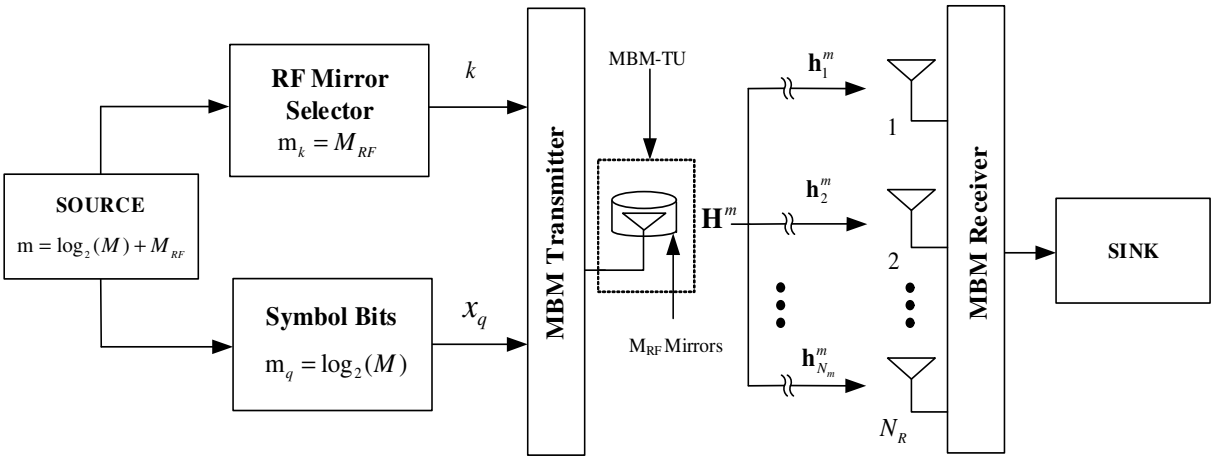

Figure 5.1: System Model for the SIMO-MBM scheme

Consider the MBM-TU with M_{RF} RF mirrors shown in Figure 5.1. If a single RF mirror gives rise to two different channel fade realizations and assuming that M_{RF} is the total number of available RF mirrors in the MBM-TU, then the total number of MAPs available is given by $N_m = 2^{M_{RF}}$. Therefore, the fading channel for an MBM-TU is represented as an $N_R \times N_m$ matrix $\mathbf{H}^m$ [33].

In each transmission interval, the source provides an input bit vector of length $m = \log_2(M) + M_{RF}$ bits, where M is the modulation order of the APM symbol. The information is divided into two parts. The first part is mapped to the RF mirror selector, such that $\mathrm{m}_k = M_{RF}$ bits are used to select a MAP index k, $k \in [1 : N_m]$, and the second part is mapped, such that $\mathrm{m}_q = \log_2 M$ bits are used to select a Gray-coded M-QAM or M-PSK signal constellation symbol x_q, $q \in [1 : M]$, to convey information. The spectral efficiency of SIMO-MBM is given as [34]:

$$\eta_{SIMO-MBM} = \log_2 M + M_{RF} \quad \text{b/s/Hz.} \tag{5.1}$$

As shown in (5.1), the spectral efficiency of SIMO-MBM can be increased linearly by increasing the number of M_{RF} mirrors or by increasing the modulation order of the APM symbol. The example illustrated in Table 5.1 demonstrates the mapping procedure for a Gray-coded 4-QAM SIMO-MBM system with $M_{RF} = 4$, and spectral efficiency of 6 b/s/Hz. Only a few random data streams are considered.

Table 5.1: Illustration of the mapping procedure for SIMO-MBM

Source Bits m	**MAP Index** k	M**-QAM Symbol** x_q
$[\,0\,0\,1\,0\,0\,0\,]$	$[\,0\,0\,1\,0\,] = 3$	$[\,0\,0\,] = 1+i$
$[\,0\,1\,1\,1\,0\,1\,]$	$[\,0\,1\,1\,1\,] = 8$	$[\,0\,1\,] = -1+i$
$[\,1\,1\,0\,0\,1\,0\,]$	$[\,1\,1\,0\,0\,] = 13$	$[\,1\,0\,] = -1-i$
$[\,0\,1\,0\,1\,1\,1\,]$	$[\,0\,1\,0\,1\,] = 6$	$[\,1\,1\,] = 1-i$
$[\,1\,0\,1\,0\,0\,0\,]$	$[\,1\,0\,1\,0\,] = 11$	$[\,0\,0\,] = 1+i$

The fading channel for an MBM-TU is represented by an $N_R \times N_m$ Rayleigh frequency-flat fading channel gain matrix $\mathbf{H}^m = [\mathbf{h}_1^m \dots \mathbf{h}_{N_m}^m]$, which contains all available N_m MAPs. The M-QAM or M-PSK symbol x_q is transmitted over a fading channel selected from the MBM-TU MAP with a channel fade given by the $N_R \times 1$ vector $\mathbf{h}_k^m = [h_1^{m,k} \dots h_{N_R}^{m,k}]^T,\ k \in [1 : N_m]$ in the presence of AWGN. AWGN is represented by vector $\mathbf{n}$ of dimension $N_R \times 1$. All elements of $\mathbf{H}^m$ and $\mathbf{n}$ are assumed to be i.i.d. with Gaussian distribution of zero mean and unit variance $\sim CN(0,1)$. The received signal for SIMO-MBM is given by an $N_R \times 1$ vector $\boldsymbol{y}$:

$$\boldsymbol{y} = \sqrt{\rho}\, \mathbf{h}_k^m x_q + \mathbf{n}\,, \tag{5.2}$$

where ρ is the average SNR at each receive antenna, and $\mathbf{h}_k^m$ represents the k^{th} MAP from the MBM-TU fading channel gain matrix $\mathbf{H}^m$.

5.3 SIMO-MBM Detection

In the detection of SIMO-MBM, we assume that perfect CSI is known at the MBM receiver in all instances. The MBM receiver estimates the transmitted signal via an exhaustive ML search were all the possible signal constellation points, and MAPs are considered. The MBM receiver selects the ML calculation with the minimum argument as the estimated received signal of the transmitted information. The ML detector for SIMO-MBM is given as:

$$[\hat{x}_q, \hat{k}] = \underset{\substack{q \in [1:M] \\ k \in [1:N_m]}}{\operatorname{argmin}} \left(\|\boldsymbol{y} - \sqrt{\rho}\, \mathbf{h}_k^m x_q\|_F^2 \right). \tag{5.3}$$

If we let $\boldsymbol{g}_{qk} = \sqrt{\rho}\,\mathbf{h}_k^m x_q$ and expand the Frobenius norm in (5.3), then the ML detector can be simplified to yield:

$$[\hat{x}_q, \hat{k}] = \underset{\substack{q \in [1:M] \\ k \in [1:N_m]}}{\operatorname{argmin}} \left\{ \|\boldsymbol{g}_{qk}\|_F^2 - 2\Re\{\boldsymbol{y}^H \boldsymbol{g}_{qk}\} \right\}. \tag{5.4}$$

Note, the expression in (5.4) is the optimal ML detector for SIMO-MBM.

5.4 Performance Analysis for SIMO-MBM

In this section, the analytical lower bound performance analysis approach is used to calculate the ABEP for SIMO-MBM. The SIMO-MBM model in (5.2) may be viewed as an $N_R \times N_m$ SM system. Hence, the theoretical derivation of SM may be extended to SIMO-MBM [25, 36]. Similar to the case in SM, we denote P_m as the bit error probability for the MAP index given that the symbol is perfectly estimated, and P_d represents the bit error probability of the symbol given that the MAP index is perfectly estimated. The overall probability of error P_e for SIMO-MBM is given as a combination of both the symbol bit error probability and the MAP index error probability, and it is expressed as [23, 25]:

$$P_e \geq P_b + P_m - P_b P_m \,. \tag{5.5}$$

5.4.1 Analysis of Symbol Bit Error Probability

The symbol bit error probability is given as an approximation in [25] as:

$$P_b \cong \frac{\text{SER}}{n}, \tag{5.6}$$

where $n = \log_2 M$ is the number of bits per symbol, and SER is the average symbol error probability for M-QAM over i.i.d. Rayleigh frequency-flat fading channel [25]. The SER in [25] is given as:

$$\text{SER} = \frac{a}{c}\left[\frac{1}{2}\left(\frac{2}{b\rho+2}\right)^{N_R} - \frac{a}{2}\left(\frac{1}{b\rho+1}\right)^{N_R} + (1-a)\sum_{i=1}^{c-1}\left(\frac{\beta_i}{b\rho+\beta_i}\right)^{N_R} + \sum_{i=c}^{2c-1}\left(\frac{\beta_i}{b\rho+\beta_i}\right)^{N_R}\right], \tag{5.7}$$

where $a = 1 - \frac{1}{\sqrt{M}}$, $b = \frac{3}{M-1}$, $\beta_i = \sin^2\theta_i$, $\theta_i = \frac{i\pi}{4c}$, N_R is the number of receive antennas, and c is the number of iterations of convergence, $c = 10$.

5.4.2 Analysis of MAP Index Error Probability

The bit error probability of the MAP index is computed in a similar manner presented in [25,36]. Given that the transmit symbol is decoded perfectly, the average BER of the MAP index is calculated using the union bounded approach and is given as:

$$P_m \leq \sum_{q=1}^{M} \sum_{k=1}^{N_m} \sum_{\hat{k}=1}^{N_m} \frac{N(k,\hat{k}) P(x_{qk} \rightarrow x_{q\hat{k}})}{M N_m}, \tag{5.8}$$

where $P(x_{qk} \rightarrow x_{q\hat{k}})$ is the PEP of selecting $x_{q\hat{k}}$, given that x_{qk} was transmitted, and $N(k,\hat{k})$ is the number of bit errors between the MAP index k and the estimated MAP index $\hat{k}$. The conditional PEP of the channel matrix is given in [25] as:

$$P(x_{qk} \rightarrow x_{q\hat{k}} | \mathbf{H}^m) = P(\|\boldsymbol{y} - \sqrt{\rho}\mathbf{h}_{\hat{k}}^m x_q\|_F < \|\boldsymbol{y} - \sqrt{\rho}\mathbf{h}_k^m x_q\|_F) = Q(\sqrt{k}), \tag{5.9}$$

where k is a central chi-squared RV with $2N_R$ degrees of freedom and is defined as:

$$k = \frac{\rho}{2}\|(\mathbf{h}_k^m x_q - \mathbf{h}_{\hat{k}}^m x_q)\|_F^2 = \sum_{n=1}^{2N_R} \alpha_n^2, \tag{5.10}$$

where $\alpha_n \sim N(0, \sigma_\alpha^2)$ and the variance $\sigma_\alpha^2 = \frac{\rho}{2}|x_q|^2$. The PDF of k is defined as [25]:

$$p_k(\upsilon) = \frac{\upsilon^{N_R-1} e^{\frac{-\upsilon}{2\sigma_\alpha^2}}}{\left(2\sigma_\alpha^2\right)^{N_R}\Gamma\left(N_R\right)} \quad , \upsilon \geq 0. \tag{5.11}$$

Since the distribution of k is known, the PEP in (5.8) is calculated as [25]:

$$P(\mathbf{x}_{qk} \rightarrow \mathbf{x}_{q\hat{k}}) = \int_{\upsilon=0}^{\infty} Q(\sqrt{\upsilon}) p_k(\upsilon) \mathrm{d}\upsilon. \tag{5.12}$$

The closed-form representation for (5.12) is given as [25, 36]:

$$P(\boldsymbol{x}_{qk} \rightarrow \boldsymbol{x}_{q\hat{k}}) = \mu_\alpha^{N_R} \sum_{k=0}^{N_R-1} \binom{N_R - 1 + k}{k} [1 - \mu_\alpha]^k, \tag{5.13}$$

where $\mu_\alpha = \frac{1}{2}\left(1 - \sqrt{\frac{\sigma_\alpha^2}{\sigma_\alpha^2+1}}\right)$.

5.5 Numerical Analysis of the Analytical and Simulated BER Performance of SIMO-MBM

In this section, the ABEP for SIMO-MBM formulated using the lower bound approach is presented. Monte Carlo simulation results executed in a Matlab environment and are presented to validate the analytical result in Section 5.4. All Monte Carlo simulations are performed over i.i.d. Rayleigh frequency-flat fading channels in the presence of AWGN and Gray-coded M-QAM signal constellations are employed. It is assumed that complete CSI is known at the receiver in all instances.

Monte Carlo simulations are presented for spectral efficiencies of 4, 6, and 8 b/s/Hz, and results are presented in graphs of average BER versus SNR. The notation used to denote a SIMO-MBM system with N_R receive antennas, and M_{RF} RF mirrors is $(M, N_R, M_{RF}, \eta_{SIMO-MBM})$.

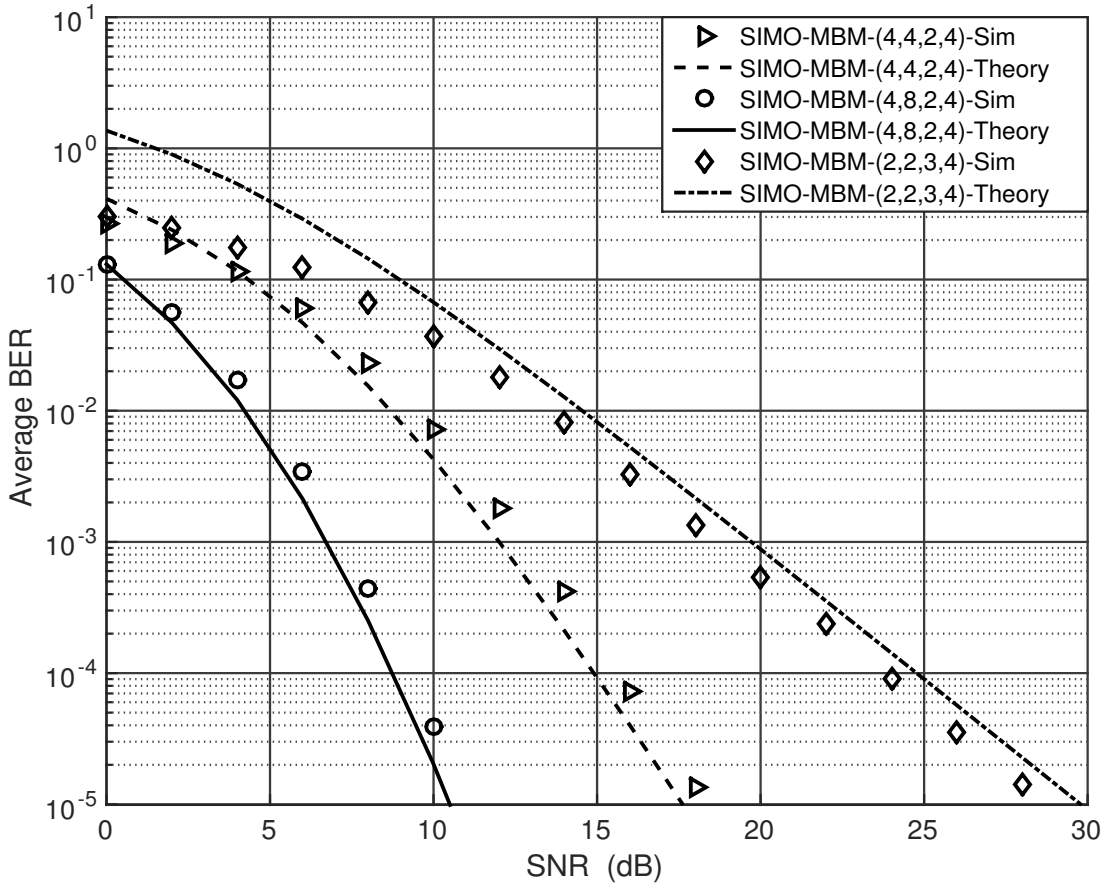

Figure 5.2: Theoretical and simulated BER performance of SIMO-MBM for $\eta_{SIMO-MBM} = 4$ b/s/Hz.

In Figure 5.2, the ABEP of the SIMO-MBM is analyzed for systems with $M_{RF} = 2$ and 3. The BER performance for 4-QAM SIMO-MBM with spectral efficiency of $\eta_{SIMO-MBM} = 4$

b/s/Hz with $N_R = 2$, 4, and 8 are presented. The Monte Carlo BER performance is relatively tight and matches the analytical BER performance, therefore, verifying the theoretical performance of SIMO-MBM. An investigation of the results shows that the BER performance of SM improves with an increase in the number of receive antennas for systems with the same spectral efficiency. For an identical M_{RF} setting, at a BER of 10^{-5}, 4-QAM SIMO-MBM with $N_R = 8$ has an approximate SNR gain of 7.5 dB over 4-QAM SIMO-MBM with $N_R = 4$.

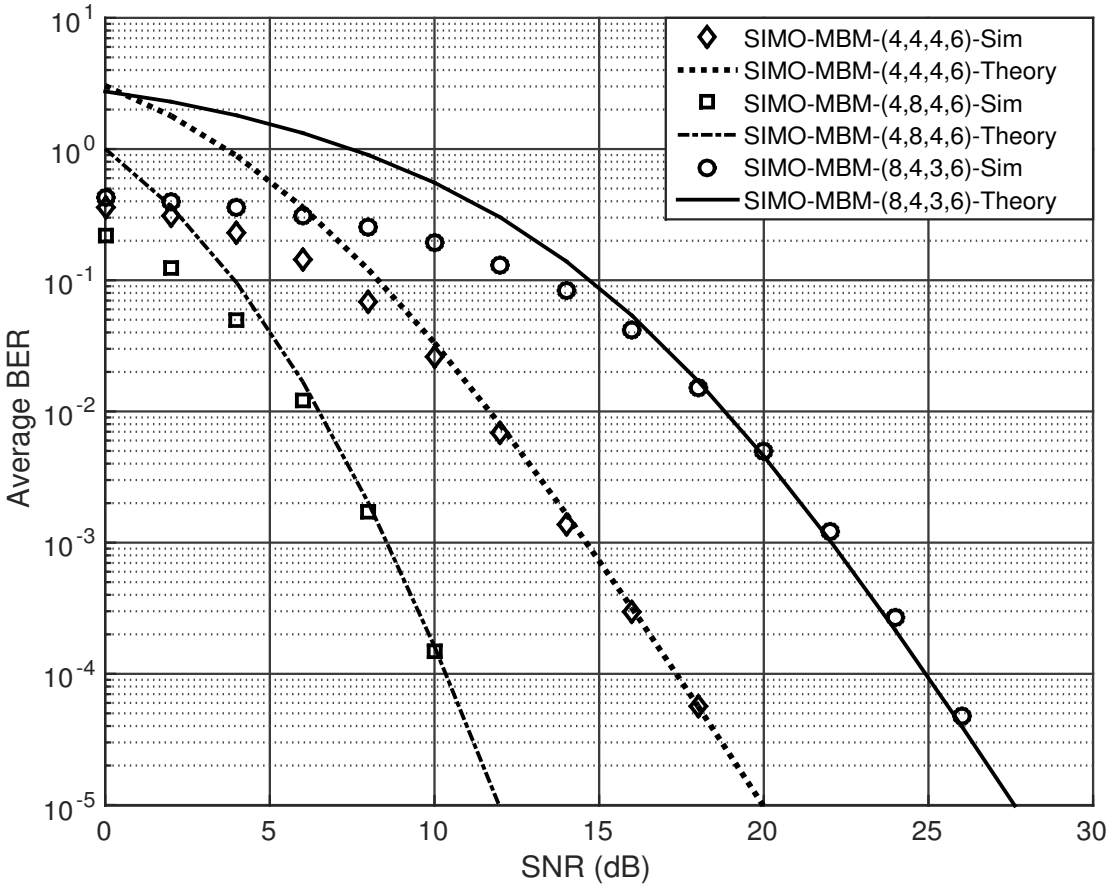

Figure 5.3: Theoretical and simulated BER performance of SIMO-MBM for $\eta_{SIMO-MBM} = 6$ b/s/Hz.

In Figure 5.3, the ABEP of the SIMO-MBM is analyzed for systems with $M_{RF} = 3$ and 4. The BER performance for 4-QAM SIMO-MBM with spectral efficiency of $\eta_{SIMO-MBM} = 6$ b/s/Hz with $N_R = 4$ and 8 are presented. The Monte Carlo simulation error performance is relatively tight with the analytical error performance, which verifies the theoretical analysis for SIMO-MBM. An increase in error performance is observed when the number of receive antennas is increased for systems with identical spectral efficiency. At a BER of 10^{-5}, 4-QAM SIMO-MBM with $N_R = 8$ has an SNR gain of 9.2 dB over 4-QAM SIMO-MBM with $N_R = 4$.

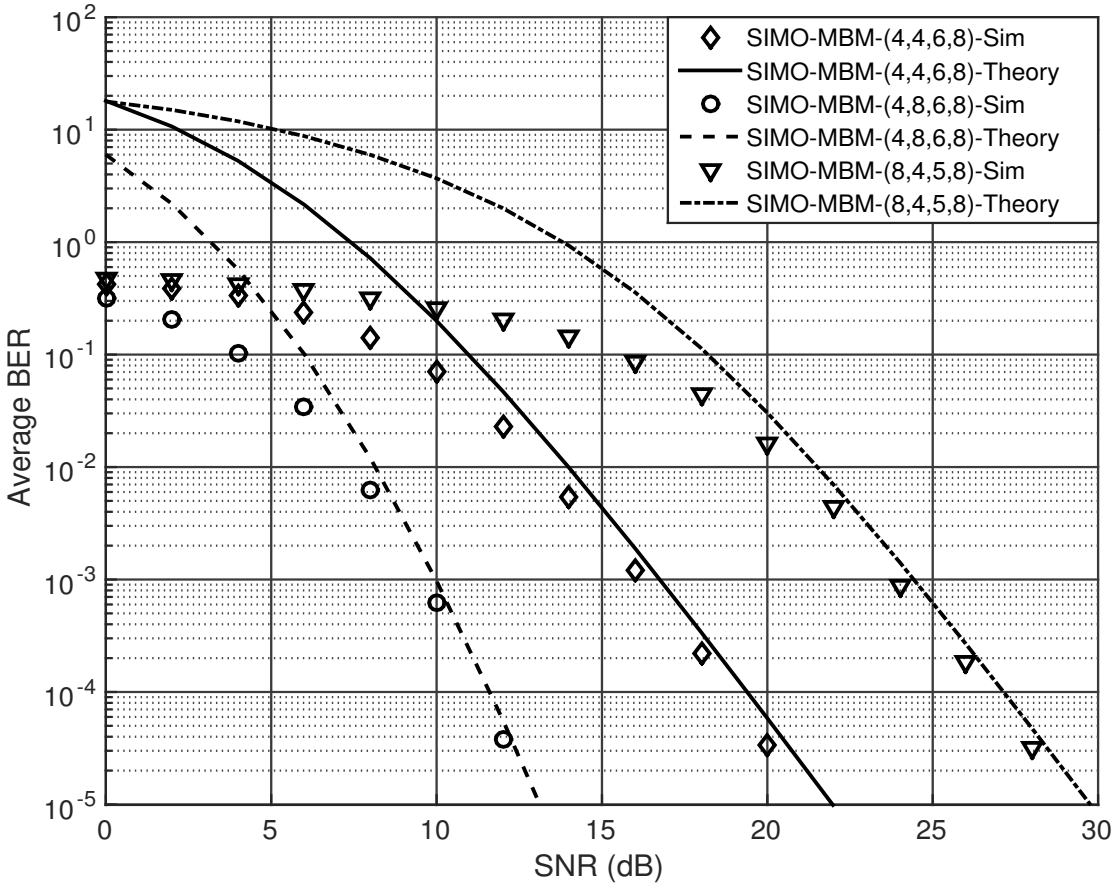

Figure 5.4: Theoretical and simulated BER performance of SIMO-MBM for $\eta_{SIMO-MBM} = 8$ b/s/Hz.

In Figure 5.4, the ABEP of the SIMO-MBM is analyzed for systems with 5 and 6 M_{RF} mirrors. The BER performance for 4-QAM SIMO-MBM with spectral efficiency of $\eta_{SIMO-MBM} = 8$ b/s/Hz with $N_R = 4$ and 8 are presented. The Monte Carlo simulation results validate the analytical performance of SIMO-MBM as it is demonstrated that the analytical results are closely matched by the simulation results. At a BER of 10^{-5}, 4-QAM SIMO-MBM with $N_R = 8$ has an SNR gain of 7.5 dB over 4-QAM SIMO-MBM with $N_R = 4$.

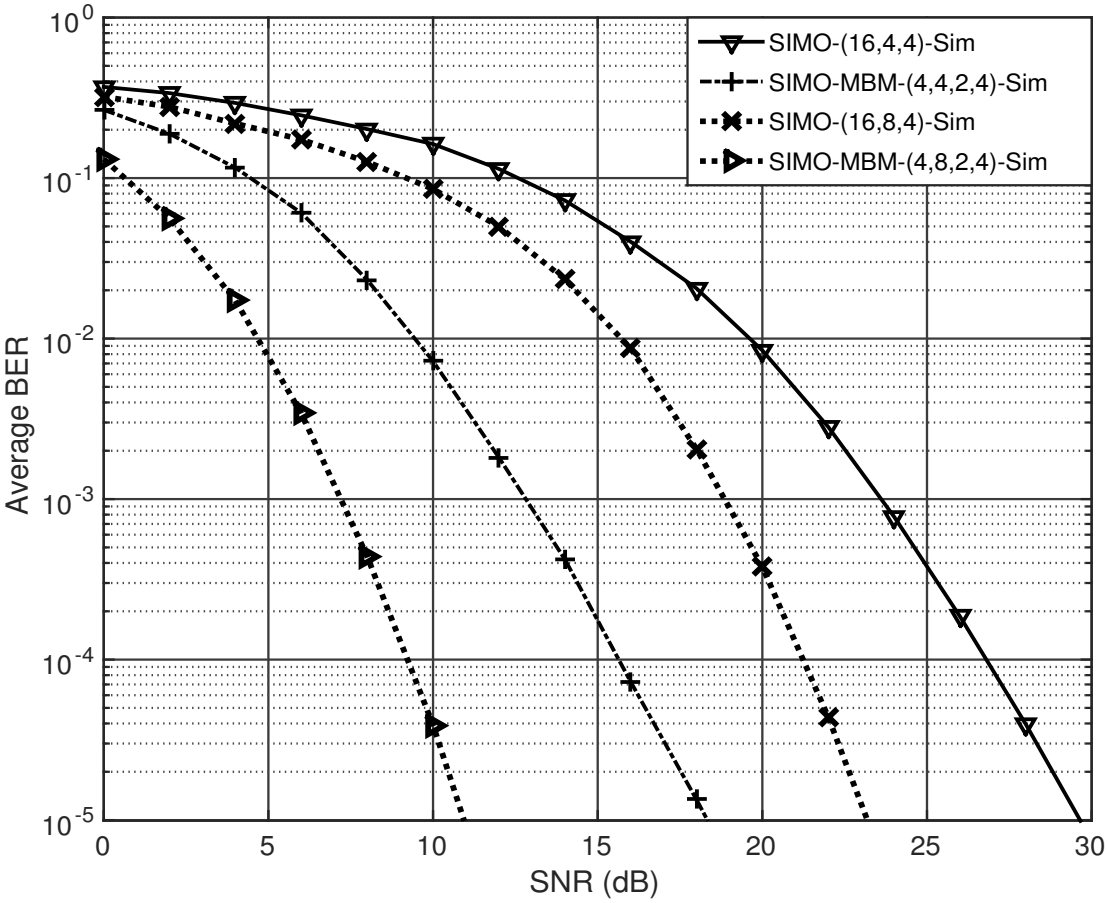

Figure 5.5: BER performance of SIMO and SIMO-MBM for $\eta_{SIMO-MBM}, \eta_{SIMO} = 8$ b/s/Hz.

In Figure 5.5, the BER performance for SIMO and SIMO-MBM with spectral efficiency of $\eta_{SIMO-MBM}$, $\eta_{SIMO} = 4$ b/s/Hz are presented. Simulation results for SIMO systems with 4 and 8 receive antennas are shown. The SIMO-MBM system employs two M_{RF} mirrors, and significant SNR gains is demonstrated. At a BER of 10^{-5}, 4-QAM SIMO-MBM has an SNR gain of 12.1 dB over 16-QAM SIMO for a system with N_R=4, and at a BER of 10^{-5}, 4-QAM SIMO-MBM has an SNR gain of 12.8 dB over 16-QAM SIMO with N_R=8.

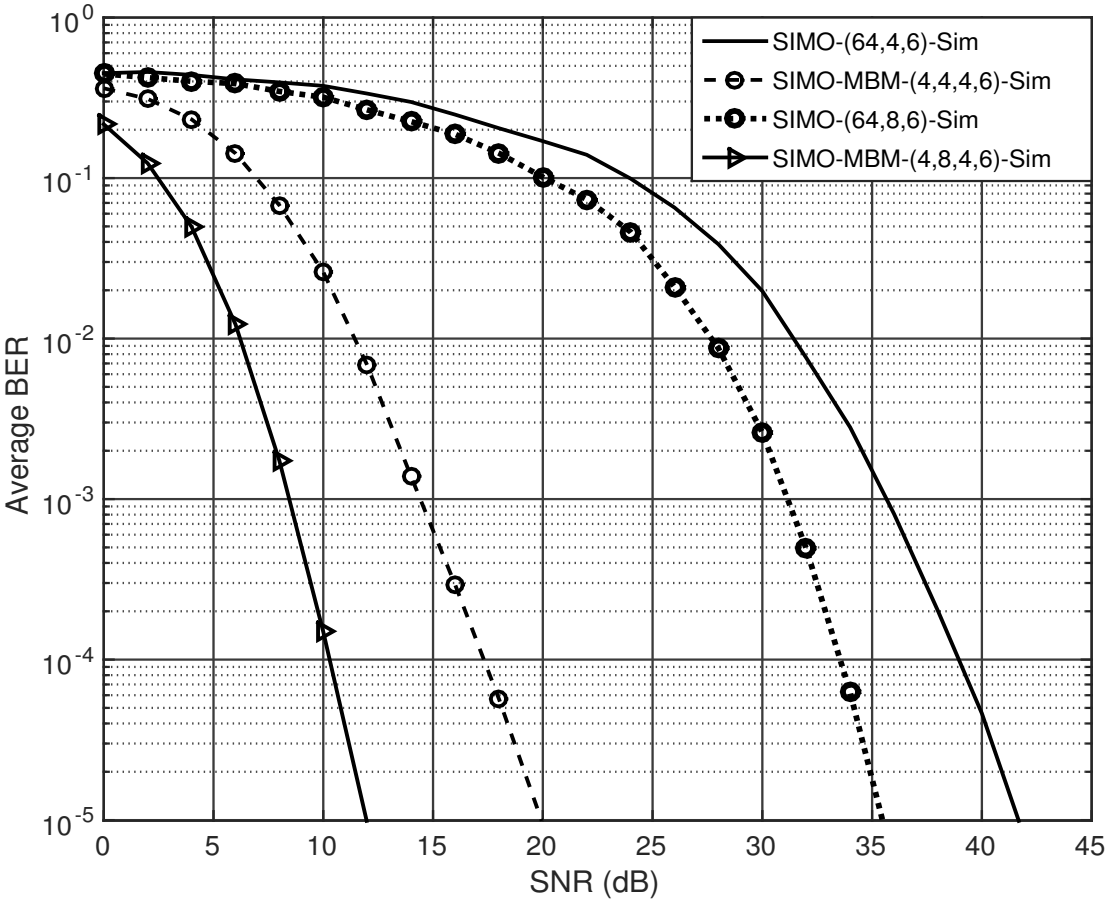

Figure 5.6: BER performance of SIMO and SIMO-MBM for $\eta_{SIMO-MBM}, \eta_{SIMO} = 6$ b/s/Hz.

In Figure 5.6, the BER performance for SIMO and SIMO-MBM with spectral efficiency of $\eta_{SIMO-MBM}$, $\eta_{SIMO} = 6$ b/s/Hz are presented. Simulation results for SIMO systems with 4 and 8 receive antennas are shown. The SIMO-MBM system employs four M_{RF} mirrors, and significant SNR gain is demonstrated. At a BER of 10^{-5}, 4-QAM SIMO-MBM has an approximate SNR gain of 21.1 dB over 64-QAM SIMO for a system with N_R=4, and at a BER of 10^{-5}, 4-QAM SIMO-MBM has an approximate SNR gain of 23.2 dB over 64-QAM SIMO for a system with N_R=8.

5.6 Summary

The performance analysis for SIMO-MBM employing the lower bound approach to calculate the average BER performance over i.i.d. Rayleigh frequency-flat fading channel was formulated. The analytical result is relatively tight with the simulated BER of SIMO-MBM, therefore, validating the analytical performance of SIMO. The simulation results for SIMO and SIMO-MBM were presented, and significant gains in error performance were demonstrated.

Chapter 6

Double Spatial Media-based Modulation

6.1 Introduction

The perpetual increase in demand for multimedia services for the next-generation WCS requires a substantial improvement in error performance and data rates. MIMO systems are considered one of the essential techniques for improving error performance and data rates. However, MIMO systems face challenges, such as ICI, IAS, and relatively high-complexity receive algorithms which therefore reduce the potential of these systems [12, 17, 18].

IM has recently been receiving much research attention as a promising candidate for next-generation wireless networks due to its capability of employing indices in communication systems, which form part of the building blocks used to convey additional information bits [21, 22]. SM is a novel MIMO based scheme that is a widespread realization of the IM technique that provides an energy efficient method by exploiting spatial multiplexing [23, 44]. Unlike the traditional MIMO, SM employs only a single active transmit antenna to transmit a signal using a single RF chain. SM has relatively low-complexity receive algorithms, ICI, and IAS [25]. However, there are growing concerns over the potential of these schemes to substantially increase their data rate and improve error performance to support next-generation wireless communications.

Several significant SM-based schemes have been proposed in the literature, which includes QSM and DSM [29, 30]. QSM is a scheme that improves the spectral efficiency of conventional SM by increasing the number of active transmit antenna indices. Additional information bits are employed to select two transmit antenna indices, therefore, increasing the spectral efficiency of

conventional SM. QSM decomposes an APM signal modulation symbol into its constituent real and imaginary parts, then transmits the components via the transmit antennas with the selected indices. QSM employs a single RF chain, therefore, relatively low-complexity receive algorithms are employed, and since the real and imaginary components of the APM signal are orthogonal, QSM mitigates ICI [29]. DSM is a recently proposed SM-based scheme that aims to double the spectral efficiency of conventional SM. DSM employs two independent SM channels that simultaneously transmit two APM symbols in a transmission interval. The key idea of DSM is that constellation rotation is applied to one of the APM signal constellation such that the symbols in independent SM channels can be distinguished at the receiver. DSM demonstrates a better error performance than QSM for systems with an identical spectral efficiency provided that the modulation order of DSM is greater than two [30].

Recently, there has been a growing interest in MBM, which has been proposed as a novel modulation scheme which intentionally varies the fading channel in a wireless system [32]. The permittivity, permeability, and resistivity of the propagation environment are altered by the information embedded in the system to produce distinct channel fade realizations [34]. MBM is facilitated by RF mirrors placed near a transmit antenna, and by changing the ON/OFF status of these RF mirrors, different channel fade realizations are created [33]. An MBM-TU contains M_{RF} RF mirror units, if each individual RF mirror has two possible channel realizations, then the total number of different fading channel realizations is given by $N_m = 2^{M_{RF}}$ [33, 34].

In order to meet the high data rate requirements for next-generation wireless networks, the MBM technique coupled with SBM techniques, have been investigated in order to improve error performance and/or spectral efficiency. Systems such as spatial media-based modulation, SIMO-MBM, and QSMBM have been investigated in literature where significant gains in error performance and/or spectral efficiency have been demonstrated [33–35, 37, 38]. Motivated by the benefits MBM, in this chapter we propose a new MBM-based scheme based on DSM called DSMBM. The investigation on DSM demonstrated that the schemes have an improved error performance over QSM, and the expectation is that the proposed scheme yields a better error performance than QSMBM, which has been presented in literature.

A majority of wireless communications systems employ FEC to improve information reliability in noisy channels [40]. It has been demonstrated in literature that soft-output detection combined with soft-input channel decoding results in a significant net coding gain when compared

to HDMLDs [41–43, 47, 48]. In this chapter, we present the system model, detection scheme, and analytical error performance of DSMBM. Furthermore, we propose a SOMLD for DSMBM, and simulation results are presented to validate the performance for the SOMLD.

6.2 System model for Double Spatial Media based Modulation

Figure 6.1 illustrates the system model for DSMBM, where N_T and N_R represent the number of transmit antennas and receive antennas, respectively, and each transmit antenna is an MBM-TU with M_{RF} RF mirrors, $M_{RF} \in 2\mathbb{N}$.

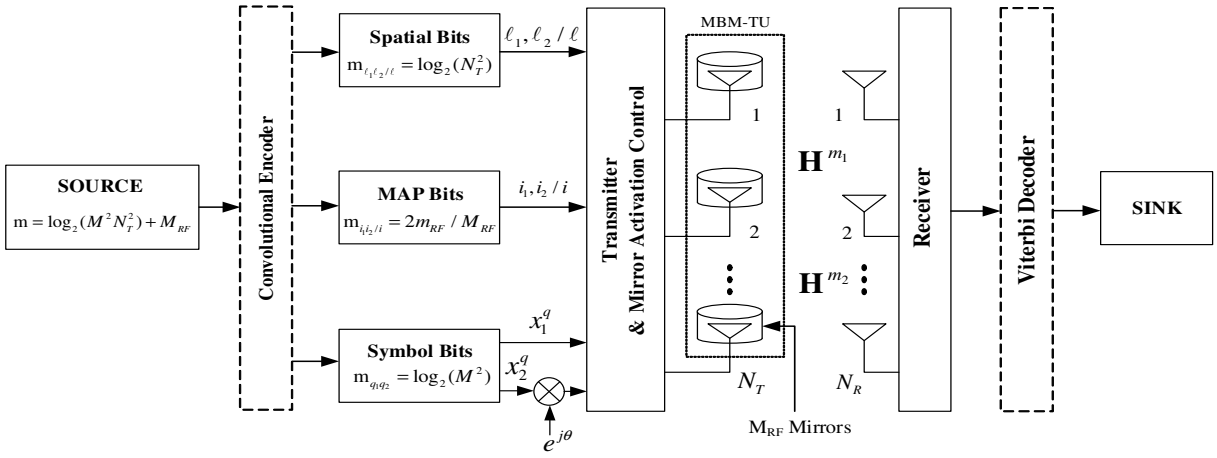

Figure 6.1: System model for the DSMBM scheme

In each transmission interval, the source provides an input vector of length $\mathrm{m} = \log_2(N_T^2 M^2) + M_{RF}$ bits, where M is the APM signal modulation order, into the DSMBM encoder. Note, we refer to the dashed convolutional encoder in Figure 6.1 as the DSMBM encoder for uncoded cases. The DSMBM encoder divides the information into six partitions. The first and second partitions are mapped, such that $\mathrm{m}_{\ell_1\ell_2} = \log_2(N_T^2)$ bits used to select two MBM-TU indices ℓ_1 and ℓ_2, $\ell_1, \ell_2 \in [1 : N_T]$, respectively. The third and fourth partitions are mapped, such that $\mathrm{m}_{q_1 q_2} = \log_2(M^2)$ bits are used to select two symbols x_1^q and x_2^q, $q \in [1 : M]$ which are drawn from a Gray-coded M-QAM or M-PSK signal constellation sets. The first data symbol x_1^q is transmitted via the active MBM-TU with index ℓ_1 whereas the second data symbol x_2^q is rotated through an optimized angle θ before transmission through the second active MBM-TU with index ℓ_2. As stated earlier, the optimized rotation angle θ is $90°, 45°$ and $30°$ for BPSK, 4-QAM and 8-QAM, respectively [30, 31]. The transmit vector is represented by an $N_R \times 1$

vector given as:

$$\mathbf{x} = \begin{matrix} & & \ell_1^{th}\text{ position} & & \ell_2^{th}\text{ position} & \\ & & \downarrow & & \downarrow & \\ \big[\,0 & \cdots & x_q^1 & & x_q^2 e^{j\theta} & \cdots\ 0\,\big]^T, \\ & \uparrow & & & & \uparrow \\ & 1^{st}\text{ position} & & & & N_T^{th}\text{ position} \end{matrix} \tag{6.1}$$

where x_1^q and $x_2^q e^{j\theta}$, $q \in [1:M]$, represents the transmit symbols drawn from M-QAM or M-PSK signal constellation sets with $E\{|x_1^q|^2\} = E\{|x_2^q e^{j\theta}|^2\} = 1$, and ℓ_1 and ℓ_2, $\ell_1, \ell_2 \in [1:N_T]$ represent active MBM-TU indices for the transmission of x_1^q and $x_2^q e^{j\theta}$, respectively.

Note that in (6.1), it is possible to have the MBM-TU indices $\ell_1 = \ell_2$, this is the case where a single MBM-TU is employed, and we use the index ℓ, $\ell \in [1:N_T]$, to represent the indices ℓ_1 and ℓ_2, respectively. Due to the rotated constellation, the corresponding data symbols can be distinguished at the receiver, and the transmitted signal at ℓ is the summation of the symbols x_1^q and $x_2^q e^{j\theta}$, respectively. Given a total of M_{RF} mirror units at each MBM-TU, if the symbols x_1^q and $x_2^q e^{j\theta}$ are mapped to a single MBM-TU, then the information bits of the fifth and sixth partitions are combined to give M_{RF} bits which are employed to select a single MAP index i, which selects one of the $N_{m_1} = 2^{M_{RF}}$ MAPs available at the MBM-TU. If the symbols x_1^q and $x_2^q e^{j\theta}$ are mapped to different MBM-TUs, then the fifth and sixth partition each employ $m_{RF} = (1/2)M_{RF}$ bits to select two MAP indices i_1 and i_2, where each index selects one of the available $N_{m_2} = 2^{m_{RF}}$ MAPs at each MBM-TU, respectively. The spectral efficiency of DSMBM is given as:

$$\eta_{DSMBM} = \log_2(N_T^2) + \log_2(M^2) + M_{RF}\ \text{b/s/Hz}. \tag{6.2}$$

The MBM-TUs are individually activated with either M_{RF} or m_{RF} RF mirrors based on whether the system is employing a single MBM-TU or dual MBM-TUs for the transmission interval, respectively. In the case of single MBM-TU activation, the fading channel gain matrix for each MBM-TU of dimension $N_R \times N_{m_1}$ is represented as $\mathbf{H}_\ell^{m_1} = [\mathbf{h}_1^{m_1,\ell} \dots \mathbf{h}_{N_{m_1}}^{m_1,\ell}]$, $\ell \in [1:N_T]$, where ℓ is the MBM-TU index and the i^{th} column vector $\boldsymbol{h}_i^{m_1,\ell}$, $i \in [1:N_{m_1}]$, of dimension $N_R \times 1$ is given as $\mathbf{h}_i^{m_1,\ell} = [h_{1,i}^{m_1,\ell} \dots h_{N_R,i}^{m_1,\ell}]^T$. To select a particular MAP with index i from the MBM-TU MAPs, we denote a vector $\mathbf{e}_i$ of dimension $N_{m_1} \times 1$, where the i^{th} entry corresponds to the only non-zero unit entry in the vector. The product of $\mathbf{H}_\ell^{m_1}$ and $\mathbf{e}_i$ selects a MAP where the channel fade is given by $\mathbf{h}_i^{m_1,\ell}$. Similarly, in the case of dual MBM-TU activation,

the fading channel gain matrix for each MBM-TU of dimension $N_R \times N_{m_2}$ is represented as $\mathbf{H}_{\ell_\varphi}^{m_2} = [\mathbf{h}_1^{m_2,\ell_\varphi} \dots \mathbf{h}_{N_{m_2}}^{m_2,\ell_\varphi}]$, $\ell_\varphi \in [1 : N_T]$, $\varphi \in [1 : 2]$, where ℓ_φ is the MBM-TU index, φ is an index for the first and second active MBM-TU, respectively, and the i_φ-th column vector $\boldsymbol{h}_{i_\varphi}^{m_1,\ell_\varphi}$, $i_\varphi \in [1 : N_{m_2}]$, of dimension $N_R \times 1$ is given as $\boldsymbol{h}_{i_\varphi}^{m_2,\ell_\varphi} = [h_{1,i_\varphi}^{m_2,\ell_\varphi} \dots h_{N_R,i_\varphi}^{m_2,\ell_\varphi}]^T$. To select a particular MAP with index i_φ from the MBM-TU MAPs, we denote a vector $\mathbf{e}_{i_\varphi}$ of dimension $N_{m_2} \times 1$, where the i_φ^{th} entry corresponds to the only non-zero unit entry in the vector. The product of $\mathbf{H}_{\ell_\varphi}^{m_2}$ and $\mathbf{e}_{i_\varphi}$ selects a MAP where the fade is given by $\mathbf{h}_{i_\varphi}^{m_2,\ell_\varphi}$.

The example illustrated in Table 6.1 demonstrates the mapping procedure for a 4×4 Gray-coded 4-QAM DSMBM system with $\theta = 45^\circ$ and $M_{RF} = 4$, yielding a spectral efficiency of $\eta_{DSMBM} = 12$ b/s/Hz, only two random data streams are considered.

Table 6.1: Illustration of the mapping procedure for DSMBM

Source Bits	**Mapping Partition**					
$\log_2 M^2 N_T^2 N_{m_1}$	1	2	3	4	5	6
0 1 1 0 1 0 1 1 1 1 0 1 $\theta = 45^\circ$ $M = 4, N_T = 4$ $m_{RF} = 1/2M_{RF} = 2$	$\log_2 M = 2$ 0 1 x_1^q $-1 - j$	$\log_2 M = 2$ 1 0 $x_2^q e^{j\theta}$ $(1 + j)\ e^{j\theta}$	$\log_2 N_T = 2$ 1 0 $\ell_1 = 3$ $\mathbf{H}_{\ell_1}^{m_2}$ $\mathbf{H}_3^{m_2}$	$\log_2 N_T = 2$ 1 1 $\ell_2 = 4$ $\mathbf{H}_{\ell_2}^{m_2}$ $\mathbf{H}_4^{m_2}$	$m_{RF} = 2$ 1 1 $i_1 = 4$ $\mathbf{H}_3^{m_2} \times \mathbf{e}_{i_1}$ $\mathbf{h}_4^{m_2,3}$	$m_{RF} = 2$ 0 1 $i_2 = 2$ $\mathbf{H}_4^{m_2} \times \mathbf{e}_{i_2}$ $\mathbf{h}_2^{m_2,4}$
0 0 1 1 1 0 1 0 1 0 0 1 $\theta = 45^\circ$ $M = 4, N_T = 4$ $M_{RF} = 4$	$\log_2 M = 2$ 0 0 x_1^q $-1 + j$	$\log_2 M = 2$ 1 1 $x_2^q\ e^{j\theta}$ $(1 - j)\ e^{j\theta}$	$\log_2 N_T = 2$ 1 0 $\ell = 3$ $\mathbf{H}_\ell^{m_1}$ $\mathbf{H}_3^{m_1}$	$\log_2 N_T = 2$ 1 0 $\ell = 3$ $\mathbf{H}_\ell^{m_1}$ $\mathbf{H}_3^{m_1}$	$M_{RF} = 4$ 1 0 0 1 $i = 10$ $\mathbf{H}_3^{m_1} \times \mathbf{e}_i$ $\mathbf{h}_{10}^{m_1,3}$	

Consider the input bit stream given by {011010111101} transmitted at some arbitrary instant in Table 6.1. In the first partition, $\log_2 M = \{01\}$ bits are used to select the modulation symbol x_1^q, similarly in the second partition, $\log_2 M = \{10\}$ bits are used to select the modulation symbol $x_2^q e^{j\theta}$. In the third partition, $\log_2 N_T = \{10\}$ bits are used to the MBM-TU index ℓ_1, and in the fourth partition, $\log_2 N_T = \{11\}$ bits are used to select the MBM-TU index ℓ_2. Since the indices $\ell_1 \neq \ell_2$, dual MBM-TUs are selected for the transmission, and active MBM-TUs employ m_{RF} mirror units with a channel gain matrix given by $\mathbf{H}^{m_2}$ for the MBM-TUs with indices $\ell_1 = 3$ and $\ell_2 = 4$, respectively. In the fifth partition, $m_{RF} = \{11\}$ bits are used to select the MAP index $i_1 = 4$, similarly in the sixth partition, $m_{RF} = \{01\}$ bits are used select the MAP index $i_2 = 2$, respectively.

The received signal for DSMBM is represented for the two cases. In single MBM-TU transmission, a signal is transmitted over a Rayleigh frequency-flat fading channel $\mathbf{H}_{\ell}^{m_1}, \ell \in [1 : N_T]$ in the presence of AWGN represented by the $N_R \times 1$ vector $\mathbf{n}_1$, and in dual MBM-TU transmission, a signal is transmitted over a Rayleigh frequency-flat fading channel $\mathbf{H}_{\ell_\varphi}^{m_2}, \ell \in [1 : N_T], \varphi \in [1 : 2]$ in the presence of AWGN represented by the $N_R \times 1$ vector $\mathbf{n}_2$. All elements of $\mathbf{H}_{\ell}^{m_1}$, $\mathbf{H}_{\ell_\varphi}^{m_2}$, $\mathbf{n}_1$ and $\mathbf{n}_2$ are assumed to be i.i.d. with Gaussian distribution of zero mean and unit variance $\sim CN(0, 1)$. Therefore, the received signal given by two $N_R \times 1$ vectors $\mathbf{y}_1$ and $\mathbf{y}_2$ for the single and dual MBM-TU transmission, respectively, as:

$$\mathbf{y}_1 = \sqrt{\frac{\rho}{2}} \mathbf{H}_{\ell}^{m_1} \mathbf{e}_i \big(x_1^q + x_2^q e^{j\theta}\big) + \mathbf{n}_1, \tag{6.3}$$

$$\mathbf{y}_2 = \sqrt{\frac{\rho}{2}} \big(\mathbf{H}_{\ell_1}^{m_2} \mathbf{e}_{i_1} x_1^q + \mathbf{H}_{\ell_2}^{m_2} \mathbf{e}_{i_2} x_2^q e^{j\theta}\big) + \mathbf{n}_2, \tag{6.4}$$

where $\frac{\rho}{2}$ is the average SNR per symbol at each receive antenna, $q \in [1 : M]$, and the vectors $\mathbf{e}_i$ and $\mathbf{e}_{i_\varphi}, i \in [1 : N_{m_1}], i_\varphi \in [1 : N_{m_2}]$ are vectors of dimension $N_{m_1} \times 1$ and $N_{m_2} \times 1$ where the i^{th} and i_φ^{th} entry of the vectors are the only non-zero elements of unit entry, respectively.

6.3 DSMBM Detection

In the detection of DSMBM, we assume that perfect CSI is known at the receiver in all instances. Based on the received signal expressions given in (6.3) and (6.4), a two-stage ML detector is formulated which considers all the possible realizations of the M-QAM/M-PSK constellation symbols x_1^q and $x_2^q e^{j\theta}$, the MBM-TU index ℓ and MAP index i for the case of a single MBM-TU activation, and the MBM-TU indices ℓ_1 and ℓ_2 and the MAP indices i_1, and i_2 for the case of dual MBM-TU activation, respectively. The ML calculation with the minimum argument is selected as the final estimated signal of the transmitted information for the two cases. Given the received signal $\mathbf{y}_2$ and $\mathbf{y}_2$, the ML detectors are given as:

$$[\hat{x}_1^q, \hat{x}_2^q, \hat{\ell}, \hat{i}] = \underset{\substack{\ell \in [1 : N_T] \\ q \in [1 : M] \\ i \in [1 : N_{m_1}]}}{\operatorname{argmin}} \left(\|\mathbf{y}_1 - \sqrt{\frac{\rho}{2}} \mathbf{H}_{\ell}^{m_1} \mathbf{e}_i (x_1^q + x_2^q e^{j\theta})\|_F^2 \right), \tag{6.5}$$

$$[\hat{x}_1^q, \hat{x}_2^q, \hat{\ell_1}, \hat{\ell_2}, \hat{i_1}, \hat{i_2}] = \underset{\substack{\ell_1, \ell_2 \in [1:N_T] \\ q \in [1:M] \\ i_1, i_2 \in [1:N_{m_2}]}}{\text{argmin}} \left(\|\mathbf{y}_2 - \sqrt{\frac{\rho}{2}}(\mathbf{H}_{\ell_1}^{m_2}\mathbf{e}_{i_1}x_1^q + \mathbf{H}_{\ell_2}^{m_2}\mathbf{e}_{i_2}x_2^q e^{j\theta})\|_F^2 \right). \tag{6.6}$$

The ML detector employed by DSMBM is shown in (6.5) and (6.6). Since the receiver has no knowledge of whether a single or dual MBM-TUs were employed, a decision metric is formulated to estimate the final received signal from the result given by the two ML detectors. The metric is given by:

$$\tau = \|\mathbf{y}_1 - \sqrt{\frac{\rho}{2}}\mathbf{H}_{\hat{\ell}}^{m_2}\mathbf{e}_{\hat{i}}(\hat{x}_1^q + \hat{x}_2^q e^{j\theta})\|_F^2 - \|\mathbf{y}_2 - \sqrt{\frac{\rho}{2}}(\mathbf{H}_{\hat{\ell}_1}^{m_2}\mathbf{e}_{\hat{i}_1}\hat{x}_1^q + \mathbf{H}_{\hat{\ell}_2}^{m_2}\mathbf{e}_{\hat{i}_2}\hat{x}_2^q e^{j\theta})\|_F^2, \tag{6.7}$$

$$\tau < 0: \quad [\hat{x}_1^q, \hat{x}_2^q, \hat{\ell}, \hat{i}],$$

$$\tau > 0: \quad [\hat{x}_1^q, \hat{x}_2^q, \hat{\ell_1}, \hat{\ell_2}, \hat{i}_1, \hat{i}_2].$$

Note, the metric in (6.7) is used to select the final estimated receive signal for the transmission in (6.3) and (6.4). If the metric $\tau < 0$, then the detector selects the estimated signal for single MBM-TU transmission, and if $\tau > 0$, then the detector selects the estimated signal for dual MBM-TU transmission [35].

6.4 Performance Analysis of DSMBM

In this section, the theoretical ABEP of DSMBM over i.i.d. Rayleigh frequency-flat fading channel employing ML detection is formulated. Considering the received signal vector in (6.3) and (6.4), the transmitted codeword in DSMBM can be represented as $\mathbf{X}_\mu,\ \mu \in [1:2]$ which is erroneously detected at the receiver as $\hat{\mathbf{X}}_{\hat{\mu}},\ \hat{\mu} \in [1:2]$, where μ and $\hat{\mu}$ are indices which represent the codeword for a case when single transmit antenna is employed, or dual antennas are employed during transmission, respectively. The ABEP of DSMBM may be defined as:

$$\text{ABEP} \leq \frac{1}{2^{M_{RF}} M^2 N_T^2} \sum_{\boldsymbol{X}_\mu} \sum_{\hat{\boldsymbol{X}}_{\hat{\mu}}} \frac{N(\boldsymbol{X}_\mu, \hat{\boldsymbol{X}}_{\hat{\mu}})\ P(\mathbf{X}_\mu \to \hat{\mathbf{X}}_{\hat{\mu}})}{\eta_{DSMBM}}, \tag{6.8}$$

where $P(\mathbf{X}_\mu \to \hat{\mathbf{X}}_{\hat{\mu}})$ is the PEP that the transmitted DSMBM codeword $\mathbf{X}_\mu$ detected as $\hat{\mathbf{X}}_{\hat{\mu}}$ at the receiver, with $\mathbf{X}_1 = \begin{bmatrix}\mathbf{e}_i(x_1^q + x_2^q e^{j\theta}) & 0\end{bmatrix}^T$ when $\ell_1 = \ell_2$ and $\hat{\mathbf{X}}_{\hat{1}} = \begin{bmatrix}\mathbf{e}_{\hat{i}}(x_1^{\hat{q}} + x_2^{\hat{q}} e^{j\theta}) & 0\end{bmatrix}^T$ when $\hat{\ell}_1 =$

$\hat{\ell}_2,\ \mathbf{X}_2 = \begin{bmatrix}\mathbf{e}_{i_1} x_1^q & \mathbf{e}_{i_2} x_2^q e^{j\theta}\end{bmatrix}^T$ when $\ell_1 \neq \ell_2$ and $\hat{\mathbf{X}}_{\hat{2}} = \begin{bmatrix}\mathbf{e}_{\hat{i}_1} x_1^{\hat{q}} & \mathbf{e}_{\hat{i}_2} x_2^{\hat{q}} e^{j\theta}\end{bmatrix}^T$ when $\hat{\ell}_1 \neq \hat{\ell}_2$, where $q \in [1:M],\ i \in [1:N_{m_1}],\ i_1, i_2 \in [1:N_{m_2}]$ and $\ell, \ell_1, \ell_2 \in [1:N_T]$. $N\big(\boldsymbol{X}_\mu, \hat{\boldsymbol{X}}_{\hat{\mu}}\big)$ is the number of bit errors associated with the corresponding PEP event $P\big(\mathbf{X}_\mu \to \hat{\mathbf{X}}_{\hat{\mu}}\big)$.

If we let $\hat{\boldsymbol{\zeta}}_1 = \sqrt{\frac{\rho}{2}} \mathbf{H}_{\hat{\ell}}^{m_1} \mathbf{e}_{\hat{i}} \big(x_1^{\hat{q}} + x_2^{\hat{q}} e^{j\theta}\big)$ and $\hat{\boldsymbol{\zeta}}_2 = \sqrt{\frac{\rho}{2}} \big(\mathbf{H}_{\hat{\ell}_1}^{m_2} \mathbf{e}_{\hat{i}_1} x_1^{\hat{q}} + \mathbf{H}_{\hat{\ell}_2}^{m_2} \mathbf{e}_{\hat{i}_2} x_2^{\hat{q}} e^{j\theta}\big)$ and consider $\mathbf{H}^{m_1}, \mathbf{H}^{m_2} \in \mathbf{H}^m$, the conditional PEP $P(\mathbf{X}_\mu \to \hat{\mathbf{X}}_{\hat{\mu}} | \mathbf{H}^m)$ may be formulated as:

$$P\bigg(\mathbf{X}_\mu \to \hat{\mathbf{X}}_{\hat{\mu}} \big| \mathbf{H}^m\bigg) = P\bigg(\big\|\mathbf{y}_\mu - \boldsymbol{\zeta}_\mu\big\|_F^2 \geq \big\|\mathbf{y}_{\hat{\mu}} - \hat{\boldsymbol{\zeta}}_{\hat{\mu}}\big\|_F^2\bigg), \tag{6.9}$$

where $\mu = \begin{cases} 1, & \ell_1 = \ell_2 \\ 2, & \ell_1 \neq \ell_2 \end{cases}$ and $\hat{\mu} = \begin{cases} 1, & \hat{\ell}_1 = \hat{\ell}_2 \\ 2, & \hat{\ell}_1 \neq \hat{\ell}_2 \end{cases}$.

The conditional PEP may be simplified using the method shown by Xu *et al.* [51] which gives:

$$P\big(\mathbf{X}_\mu \to \hat{\mathbf{X}}_{\hat{\mu}} \big| \mathbf{H}^m\big) = Q\big(\sqrt{k}\big), \tag{6.10}$$

where k is a central chi-squared RV with $2N_R$ degrees of freedom and is defined as:

$$k = \frac{\rho}{8} \|\mathbf{H}^m\|_F^2 \cdot \|\overline{\boldsymbol{\xi}}\|_F^2 = \sum_{n=1}^{2N_R} \alpha^2, \tag{6.11}$$

where $\alpha \sim N(0, \sigma_\alpha^2)$ and the variance $\sigma_\alpha^2 = \frac{\rho}{8} \cdot \|\overline{\boldsymbol{\xi}}\|_F^2$ with $\overline{\boldsymbol{\xi}} = \begin{cases} \mathbf{X}_1 - \hat{\mathbf{X}}_1 & \text{if } \ell_1 = \ell_2,\ \hat{\ell}_1 = \hat{\ell}_2 \\ \mathbf{X}_2 - \hat{\mathbf{X}}_1 & \text{if } \ell_1 \neq \ell_2,\ \hat{\ell}_1 = \hat{\ell}_2 \\ \mathbf{X}_1 - \hat{\mathbf{X}}_2 & \text{if } \ell_1 = \ell_2,\ \hat{\ell}_1 \neq \hat{\ell}_2 \\ \mathbf{X}_2 - \hat{\mathbf{X}}_2 & \text{if } \ell_1 \neq \ell_2,\ \hat{\ell}_1 \neq \hat{\ell}_2 \end{cases}$.

The PDF of k is defined as:

$$f_k(\upsilon) = \frac{\upsilon^{N_R - 1} e^{\frac{-\upsilon}{2\sigma_\alpha^2}}}{\big(2\sigma_\alpha^2\big)^{N_R} (N_R - 1)!} \quad ,\ \upsilon \geq 0. \tag{6.12}$$

Averaging the conditional PEP over the i.i.d. RVs we arrive at:

$$P\big(\mathbf{X}_\mu \to \hat{\mathbf{X}}_{\hat{\mu}}\big) = \int_0^\infty P\big(\mathbf{X}_\mu \to \hat{\mathbf{X}}_{\hat{\mu}} | \mathbf{H}^m\big) \cdot f_k(\upsilon) \partial\upsilon. \tag{6.13}$$

Employing the trapezoidal rule approximation of the Q-function $Q(x) = \frac{1}{\pi} \int_0^{\frac{\pi}{2}} \exp(-x^2 / \sin^2\theta) \partial\theta$

which is given as:

$$Q\big(\sqrt{k}\big) \approx \frac{1}{2c}\left[\frac{1}{2}\exp\left(\frac{-k}{2}\right) + \sum_{k=1}^{c-1}\exp\left(\frac{-k}{2\sin^2\left(\frac{k\pi}{2c}\right)}\right)\right], \tag{6.14}$$

where c is the number of iterations of convergence, $c > 10$. Using the MGF, we arrive at the unconditional PEP given as [49]:

$$P\big(\mathbf{X}_\mu \to \hat{\mathbf{X}}_{\hat{\mu}}\big) = \frac{1}{2c}\left[\frac{1}{2}M\left(\frac{1}{2}\right) + \sum_{k=1}^{c-1}M\left(\frac{1}{2\sin^2\left(\frac{k\pi}{2c}\right)}\right)\right], \tag{6.15}$$

where $M(\cdot)$ is the MGF defined as:

$$M(s) = \int_0^\infty e^{s\upsilon}\frac{\upsilon^{N_R-1}e^{\frac{-\upsilon}{2\sigma_\alpha^2}}}{\big(2\sigma_\alpha^2\big)^{N_R}\big(N_R-1\big)!}\partial\upsilon = \left(\frac{1}{1+2\sigma_\alpha^2 s}\right)^{N_R}. \tag{6.16}$$

6.5 DSMBM Soft-Output Detector

The system model in Figure 6.1 is extended to include channel coding and decoding, and we refer to the dashed line blocks in Figure 6.1 for the coded model understudy in this section. For the proposed soft-output detector, we assume the following [42]:

1. Data symbols and antenna indices are uncorrelated.
2. Data symbols are independent and generated with equal probability.
3. Antenna bits are independent and generated with equal probability.
4. RF mirror bits are independent and generated with equal probability.
5. Full CSI is available at the receiver.

6.5.1 DSMBM SOMLD

The SOMLD for DSMBM is calculated as an LLR expression based on the ML detectors for the two transmission cases given in (6.3) and (6.4), respectively. The SOMLD based on (6.3) calculates the LLR expression for the first symbol $x_{a_1}^q$, the second symbol $x_{b_1}^q$ the MBM-TU index ℓ_c, and the MAP index i_c. The LLR expression of the first antenna index $x_{a_1}^q$ is formulated as :

$$LLR(x_{a_1}^q) = \log\frac{P\big(x_{a_1}^q = 1|\mathbf{y}_1\big)}{P\big(x_{a_1}^q = 0|\mathbf{y}_1\big)}. \tag{6.17}$$

The LLR expression in (6.8) can be written as:

$$LLR(x_{a_1}^q) = \log \frac{\sum\limits_{\substack{\hat{x}_{a_1}^q \in \mathbf{\Omega}_{a_1}^1 \\ \hat{x}_{b_1}^q \in \mathbf{\Omega}_{b_1}}} \sum\limits_{\hat{\ell}_c \in \mathbf{L}_c} \sum\limits_{\hat{i}_c \in \mathbf{S}_c} P\big(\mathbf{y}_1 | x_{a_1}^q = \hat{x}_{a_1}^q, x_{b_1}^q = \hat{x}_{b_1}^q, \ell_c = \hat{\ell}_c, i_c = \hat{i}_c,\big) P\big(x_{a_1}^q = \hat{x}_{a_1}^q\big)}{\sum\limits_{\substack{\hat{x}_{a_1}^q \in \mathbf{\Omega}_{a_1}^0 \\ \hat{x}_{b_1}^q \in \mathbf{\Omega}_{b_1}}} \sum\limits_{\hat{\ell}_c \in \mathbf{L}_c} \sum\limits_{\hat{i}_c \in \mathbf{S}_c} P\big(\mathbf{y}_1 | x_{a_1}^q = \hat{x}_{a_1}^q, x_{b_1}^q = \hat{x}_{b_1}^q, \ell_c = \hat{\ell}_c, i_c = \hat{i}_c\big) P\big(x_{a_1}^q = \hat{x}_{a_1}^q\big)}, \tag{6.18}$$

where $\mathbf{\Omega}_{a_1}^1$ and $\mathbf{\Omega}_{a_1}^0$ are vectors which contain the indices of the first symbol $\hat{x}_{a_1}^q$ with binary '1' and '0' that corresponds to a particular significant bit of the binary data of the symbol in question, respectively, $\mathbf{\Omega}_b$ is a set representing all possible $\hat{x}_{b_1}^q$ symbols, $\mathbf{L}_c$ is the set of all possible for the antenna indices $\hat{\ell}_c$, and $\mathbf{S}_c$ is a set that represents all possible MAP indices $\hat{i}_c$. Applying Bayes' theorem on the demodulator output given in (6.9), the LLR for the first symbol $x_{a_1}^q$ is calculated as:

$$LLR(x_{a_1}^q) = \log \frac{\sum\limits_{\hat{x}_{a_1}^q \in \mathbf{\Omega}_a^1} \sum\limits_{\hat{x}_{b_1}^q \in \mathbf{\Omega}_b} \sum\limits_{\hat{\ell}_c \in \mathbf{L}_c} \sum\limits_{\hat{i}_c \in \mathbf{S}_c} \exp(C)}{\sum\limits_{\hat{x}_{a_1}^q \in \mathbf{\Omega}_{a_1}^0} \sum\limits_{\hat{x}_{b_1}^q \in \mathbf{\Omega}_b} \sum\limits_{\hat{\ell}_c \in \mathbf{L}_c} \sum\limits_{\hat{i}_c \in \mathbf{S}_c} \exp(D)}, \tag{6.19}$$

where $C = D = \frac{-\|\mathbf{y}_1 - \sqrt{\frac{\rho}{2}} \mathbf{H}_{\hat{\ell}_c}^{m_1} \mathbf{e}_{\hat{i}_c} \left(\hat{x}_{a_1}^q + \hat{x}_{b_1}^q e^{j\theta}\right)\|_F^2}{2\sigma^2}$ and σ^2 the variance of the AWGN channel in (6.3). Based on the procedure in (6.9) and (6.10), the LLR for the second symbol $x_{b_1}^q$ is calculated as:

$$LLR(x_{b_1}^q) = \log \frac{\sum\limits_{\hat{x}_{b_1}^q \in \mathbf{\Omega}_b^1} \sum\limits_{\hat{x}_{a_1}^q \in \mathbf{\Omega}_a} \sum\limits_{\hat{\ell}_c \in \mathbf{L}_c} \sum\limits_{\hat{i}_c \in \mathbf{S}_c} \exp(C)}{\sum\limits_{\hat{x}_{b_1}^q \in \mathbf{\Omega}_b^0} \sum\limits_{\hat{x}_{a_1}^q \in \mathbf{\Omega}_a} \sum\limits_{\hat{\ell}_c \in \mathbf{L}_c} \sum\limits_{\hat{i}_c \in \mathbf{S}_c} \exp(D)}, \tag{6.20}$$

where $\mathbf{\Omega}_b^1$ and $\mathbf{\Omega}_b^0$ are vectors which contain the indices of the second symbol $\hat{x}_{b_1}^q$ with binary '1' and '0' that corresponds to a particular significant bit of the binary data of the symbol, respectively, and $\mathbf{\Omega}_a$ is a set representing all possible $\hat{x}_{a_1}^q$ symbols. The LLR for the transmit

antenna index ℓ_c is calculated using the procedure shown in (6.9) and (6.10), and it is given as:

$$LLR(\ell_c) = \log \frac{\sum_{\hat{\ell}_c \in \boldsymbol{\ell}_c^1} \sum_{\hat{x}_{a_1}^q \in \boldsymbol{\Omega}_a} \sum_{\hat{x}_{b_1}^q \in \boldsymbol{\Omega}_b} \sum_{\hat{i}_c \in \mathbf{S}_c} \exp(C)}{\sum_{\hat{\ell}_c \in \boldsymbol{\ell}_c^0} \sum_{\hat{x}_{a_1}^q \in \boldsymbol{\Omega}_a} \sum_{\hat{x}_{b_1}^q \in \boldsymbol{\Omega}_b} \sum_{\hat{i}_c \in \mathbf{S}_c} \exp(D)}, \tag{6.21}$$

where $\boldsymbol{\ell}_c^1$ and $\boldsymbol{\ell}_c^0$ are vectors which contain the indices of the transmit antenna index with binary '1' and '0' that corresponds to a particular significant bit of the binary data of the antenna index, respectively. Lastly, the LLR for the MAP index i_c is calculated using the procedure shown in (6.9) and (6.10), and it is given as:

$$LLR(i_c) = \log \frac{\sum_{\hat{i}_c \in \mathbf{S}_c^1} \sum_{\hat{x}_{a_1}^q \in \boldsymbol{\Omega}_a} \sum_{\hat{x}_{b_1}^q \in \boldsymbol{\Omega}_b} \sum_{\hat{\ell}_c \in \mathbf{L}_c} \exp(C)}{\sum_{\hat{i}_c \in \mathbf{S}_c^0} \sum_{\hat{x}_{a_1}^q \in \boldsymbol{\Omega}_a} \sum_{\hat{x}_{b_1}^q \in \boldsymbol{\Omega}_b} \sum_{\hat{\ell}_c \in \mathbf{L}_c} \exp(D)}, \tag{6.22}$$

where $\mathbf{S}_c^1$ and $\mathbf{S}_c^0$ are vectors which contain the indices of the MAP index i_c with binary '1' and '0' that corresponds to a particular significant bit of the binary data for the MAP index, respectively.

The SOMLD based on (6.4) calculates the LLR expression for the first symbol $x_{a_2}^q$, second symbol $x_{b_2}^q$, MBM-TU index ℓ_{a_2}, MBM-TU index ℓ_{b_2}, MAP index i_{a_2} and lastly the MAP index i_{b_2}. The LLR expressions are formulated using the procedure in (6.9) and (6.10) and applying Bayes' theorem to the output, the LLR expression for the first symbol x_{a_2} is given as:

$$LLR(x_{a_2}^q) = \log \frac{\sum_{\hat{x}_{a_2}^q \in \boldsymbol{\Omega}_a^1} \sum_{\hat{x}_{b_2}^q \in \boldsymbol{\Omega}_b} \sum_{\hat{\ell}_{a_2} \in \mathbf{L}_a} \sum_{\hat{\ell}_{b_2} \in \mathbf{L}_b} \sum_{\hat{i}_{a_2} \in \mathbf{S}_a} \sum_{\hat{i}_{b_2} \in \mathbf{S}_b} \exp(E)}{\sum_{\hat{x}_{a_2}^q \in \boldsymbol{\Omega}_a^0} \sum_{\hat{x}_{b_2}^q \in \boldsymbol{\Omega}_b} \sum_{\hat{\ell}_{a_2} \in \mathbf{L}_a} \sum_{\hat{\ell}_{b_2} \in \mathbf{L}_b} \sum_{\hat{i}_{a_2} \in \mathbf{S}_a} \sum_{\hat{i}_{b_2} \in \mathbf{S}_b} \exp(F)}, \tag{6.23}$$

where $\boldsymbol{\Omega}_a^1$ and $\boldsymbol{\Omega}_a^0$ are vectors which contain indices of the symbol $x_{a_2}^q$ with binary '1' and '0' which corresponds to a particular significant bit of the binary data of the symbol, respectively, $\boldsymbol{\Omega}_b$ is the set of all possible $\hat{x}_{b_2}^q$ symbols, $\mathbf{L}_a$ and $\mathbf{L}_b$ are sets of all possible for the antenna indices $\hat{\ell}_{a_2}$ and $\hat{\ell}_{b_2}$, respectively, $\mathbf{S}_a$ and $\mathbf{S}_b$ are sets of all possible MAP indices for $\hat{i}_{a_2}$ and $\hat{i}_{b_2}$, respectively, $E = F = \frac{-\|\mathbf{y}_2 - \sqrt{\frac{p}{2}}\left(\mathbf{H}_{\hat{\ell}_{a_2}}^{m_2} \mathbf{e}_{\hat{i}_{a_2}} \hat{x}_{a_2}^q + \mathbf{H}_{\hat{\ell}_{b_2}}^{m_2} \mathbf{e}_{\hat{i}_{b_2}} \hat{x}_{b_2}^q e^{j\theta}\right)\|_F^2}{2\sigma^2}$, where σ^2 the variance of the AWGN in channel (6.4). Employing the same procedure as in (6.14), the LLR expression for the second symbol $x_{b_2}^q$ is given by:

$$LLR(x^q_{b_2}) = \log \frac{\sum_{\hat{x}^q_{b_2} \in \mathbf{\Omega}^b_1} \sum_{\hat{x}^q_{a_2} \in \mathbf{\Omega}_a} \sum_{\hat{\ell}_{a_2} \in \mathbf{L}_a} \sum_{\hat{\ell}_{b_2} \in \mathbf{L}_b} \sum_{\hat{i}_{a_2} \in \mathbf{S}_a} \sum_{\hat{i}_{b_2} \in \mathbf{S}_b} \exp(E)}{\sum_{\hat{x}^q_{b_2} \in \mathbf{\Omega}^0_b} \sum_{\hat{x}^q_{a_2} \in \mathbf{\Omega}_a} \sum_{\hat{\ell}_{a_2} \in \mathbf{L}_a} \sum_{\hat{\ell}_{b_2} \in \mathbf{L}_b} \sum_{\hat{i}_{a_2} \in \mathbf{S}_a} \sum_{\hat{i}_{b_2} \in \mathbf{S}_b} \exp(F)}, \tag{6.24}$$

where $\mathbf{\Omega}^1_b$ and $\mathbf{\Omega}^0_b$ are vectors which contain the indices of the second symbol with binary '1' and '0' that corresponds to a particular significant bit for the symbol binary data, and $\mathbf{\Omega}_a$ is the set of all possible $\hat{x}^q_{a_2}$ symbols. Employing the procedure in (6.14), the LLR expression for the MBM-TU index ℓ_{a_2} is calculated as:

$$LLR(\ell_{a_2}) = \log \frac{\sum_{\hat{\ell}_{a_2} \in \boldsymbol{\ell}^1_a} \sum_{\hat{\ell}_{b_2} \in \mathbf{L}_b} \sum_{\hat{x}^q_{a_2} \in \mathbf{\Omega}_a} \sum_{\hat{x}^q_{b_2} \in \mathbf{\Omega}_b} \sum_{\hat{i}_{a_2} \in \mathbf{S}_a} \sum_{\hat{i}_{b_2} \in \mathbf{S}_b} \exp(E)}{\sum_{\hat{\ell}_{a_2} \in \boldsymbol{\ell}^0_a} \sum_{\hat{\ell}_{b_2} \in \mathbf{L}_b} \sum_{\hat{x}^q_{a_2} \in \mathbf{\Omega}_a} \sum_{\hat{x}^q_{b_2} \in \mathbf{\Omega}_b} \sum_{\hat{i}_{a_2} \in \mathbf{S}_a} \sum_{\hat{i}_{b_2} \in \mathbf{S}_b} \exp(F)}, \tag{6.25}$$

where $\boldsymbol{\ell}^1_a$ and $\boldsymbol{\ell}^0_a$ are vectors which contain the antenna indices for ℓ_{a_2} with binary '1' and '0' that corresponds to a particular significant bit for the index binary data, respectively, $\mathbf{L}_b$ is the set of all possible for the second antenna index positions $\hat{\ell}_{b_2}$, $\mathbf{\Omega}_a$ and $\mathbf{\Omega}_b$ represents a set of all possible $\hat{x}_{a_2}$ and $\hat{x}_{b_2}$, respectively, $\mathbf{S}_a$ and $\mathbf{S}_b$ represents a set of all possible $\hat{i}_{a_2}$ and $\hat{i}_{b_2}$, respectively. Similarly, the LLR for the antenna index ℓ_{b_2} is calculated as:

$$LLR(\ell_{b_2}) = \log \frac{\sum_{\hat{\ell}_{b_2} \in \boldsymbol{\ell}^1_b} \sum_{\hat{\ell}_{a_2} \in \mathbf{L}_a} \sum_{\hat{x}^q_{a_2} \in \mathbf{\Omega}_a} \sum_{\hat{x}^q_{b_2} \in \mathbf{\Omega}_b} \sum_{\hat{i}_{a_2} \in \mathbf{S}_a} \sum_{\hat{i}_{b_2} \in \mathbf{S}_b} \exp(E)}{\sum_{\hat{\ell}_{b_2} \in \boldsymbol{\ell}^0_b} \sum_{\hat{\ell}_{a_2} \in \mathbf{L}_a} \sum_{\hat{x}^q_{a_2} \in \mathbf{\Omega}_a} \sum_{\hat{x}^q_{b_2} \in \mathbf{\Omega}_b} \sum_{\hat{i}_{a_2} \in \mathbf{S}_a} \sum_{\hat{i}_{b_2} \in \mathbf{S}_b} \exp(F)}, \tag{6.26}$$

where $\boldsymbol{\ell}^1_b$ and $\boldsymbol{\ell}^0_b$ are vectors which contain the antenna indices for ℓ_{b_2} with binary '1' and '0', that corresponds to a particular significant bit for the index binary data, respectively, $\mathbf{L}_a$ is the set of all possible indices for the antenna indices $\hat{\ell}_{a_2}$. The LLR expression for the MAP indices is calculated using the same procedure as (6.12) and applying Bayes' theorem to output. The MAP index LLR expression is given as:

$$LLR(i_{a_2}) = \log \frac{\sum_{\hat{i}_{a_2} \in \mathbf{S}^1_a} \sum_{\hat{i}_{b_2} \in \mathbf{S}_b} \sum_{\hat{\ell}_{a_2} \in \mathbf{L}_a} \sum_{\hat{\ell}_{b_2} \in \mathbf{L}_b} \sum_{\hat{x}^q_{a_2} \in \mathbf{\Omega}_a} \sum_{\hat{x}^q_{b_2} \in \mathbf{\Omega}_b} \exp(E)}{\sum_{\hat{i}_{a_2} \in \mathbf{S}^0_a} \sum_{\hat{i}_{b_2} \in \mathbf{S}_b} \sum_{\hat{\ell}_{a_2} \in \mathbf{L}_a} \sum_{\hat{\ell}_{b_2} \in \mathbf{L}_b} \sum_{\hat{x}^q_{a_2} \in \mathbf{\Omega}_a} \sum_{\hat{x}^q_{b_2} \in \mathbf{\Omega}_b} \exp(F)}, \tag{6.27}$$

where $\mathbf{S}^a_1$ and $\mathbf{S}^a_0$ are vectors that contain the MAP indices i_{a_2} with binary '1' and '0', which corresponds to a particular significant bit for the MAP index binary data, respectively. Lastly,

the LLR for the MAP index i_{b_2} is calculated as :

$$LLR(i_{b_2}) = \log \frac{\sum_{\hat{i}_{b_2} \in \mathbf{S}_b^1} \sum_{\hat{i}_{a_2} \in \mathbf{S}_a} \sum_{\hat{\ell}_{a_2} \in \mathbf{L}_a} \sum_{\hat{\ell}_{b_2} \in \mathbf{L}_b} \sum_{\hat{x}_{a_2}^q \in \mathbf{\Omega}_a} \sum_{\hat{x}_{b_2}^q \in \mathbf{\Omega}_b} \exp(E)}{\sum_{\hat{i}_{b_2} \in \mathbf{S}_b^0} \sum_{\hat{i}_{a_2} \in \mathbf{S}_a} \sum_{\hat{\ell}_{a_2} \in \mathbf{L}_a} \sum_{\hat{\ell}_{b_2} \in \mathbf{L}_b} \sum_{\hat{x}_{a_2}^q \in \mathbf{\Omega}_a} \sum_{\hat{x}_{b_2}^q \in \mathbf{\Omega}_b} \exp(F)}, \tag{6.28}$$

where $\mathbf{S}_1^b$ and $\mathbf{S}_0^b$ are vectors that contain the MAP indices i_{b_2} with binary '1' and '0', which correspond to a particular significant bit for the MAP index binary data, respectively.

The output of the LLR expressions for DSMBM is first used to determine the HDMLD output of the two transmission cases. An HDMLD output for a SOMLD is given when the LLR expression assigns binary "1" if the LLR output is greater than zero; otherwise, it assigns binary "0". Only a single HDMLD output for DSMBM is desired for each transmission; therefore, a decision metric is formulated to select a final HDMLD output from the two cases. Similar to the metric in (6.5), the decision matric for the HDMLD is given as:

$$\lambda = \|\mathbf{y}_1 - \sqrt{\frac{\rho}{2}}\mathbf{H}_{\bar{\ell}_c}^{m_2}\mathbf{e}_{\bar{i}_c}(\bar{x}_{a_1}^q + \bar{x}_{b_1}^q e^{j\theta})\|_F^2 - \|\mathbf{y}_2 - \sqrt{\frac{\rho}{2}}(\mathbf{H}_{\bar{\ell}_{a_1}}^{m_2}\mathbf{e}_{\bar{i}_{a_2}}\bar{x}_{b_2}^q + \mathbf{H}_{\bar{\ell}_{b_2}}^{m_2}\mathbf{e}_{\bar{i}_{b_2}}\bar{x}_{b_2}^q e^{j\theta})\|_F^2, \tag{6.29}$$

$$\lambda < 0: \quad \left[\bar{x}_{a_1}^q, \bar{x}_{b_1}^q, \bar{\ell}_c, \bar{i}_c\right],$$

$$\lambda > 0: \quad \left[\bar{x}_{a_2}^q, \bar{x}_{b_2}^q, \bar{\ell}_{a_2}, \bar{\ell}_{b_2}, \bar{i}_{a_2}, \bar{i}_{b_2}\right],$$

where λ is the output of the decision metric, $\bar{x}_{a_1}^q$, $\bar{x}_{b_1}^q$, $\bar{\ell}_c$ and $\bar{i}_c$ are the first symbol, second symbol, MBM-TU index, and MAP index estimated by the HDMLD for a single transmission case, respectively. In the dual transmission case, $\bar{x}_{a_2}^q$, $\bar{x}_{b_2}^q$, $\bar{\ell}_{a_2}^q$, $\bar{\ell}_{b_2}^q$, $\bar{i}_{a_2}^q$ and $\bar{i}_{b_2}^q$ are the first symbol, second symbol, first MBM-TU index, second MBM-TU index, first MAP index, and second MAP index estimated by the HDMLD, respectively. If the metric above $\lambda < 0$, then the HDMLD output for the single MBM-TU transmission is considered the final output, whereas if $\lambda > 0$, then the final HDMLD output considered is for the dual MBM-TU transmission [35]. The SOMLD for DSMBM selects the output of the LLR expression that corresponds result of the decision metric in (6.20). Improvement in error performance is shown when the output of the SOMLD is fed into a soft-input Viterbi channel decoder [41, 48, 50].

6.6 Numerical Analysis of the Analytical and Simulated BER performance of DSMBM

In this section, the ABEP for DSMBM that is formulated using the union bound approach in Section 6.5 is presented. Monte Carlo simulation results executed in a Matlab environment are presented and serve to validate the analytical result. In all simulations, we consider i.i.d. Rayleigh frequency-flat fading channels in the presence of AWGN. As stated earlier, complete CSI is known at the receiver at all instances.

In Section 6.2, uncoded data is transmitted, and Gray-coded M-ary constellation sets are employed. Monte Carlo simulations are presented for spectral efficiencies of 6, 8, 10, and 12 b/s/Hz, and results are presented in terms of average BER vs. SNR. The notation used to denote $N_R \times N_T$ DSMBM configuration is $(N_T, N_R, M, m_{RF}, M_{RF}, \eta_{DSMBM})$.

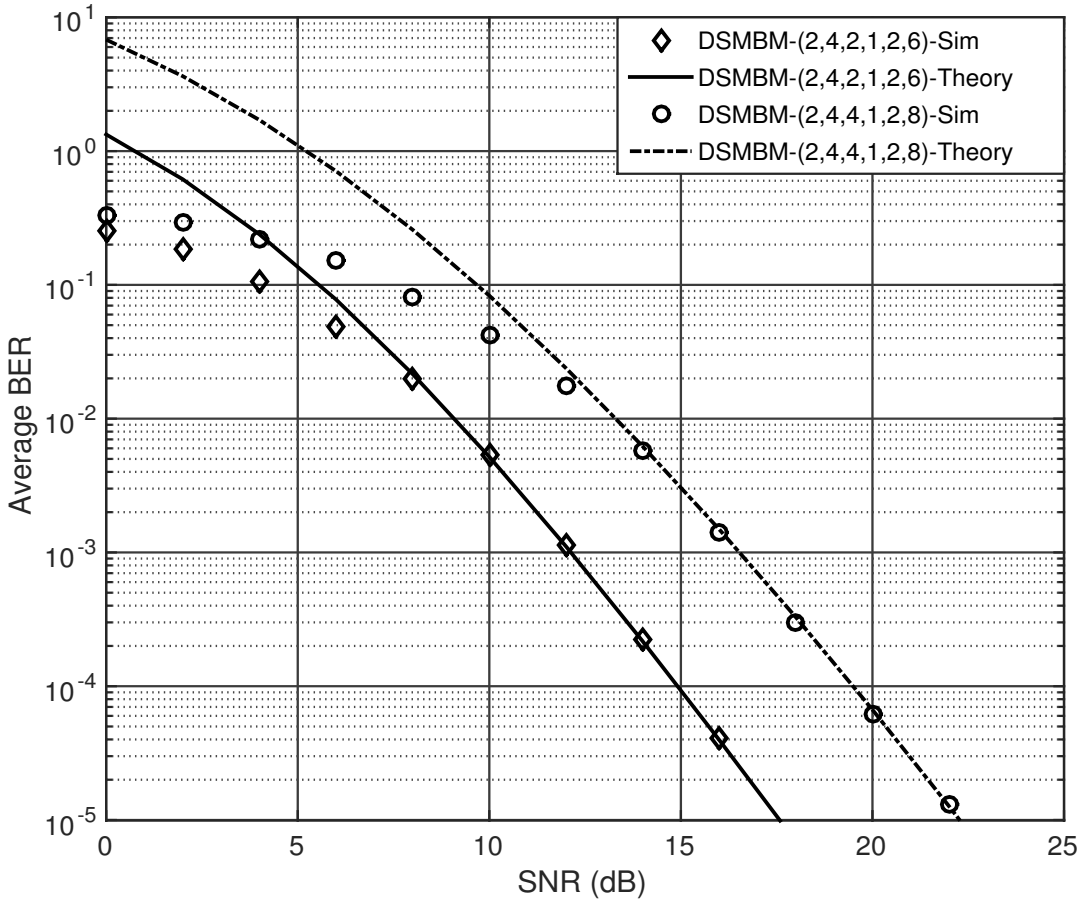

Figure 6.2: Theoretical and simulated BER performance DSMBM for η_{DSMBM}= 6, 8 b/s/Hz.

In Figure 6.2, analytical and Monte Carlo simulation results for 2×4 DSMBM BPSK and 4-QAM signal constellations with $M_{RF} = 2$ and spectral efficiency of $\eta_{DSMBM} = 6$ and 8 b/s/Hz are presented. The Monte Carlo simulation results validate the analytical performance

of DSMBM as the error performance of the simulation is relatively tight with the analytical performance at high SNR regions. This is the expected result since the upper bound approach is used to derive the theoretical performance.

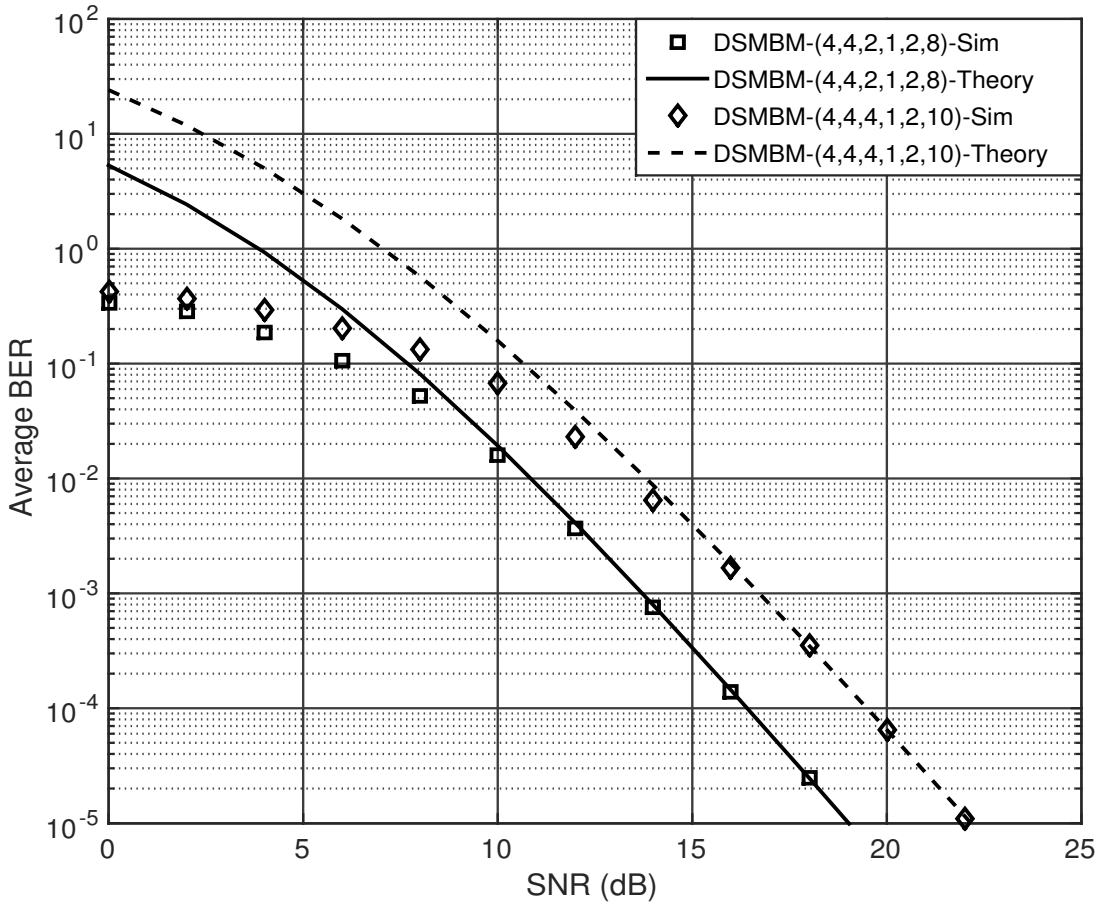

Figure 6.3: Theoretical and simulated BER performance DSMBM for η_{DSMBM}= 8, 10 b/s/Hz.

In Figure 6.3, analytical and Monte Carlo simulation results for 4×4 DSMBM BPSK and 4-QAM signal constellations with $M_{RF} = 4$ and spectral efficiency of $\eta_{DSMBM} = 8$ and 10 b/s/Hz are presented. The Monte Carlo simulation results validate the analytical performance of DSMBM as the error performance of the simulation is relatively tight with the analytical performance at high SNR regions.

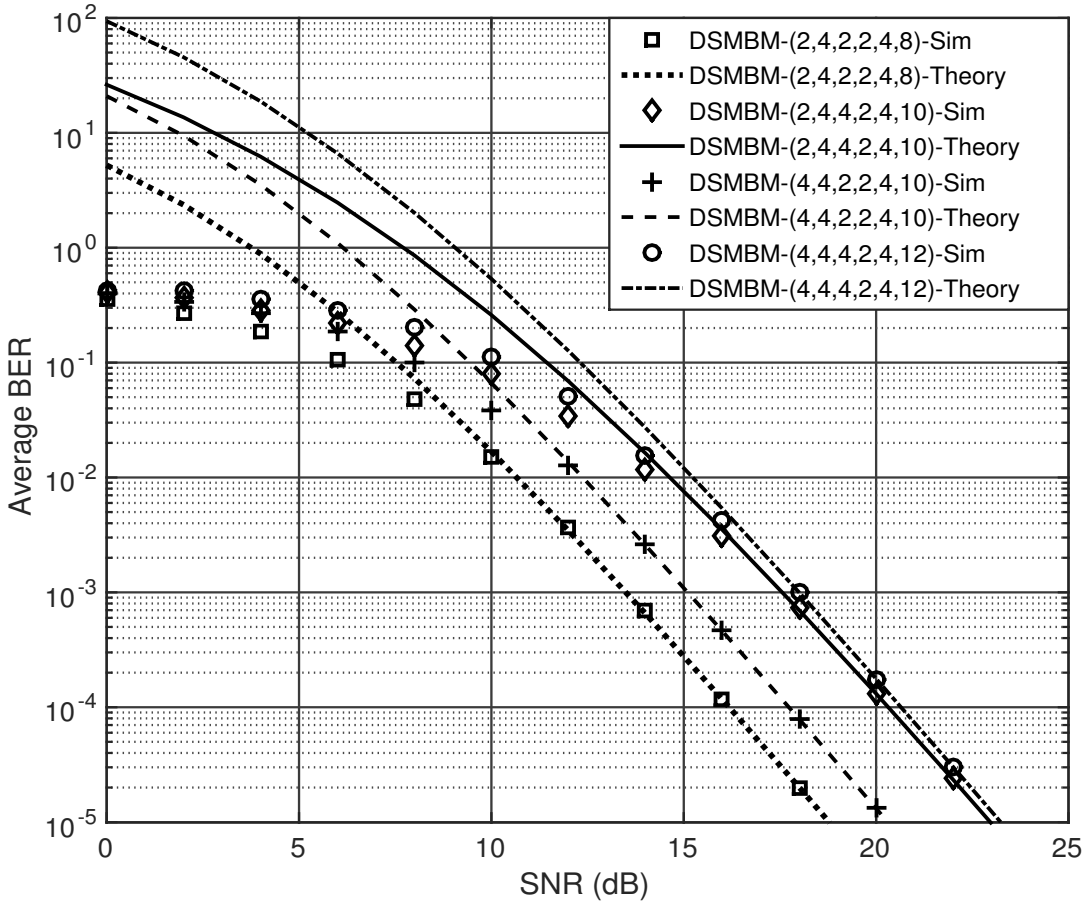

Figure 6.4: Theoretical and simulated BER performance DSMBM for η_{DSMBM}= 8, 10, 12 b/s/Hz.

In Figure 6.4, the ABEP of the DSMBM system is analyzed for BPSK and 4-QAM signal constellations with $M_{RF} = 4$. The BER performance for a 2×4 and 4×4 MIMO configurations with spectral efficiencies of $\eta_{DSMBM} = 8,\ 10$, and 12 b/s/Hz are presented. The Monte Carlo simulation results validate the analytical performance of DSM as the error performance of the simulation closely matches the analytical result at high SNR values. It is observed that at the same spectral efficiency and RF mirror configuration, 4×4 DSMBM systems have a better error performance as compared to the 2×4 DSMBM counterpart.

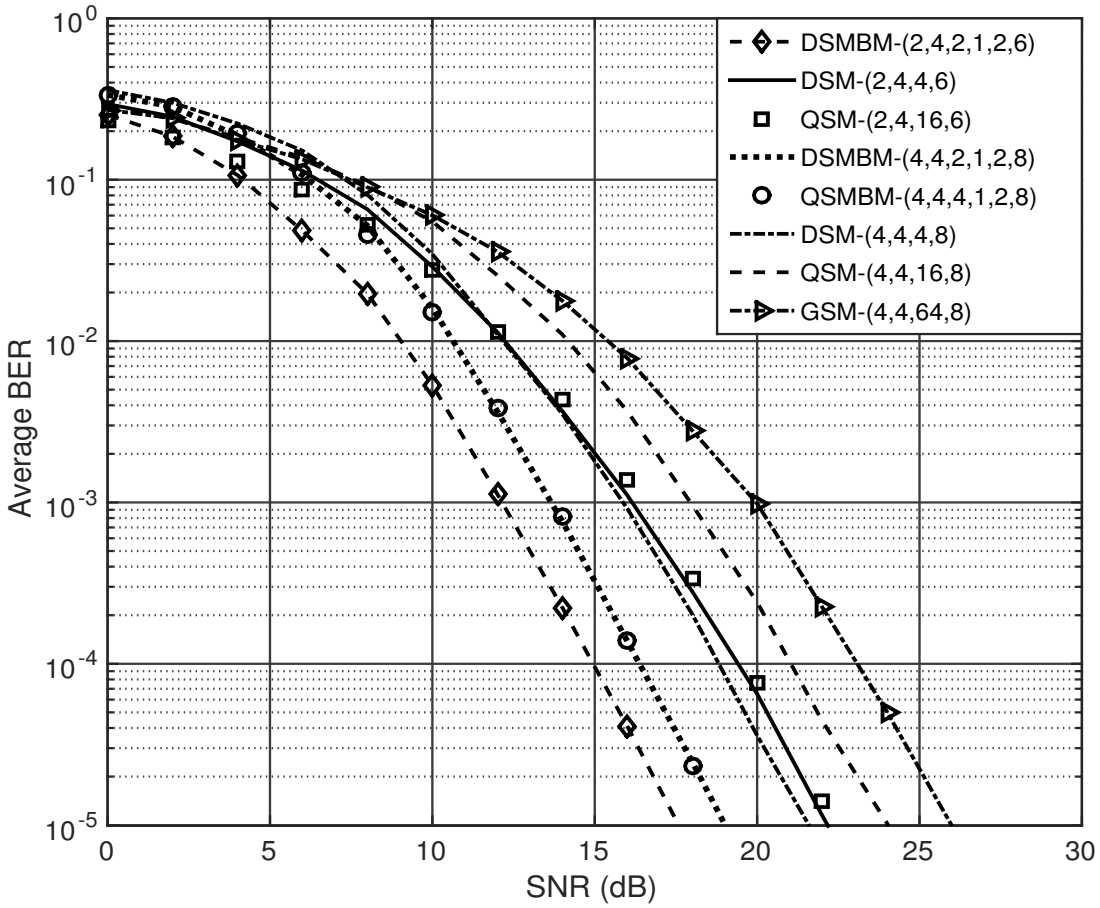

Figure 6.5: BER performance of DSMBM as compared to schemes with η= 6, 8 b/s/Hz.

In Figure 6.5, the BER performance of DSMBM is compared to other modulation schemes that have a 2×4 and 4×4 MIMO configuration. The BER performance for DSM, QSM, GSM, and QSMBM are presented for systems with identical spectral efficiency. The notation employed for QSM, DSM, GSM, and QSMBM is $(N_T, N_R, M, \eta_{QSM})$, $(N_T, N_R, M, \eta_{DSM})$, $(N_T, N_R, M, \eta_{GSM})$ and $(N_T, N_R, M, m_{RF}, M_{RF}, \eta_{QSMBM})$, respectively. It can be noted that DSMBM shows an improved BER performance as compared to the DSM, QSM, and GSM schemes.

For 2×4 systems with a spectral efficiency $\eta = 6$ b/s/Hz, at a BER of 10^{-5}, DSMBM with $M_{RF} = 2$ has an SNR gain of 4.5 dB over DSM and an SNR gain of 4.7 dB over QSM. For 4×4 systems with a spectral efficiency $\eta = 8$ b/s/Hz, at a BER of 10^{-5}, DSMBM with $M_{RF} = 2$ has an SNR gain of 2.6 dB over DSM, an SNR gain of 5.3 dB over QSM, and an SNR gain of 7.1 dB over GSM. Note that, the error performance of 4×4 DSMBM with a BSPK signal constellation and the error performance of 4×4 QSMBM with a 4-QAM signal constellation are identical. In DSMBM, the BSPK signal constellation for the second symbol $x_q^2 e^{j\theta}$ is rotated through an

optimum angle of 90°, which fundamentally gives the symbol as $(\pm j)$, whereas the first symbol $x_1^q = (\pm 1)$. Adding these two symbols essentially gives a 4-QAM constellation symbol as $(\pm 1 \pm j)$; therefore, the error performance of DSMBM and QSMBM is matched due to identical constellations. [30] As the APM modulation order increases, DSMBM error performance is better than QSMBM error performance.

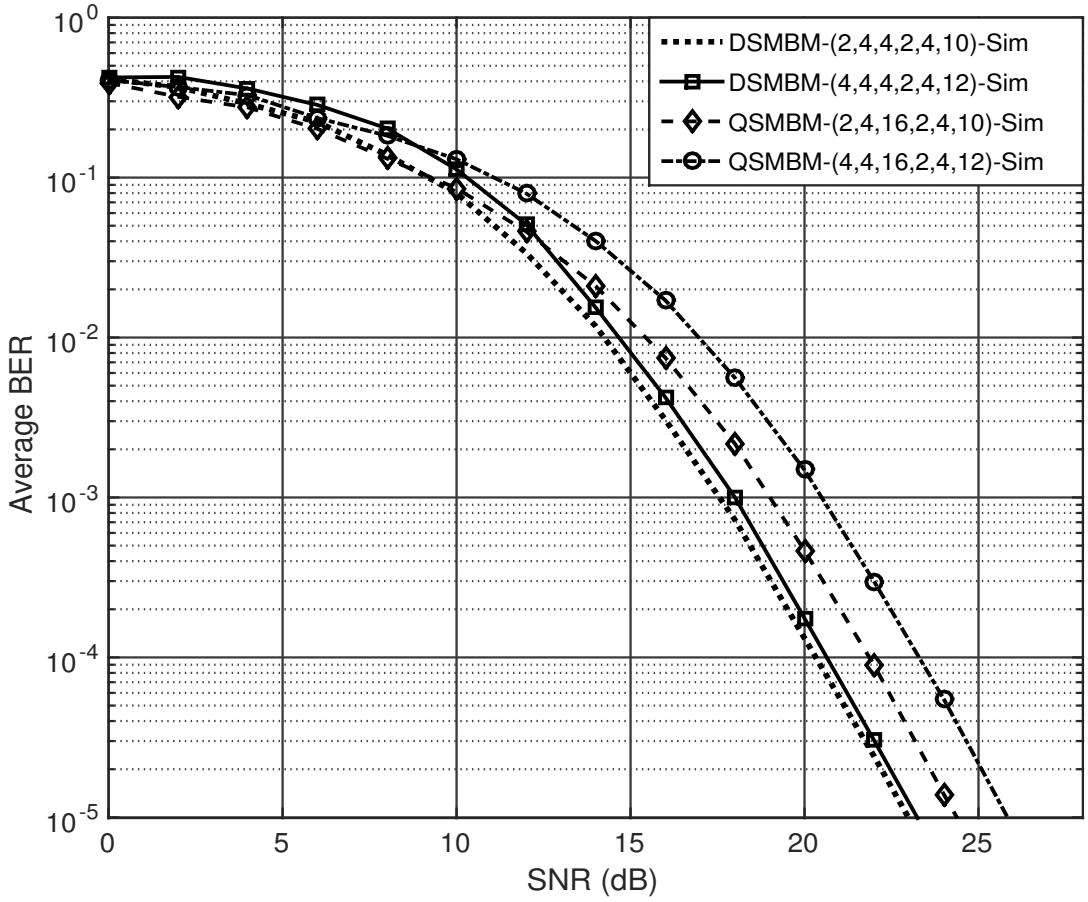

Figure 6.6: BER performance of DSMBM and QSMBM at $\eta_{DSMBM} = \eta_{QSMBM}$= 10, 12 b/s/Hz.

In Figure 6.6, the BER performance of 2×4 and 4×4 DSMBM and QSMBM systems are compared for a spectral efficiencies $\eta_{DSMBM} = \eta_{QSMBM} = 10$ and 12 b/s/Hz, respectively. At a BER of 10^{-5}, DSMBM with $\eta_{DSMBM} = 10$ b/s/Hz has an SNR gain of 1.4 dB over QSMBM with $\eta_{QSMBM} = 10$ b/s/Hz, and DSMBM with $\eta_{DSMBM} = 12$ b/s/Hz has an SNR gain of 2.7 dB over QSMBM with $\eta_{QSMBM} = 12$ b/s/Hz. DSMBM exhibits an SNR gain because as modulation order increases, the minimum Euclidean distance between signal constellation points decreases. Since QSMBM is always at a higher modulation order than DSMBM at the same spectral efficiency, DSMBM has an error performance that is inherently better than QSMBM. The advantage of employing RF mirrors to DSM systems is demonstrated by the improvement in the error performance as compared to QSMBM.

6.6.1 BER performance of DSMBM SOMLD

In Section 6.4, for all coded cases, a $\frac{1}{2}$-rate convolutional encoder was employed to encode the information bits under the constraint length 9 with code generator matrices $g_1 = (561)_{octal}$; $g_2(753)_{octal}$ [41,42,50]. At the detector, the proposed SOMLD is employed, and the output is fed into a soft-input Viterbi channel decoder in order to estimate the transmitted information [40]. Figure 6.2 shows the BER performance of BPSK DSM, using the optimal detector in Section 6.3. All configurations are compared to the analytical performance presented in Section 6.5.

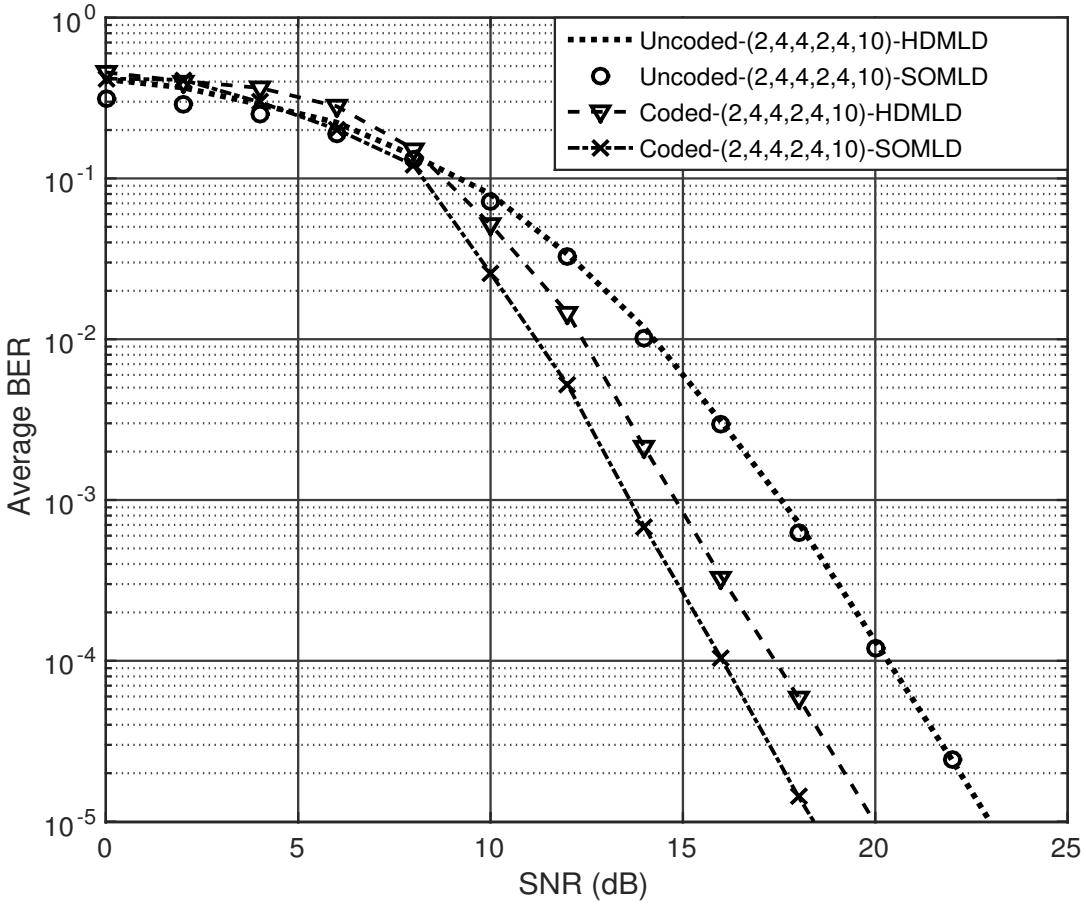

Figure 6.7: BER performance of DSMBM for SOMLD and HDMLD with $M_{RF} = 4$ and $\eta_{DSMBM} = 10$ b/s/Hz

Figure 6.7 shows the simulation results for coded and uncoded channels for the proposed SOMLD and the HDMLD for 2×4 DSMBM with $M_{RF} = 4$ at spectral efficiency of η_{DSMBM}= 10 b/s/Hz. The detector given in (6.5) is regarded as the HDMLD for DSMBM. The uncoded simulation shows that the SOMLD matches the HDMLD error performance. This is the expected result since SOMLDs only have an effect in coded channels with a soft input decoder at the receiver can give coding gain [50]. For coded channels, the proposed SOMLD for DSMBM demonstrates coding gain over the uncoded SOMLD. At a BER of 10^{-5}, coded SOMLD has an SNR gain of 4.6 dB over uncoded SOMLD, and coded HDMLD has an SNR gain of 3.0 dB as compared

to uncoded HDMLD. Hence, the advantage of soft-output demodulation followed by soft-input decoding is demonstrated.

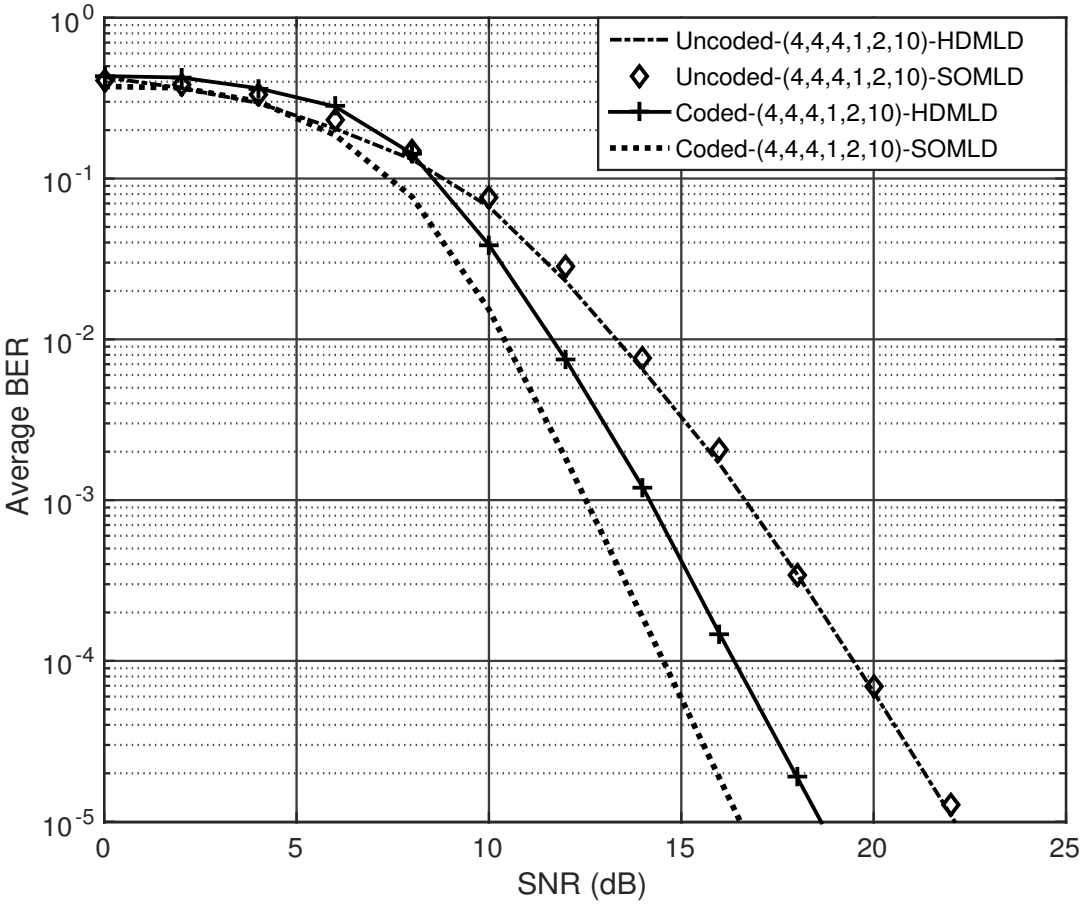

Figure 6.8: BER performance of DSMBM for SOMLD and HDMLD with $M_{RF} = 2$ and $\eta_{DSMBM} = 10$ b/s/Hz

Figure 6.8 shows the simulation results for coded and uncoded channels for the proposed SOMLD and the HDMLD for 4×4 DSMBM with $M_{RF} = 2$ at spectral efficiency of η_{DSMBM}= 10 b/s/Hz. The detector given in (6.5) is regarded as the HDMLD for DSMBM. The uncoded simulation shows that the SOMLD matches the HDMLD error performance. This is the expected result since SOMLDs only have an effect in coded channels with a soft input decoder at the receiver can give coding gain [50]. For coded channels, the proposed SOMLD for DSMBM demonstrates coding gain over the uncoded SOMLD. At a BER of 10^{-5}, coded SOMLD has an SNR gain of 4.6 dB over uncoded SOMLD, and coded HDMLD has an SNR gain of 3.0 dB as compared to uncoded HDMLD. Hence, the advantage of soft-output demodulation followed by soft-input decoding is demonstrated.

6.7 Summary

The performance analysis for DSMBM employing the union bound approach to calculate the average BER performance of over i.i.d. Rayleigh frequency-flat fading with zero mean and unit variance was formulated. Furthermore, a SOMLD based on the ML principle employing an LLR is proposed. Monte Carlo simulations are used to validate the analytical result of DSMBM in Section 6.6. The proposed SOMLD is validated by the results shown by the simulation of the uncoded HDMLD and SOMLD channels. In coded channels, both the HDMLD and SOMLD showed significant SNR gains.

Chapter 7

Conclusion

7.1 Research Contribution

In this dissertation, several-next generation modulation schemes were investigated. DSMBM and the SOMLDs for DSMBM and DSM are the contributions outputs of this dissertation.

In Chapter 2, an investigation of the fundamental SM scheme was performed. The ABEP for SM was presented, and the results demonstrated that Monte Carlo simulations were relatively tight and consistent with the analytical error performance, verifying the scheme. In Chapter 3, QSM was presented, and the investigation on the ABEP displayed Monte Carlo simulations that were tightly bound to the analytical error performance at high SNR regions, verifying the scheme. The BER performance for QSM and SM was presented to investigate the improvement in error performance of QSM. Table 7.1 summarizes the SNR gains demonstrated by QSM over SM.

Table 7.1: SNR (dB) gain of QSM as compared to SM at a BER of 10^{-5}

Configuration	**SNR gain of QSM at a BER of** 10^{-5}		
	4 b/s/Hz	6 b/s/Hz	8 b/s/Hz
$N_T = 2,\ N_R = 4$	1.9	–	–
$N_T = 4,\ N_R = 4$	–	2.9	2.3
$N_T = 8,\ N_R = 4$	–	–	2.2

In Chapter 4, DSM was presented. The initial investigation displayed the optimal rotation angle for signal constellations that minimize BER. Table 7.2 summarizes the optimal rotation angles and conditions in which angles where obtained.

Table 7.2: Optimal rotation angles for the DSM scheme

Modulation	**Configuration**	**SNR** (dB)	**Angle** θ°
BPSK	$N_R = 4, N_T = 4$	16	90
4-QAM	$N_R = 4, N_T = 4$	16	45, 135
8-QAM	$N_R = 4, N_T = 4$	20	60, 120

The ABEP of DSM was presented, and Monte Carlo simulations matched the analytical error performance at high SNR values to validate DSM. The BER performance for DSM and QSM was presented to verify the improvement in error performance of the scheme. Table 7.3 summarises the SNR gains demonstrated by DSM over QSM.

Table 7.3: SNR (dB) gain of DSM as compared to QSM at a BER of 10^{-5}

Configuration	**SNR gain of DSM at a BER of** 10^{-5}		
	6 b/s/Hz	8 b/s/Hz	10 b/s/Hz
$N_T = 4,\ N_R = 4$	0	2.9	2.3

The concept of soft-output detection was introduced to DSM, and consequently, an SOMLD was proposed. In uncoded channels, the error performance of the SOMLD was relatively tight and consistent with the HDMLD error performance at all SNR values, validating the SOMLD. In coded channels, the SOMLD coupled with a soft-input decoder at the receiver, demonstrated significant SNR gains when compared to the error performance of the uncoded HDMLD. Table 7.4 summarizes the SNR gains demonstrated by the SOMLD and HDMLD of DSM at a BER of 10^{-5}.

In Chapter 5, MBM was presented with the intention to demonstrate its application on SIMO. The ABEP of SIMO-MBM was presented, and investigations showed that Monte Carlo simulations were relatively tight and consistent with the ABEP of SIMO-MBM. The BER performance of SIMO-MBM and SIMO was presented, and significant gains in SNR were displayed. Table 7.5 summarizes the SNR gains demonstrated by SIMO-MBM over SIMO.

Table 7.4: SNR (dB) gain of DSM SOMLD and HDMLD detectors at a BER of 10^{-5}

η_{DSM}	**Detection**	**Configuration**	**SNR at a BER of 10^{-5}**		
			Uncoded	**Coded**	**Gain**
6	SOMLD	$N_T = 2, N_R = 4$	22.1	12.6	9.5
	HDMLD		22.1	15.3	6.8
8	SOMLD	$N_T = 4, N_R = 4$	21.6	11.9	9.7
	HDMLD		21.6	16.8	4.8

Table 7.5: SNR (dB) gain of SIMO-MBM as compared to SIMO at a BER of 10^{-5}

η_{SIMO} $\eta_{SIMO-MBM}$	**SIMO Configuration**	**SIMO-MBM Configuration**	**SNR at a BER of 10^{-5}**		
			SIMO	**SIMO-MBM**	**Gain**
4 b/s/Hz	$M = 16$ $N_R = 4$	$M = 4$ $N_R = 4$ $M_{RF} = 2$	29.7	18.2	11.2
4 b/s/Hz	$M = 16$ $N_R = 8$	$M = 4$ $N_R = 8$ $M_{RF} = 2$	23.3	10.9	12.4
6 b/s/Hz	$M = 64$ $N_R = 4$	$M = 4$ $N_R = 4$ $M_{RF} = 4$	41.7	19.8	21.9
6 b/s/Hz	$M = 64$ $N_R = 8$	$M = 4$ $N_R = 8$ $M_{RF} = 4$	35.5	12.0	13.5

In Chapter 6, DSMBM was presented. The ABEP for DSMBM was formulated, and Monte Carlo simulations displayed were relatively tight and consistent with the analytical error performance at high SNR regions, validating the scheme. SNR gains were demonstrated when DSMBM was compared to other schemes, which include QSM, GSM, and DSM. Table 7.6 summarizes the SNR gains demonstrated by DSMBM over QSM, GSM, and DSM.

Table 7.6: SNR (dB) gain of DSMBM compared to DSM, QSM, and GSM at a BER of 10^{-5}

η	**Scheme**	**Configuration**	**SNR at a BER of 10^{-5} Gain**
6 b/s/Hz	DSM	$N_T = 2, N_R = 4$	4.5
	QSM	$N_T = 2, N_R = 4$	4.7
8 b/s/Hz	DSM	$N_T = 4, N_R = 4$	2.6
	QSM	$N_T = 4, N_R = 4$	5.3
	GSM	$N_T = 4, N_R = 4$	7.1

The error performance of DSMBM and QSMBM was investigated, and results demonstrated that DSMBM has better performance when compared to QSMBM. Table 7.7 summarized the SNR gains demonstrated by DSMBM over QSMBM.

Table 7.7: SNR (dB) gain of DSMBM as compared to QSMBM at a BER of 10^{-5}

Configuration	**SNR gain of DSMBM at a BER of** 10^{-5}		
	8 b/s/Hz	10 b/s/Hz	12 b/s/Hz
$N_T = 2,\ N_R = 4,\ M_{RF} = 4$	–	1.4	–
$N_T = 4,\ N_R = 4,\ M_{RF} = 2$	0	–	–
$N_T = 4,\ N_R = 4,\ M_{RF} = 4$	–	–	2.7

Finally, the SOMLD detector for DSMBM was presented. In uncoded channels, the error performance of the SOMLD was consistent with the HDMLD error performance. In coded channels, the SOMLD coupled with a soft-input decoder at the receiver, demonstrated significant SNR gains when compared to uncoded cases. Table 7.8 summarizes the SNR gains achieved by the SOMLD and HDMLD of DSMBM at a BER of 10^{-5}.

Table 7.8: SNR (dB) gain of DSMBM SOMLD and HDMLD detectors at a BER of 10^{-5}

η_{DSMBM}	**Detection**	**Configuration**	**SNR at a BER of 10^{-5}**		
			Uncoded	**Coded**	**Gain**
10	SOMLD	$N_T = 2, N_R = 4$	23.0	18.4	4.6
	HDMLD	$M_{RF} = 4$	22.9	20.0	2.9
10	SOMLD	$N_T = 4, N_R = 4$	22.1	16.5	5.6
	HDMLD	$M_{RF} = 2$	22.2	18.6	3.6

7.2 Future Work

Future work can be aimed at providing research advancements in the following direction.

1. To reduce the computational complexity of DSM and DSMBM, research can be conducted to introduce low-complexity detectors for the schemes.
2. Research can be conducted to introduce differential detection schemes for DSM and DSMBM.
3. Practical implementation of the DSM and DSMBM scheme.

Bibliography

[1] A. Goldsmith, *Wireless Communications*. 1^{st} ed., New York: Cambridge University Press, 2005.

[2] L. J. Vora, "Evolution of mobile generation technology: 1G to 5G and review of upcoming wireless technology 5G," *International Journal of Modern Trends in Engineering and Research*, vol. 2, no. 10, pp. 281–290, Oct. 2015.

[3] J. A. del Peral-Rosado, R. Raulefs, J. A. López-Salcedo, and G. Seco-Granados, "Survey of cellular mobile radio localization methods: From 1G to 5G," *IEEE Communications Surveys & Tutorials*, vol. 20, no. 2, pp. 1124–1148, Dec. 2017.

[4] P. Sharma, "Evolution of mobile wireless communication networks-1G to 5G as well as future prospective of next generation communication network," *International Journal of Computer Science and Mobile Computing*, vol. 2, no. 8, pp. 47–53, Aug. 2013.

[5] F. Hillebrand, "The creation of standards for global mobile communication: GSM and UMTS standardization from 1982 to 2000," *IEEE Wireless Communications*, vol. 20, no. 5, pp. 24–33, Oct. 2013.

[6] D. X. Li, W. He, and S. Li, "Internet of things in industries: A survey," *IEEE Transactions on Industrial Informatics*, vol. 10, no. 4, pp. 2233 –2243, Nov. 2014.

[7] L. Yi, K. Miao, and A. Liu, "A comparative study of WiMAX and LTE as the next generation mobile enterprise network," in *Proceedings of the 13th International Conference on Advanced Communication Technology*, pp. 654–658, Feb. 2011.

[8] U. R. Mori, P. M. Chandarana, G. V. Gajjar, and S. Dasi, "Performance comparison of different modulation schemes in advanced technologies WiMAX and LTE," in *Proceedings of 2015 IEEE International Advance Computing Conference*, pp. 286–289, Jun. 2015.

[9] M. Jaber, M. A. Imran, R. Tafazolli, and A. Tukmanov, "5G backhaul challenges and emerging research directions: A survey," *IEEE Access*, vol. 4, pp. 1743–1766, Mar. 2016.

[10] C. X. Wang, J. Bian, J. Sun, W. Zhang, and M. Zhang, "A survey of 5G channel measurements and models," *IEEE Communications Surveys & Tutorials*, vol. 20, no. 4, pp. 3142–3168, Aug. 2018.

[11] A. B. Idris, R. F. B. Rahim, *et al.*, "The effect of additive white Gaussian noise and multipath Rayleigh fading on BER statistic in digital cellular network," in *Proceedings of the International RF and Microwave Conference*, pp. 97–100, Sep. 2006.

[12] M. K. Simon and M. S. Alouini, *Digital communication over fading channels.* 1^{st} ed., John Wiley & Sons, 2002.

[13] V. Tarokh, H. Jafarkhani, and A. R. Calderbank, "Space-time block codes from orthogonal designs," *IEEE Transactions on Information Theory*, vol. 45, no. 5, pp. 1456–1467, Jul. 1999.

[14] S. M. Alamouti, "A simple transmit diversity technique for wireless communications," *IEEE Journal on Selected Areas in Communications*, vol. 16, no. 8, pp. 1451–1458, Oct. 1998.

[15] P. O. Akuon and H. Xu, "Optimal error analysis of receive diversity schemes on arbitrarily correlated Rayleigh fading channels," *IET Communications*, vol. 10, no. 7, pp. 854–861, May. 2016.

[16] E. Telatar, "Capacity of multi-antenna Gaussian channels," *Transactions on Emerging Telecommunications Technologies*, vol. 10, no. 6, pp. 585–595, Nov. 1999.

[17] J. Mietzner, R. Schober, L. Lampe, W. H. Gerstacker, and P. A. Hoeher, "Multiple-antenna techniques for wireless communications - A comprehensive literature survey," *IEEE Communications Surveys & Tutorials*, vol. 11, no. 2, pp. 87–105, Jun. 2009.

[18] N. Ebrahimi-Tofighi, M. ArdebiliPour, and M. Shahabadi, "Receive and transmit array antenna spacing and their effect on the performance of SIMO and MIMO systems by using an RCS channel model," *World Academy of Science, Engineering and Technology*, vol. 36, pp. 1–5, Jan. 2007.

[19] E. G. Larsson, O. Edfors, F. Tufvesson, and T. L. Marzetta, "Massive MIMO for next generation wireless systems," *IEEE Communications Magazine*, vol. 52, no. 2, pp. 186–195, Feb. 2014.

[20] C. X. Wang, S. Wu, L. Bai, X. You, J. Wang, and I. Chih-Lin, "Recent advances and future challenges for massive MIMO channel measurements and models," *Science China Information Sciences*, vol. 59, no. 2, pp. 1–16, Feb. 2016.

[21] E. Basar, "Index modulation techniques for 5G wireless networks," *IEEE Communications Magazine*, vol. 54, no. 7, pp. 168–175, Jul. 2016.

[22] S. Sanayei and A. Nosratinia, "Antenna selection in MIMO systems," *IEEE Communications Magazine*, vol. 42, no. 10, pp. 68–73, Oct. 2004.

[23] R. Y. Mesleh, H. Haas, S. Sinanovic, C. W. Ahn, and S. Yun, "Spatial modulation," *IEEE Transactions on Vehicular Technology*, vol. 57, no. 4, pp. 2228–2241, Jul. 2008.

[24] E. Aydın and H. Ilhan, "A novel SM-based mimo system with index modulation," *IEEE Communications Letters*, vol. 20, no. 2, pp. 244–247, Dec. 2015.

[25] N. R. Naidoo, H. Xu, and T. A. Quazi, "Spatial modulation: optimal detector asymptotic performance and multiple-stage detection," *IET Communications*, vol. 5, no. 10, pp. 1368–1376, Jul. 2011.

[26] A. Younis, N. Serafimovski, R. Mesleh, and H. Haas, "Generalised spatial modulation," in *Proceedings of 2010 Conference Record of the Forty Fourth Asilomar Conference on Signals, Systems and Computers*, pp. 1498–1502, Nov. 2010.

[27] M. Di Renzo, H. Haas, A. Ghrayeb, S. Sugiura, and L. Hanzo, "Spatial modulation for generalized MIMO: Challenges, opportunities, and implementation," *Proceedings of the IEEE*, vol. 102, no. 1, pp. 56–103, Dec. 2013.

[28] J. Wang, S. Jia, and J. Song, "Generalised spatial modulation system with multiple active transmit antennas and low complexity detection scheme," *IEEE Transactions on Wireless Communications*, vol. 11, no. 4, pp. 1605–1615, Mar. 2012.

[29] R. Mesleh, S. S. Ikki, and H. M. Aggoune, "Quadrature spatial modulation," *IEEE Transactions on Vehicular Technology*, vol. 64, no. 6, pp. 2738–2742, Jul. 2014.

[30] Z. Yigit and E. Basar, "Double spatial modulation: A high-rate index modulation scheme for MIMO systems," in *Proceedings of 2016 International Symposium on Wireless Communication Systems*, pp. 347–351, Sep. 2016.

[31] M. Mohaisen and S. Lee, "Complex quadrature spatial modulation," *Electronics and Telecommunications Research Institute Journal*, vol. 39, no. 4, pp. 514–524, Aug. 2017.

[32] A. K. Khandani, "Media-based modulation: A new approach to wireless transmission," in *Proceedings of 2013 IEEE International Symposium on Information*, pp. 3050–3054, Jul. 2013.

[33] Y. Naresh and A. Chockalingam, "On media-based modulation using RF mirrors," *IEEE Transactions on Vehicular Technology*, vol. 66, no. 6, pp. 4967–4983, Oct. 2017.

[34] E. Basar, "Media-based modulation for future wireless systems: A tutorial," *IEEE Wireless Communications*, vol. 26, no. 5, p. 160, Jul. 2019.

[35] N. Pillay and H. Xu, "Quadrature spatial media-based modulation with RF mirrors," *IET Communications*, vol. 11, no. 16, pp. 2440–2448, Aug. 2017.

[36] B. S. Adejumobi, N. Pillay, and S. H. Mneney, "A study of spatial media-based modulation using RF mirrors," in *Proceedings of 2017 IEEE AFRICON*, pp. 336–341, Sep. 2017.

[37] Y. Zehra and E. Basar, "Space-time media-based modulation," *IEEE Communications Letters*, vol. 67, no. 9, pp. 2389–2398, May 2019.

[38] B. S. Adejumobi and N. Pillay, "RF mirror media-based space-time block coded spatial modulation techniques for two time-slots," *IET Communications*, vol. 13, no. 15, pp. 2313–2321, Jun. 2019.

[39] N. Pillay and H. Xu, "Uncoded space-time labeling diversity - application of media-based modulation with RF mirrors," *IEEE Communications Letters*, vol. 22, no. 2, pp. 272–275, Nov. 2017.

[40] T. K. Moon, *Error Correction Coding: Mathematical Methods and Algorithms*. 1^{st} ed.,John Wiley & Sons, Jun. 2005.

[41] Q. Tang, Y. Xiao, P. Yang, Q. Yu, and S. Li, "A new low-complexity near-ML detection algorithm for spatial modulation," *IEEE Wireless Communications Letters*, vol. 2, no. 1, pp. 90–93, Dec. 2012.

[42] A. A. Tijani, N. Pillay, and H. Xu, "Soft-output decision-based detection of SSK, BI-SSK and QSM," *South African Institute of Electrical Engineers Africa Research Journal*, vol. 109, no. 3, pp. 182–190, Dec. 2018.

[43] S. U. Hwang, S. Jeon, S. Lee, and J. Seo, "Soft-output ML detector for spatial modulation OFDM systems," *Institute of Electronics, Information and Communication Engineers Electronics Express*, vol. 6, no. 19, pp. 1426–1431, 2009.

[44] J. Jeganathan, A. Ghrayeb, and L. Szczecinski, "Spatial modulation: Optimal detection and performance analysis.," *IEEE Communications Letters*, vol. 12, no. 8, pp. 545–547, Aug. 2008.

[45] R. Mesleh and S. S. Ikki, "A high spectral efficiency spatial modulation technique," in *Proceedings of 2014 IEEE 80th Vehicular Technology Conference*, pp. 1–5, Sep. 2014.

[46] G. Kaddoum and E. Soujeri, "On the comparison between code-index modulation and spatial modulation techniques," in *Proceedings of the International Conference on Information and Communication Technology Research*, pp. 24–27, May. 2015.

[47] C. Li, J. Wang, Y. Cheng, and Y. Huang, "Low-complexity soft-decision aided detectors for coded spatial modulation MIMO systems," *EURASIP Journal on Wireless Communications and Networking*, vol. 2016, no. 1, p. 34, Dec. 2016.

[48] L. Xiao, P. Yang, Y. Xiao, J. Liu, S. Fan, B. Dong, and S. Li, "An improved soft-input soft-output detector for generalized spatial modulation," *IEEE Signal Processing Letters*, vol. 23, no. 1, pp. 30–34, Nov. 2016.

[49] H. Xu, "Symbol error probability for generalized selection combining reception of M-QAM," *South African Institute of Electrical Engineers Africa Research Journal*, vol. 100, no. 3, pp. 68–71, Sep. 2009.

[50] R. Govender, N. Pillay, and H. Xu, "Soft-output space-time block coded spatial modulation," *IET Communications*, vol. 8, no. 16, pp. 2786–2796, Aug. 2014.

[51] H. Xu, K. Govindasamy, and N. Pillay, "Uncoded space-time labeling diversity," *IEEE Communications Letters*, vol. 20, no. 8, pp. 1511–1514, Jun. 2016.